

## **## Replies are in blue colour and italics**

Review of “Evaluating the simulated radiative forcings, aerosol properties and stratospheric warmings from the 1963 Agung, 1982 El Chichón and 1991 Mt Pinatubo volcanic aerosol clouds” by Sandip S. Dhomse et al.

### **Review #1 by Daniel Visioni**

This article gives an overview of the results from the UM-UKCA model simulations of the three biggest volcanic eruptions of the 20<sup>th</sup> century, and compares against available datasets. All simulations are run following the design of ISA-MIP. In light of both CMIP6 and the release of the new generation of models, and also of ISA-MIP, of which this study is most likely the first showing results of the simulations described in Timmreck et al. (2018), I believe this study to be of great importance and a very good fit for ACP. I have some suggestions to improve the presentation of the results and the discussion in this paper before it can be published. After these minor comments are addressed, the study can certainly be published in ACP.

--> *We thank Dr Visioni for these positive comments.*

### **Some broad comments:**

“Evaluation dataset” section: this section is a bit confused and hard to follow. I suggest a table for the supplementary (similar to Table 1), at least, that sums up all of this information, including columns for timespan, type of observation and link to the dataset.

--> *Thank you for a very useful suggestion. We decided to add the suggested table into the main article (new Table 2) rather than the supplementary, so as to provide a summary of the important details for each observation dataset (wavelengths, data source) and to reference the papers and/or web-links to the individual datasets.*

*We have pasted below the Table 2 added to the dataset, the process also alerting us to correct some aspects of the text of the evaluation datasets section (see track-changes manuscript). For example, we improved the text re: the Pinatubo period in GloSSAC to read:*

“For the Pinatubo period, GloSSAC is an updated version of the gap-filled dataset described in \citet[] [chapter 4]{SPARC2006}, combining SAGE II aerosol extinction (in the solar part of the spectrum), with HALOE and CLAES aerosol extinction in the infra-red \citet[see][]{Thomason2018}. For the period where the SAGE-II signal was saturated (e.g. Thomason, 1992), GloSSAC applies an improved gap-fill method in mid-latitudes, but in the tropics is still based on the composite dataset from \citet[] [pages 140-147]{SPARC2006}, combining with ground-based lidar measurements from Mauna Loa, Hawaii (19.5°N, \citet{Barnes1997}), and after January 1992 also with lidar measurements from Camaguey, Cuba \citet[23°N, see][]{Antuna1996}.”

Table 2: Some important aspects of the evaluation dataset.

Aerosol property	Key Aspects
<b>Global stratospheric sulphur burden</b>	
High-resolution Infrared Radiation Sounder (HIRS)	<p>1.1 Derived from HIRS measurements onboard NOAA-10, -11, -12 satellites</p> <p>1.2 Aqueous sulphuric acid aerosol retrieval using <math>8.2\mu\text{m}</math> and <math>12.5\mu\text{m}</math> HIRS water vapour channels (Baran et al., 1993).</p> <p>1.3 Derived sulphur burden based on assumed aerosol composition of 75% weight aqueous sulphuric acid solution droplets.</p> <p>1.4 Global sulphur burden dataset is digitized from Figure 3 of Baran and Foot (1994)</p>
<b>Stratospheric AOD (<math>\text{sAOD}_{550}</math>) and extinction (<math>\text{ext}_{550}</math>) at 550 nm</b>	
The CMIP6-GloSSAC forcing dataset <a href="https://eosweb.larc.nasa.gov/project/glossac/glossac">https://eosweb.larc.nasa.gov/project/glossac/glossac</a>	<p>2.1 Pinatubo aerosol cloud primarily from SAGE-II, HALOE and CLAES observations (Thomason et al., 2018).</p> <p>2.2 Improved Pinatubo gap-fill in mid-latitudes from combining SAGE-II with CLAES</p> <p>2.3 Tropical Pinatubo gap-fill from combining SAGE-II with Mauna Loa lidar (SPARC, 2006).</p> <p>2.4 El Chichon aerosol cloud mostly derived from high-latitude SAM-II data (<math>64^{\circ}\text{N}</math>-<math>82^{\circ}\text{N}</math> and <math>64^{\circ}\text{S}</math>-<math>84^{\circ}\text{S}</math>)</p> <p>2.5 Tropical and mid-latitude El Chichon cloud from combining SAM-II with lidar data from 5 aircraft surveys (<math>13^{\circ}\text{N}</math> to <math>80^{\circ}\text{N}</math>) and from Hampton, Virginia (<math>37^{\circ}\text{N}</math>).</p>
The CMIP6-AER2D forcing dataset ( <a href="ftp://iacftp.ethz.ch/pub/read/luo/CMIP6/">ftp://iacftp.ethz.ch/pub/read/luo/CMIP6/</a> )	<p>3.1 From 2D interactive stratospheric aerosol simulations (Arleuille et al., 2014).</p> <p>3.2 Primarily from the 8 major eruption clouds in 1850-1979 (29 in 1600-present dataset).</p> <p>3.3 Additional minor eruption clouds from Stothers (1996) are also included.</p>
The CMIP5-Sato forcing dataset ( <a href="https://data.giss.nasa.gov/modelforce/strataer/">https://data.giss.nasa.gov/modelforce/strataer/</a> )	<p>4.1 NASA GISS observation-based forcing data for 1850-2012 (<math>\text{sAOD}_{550}</math> only).</p> <p>4.2 Satellite era, uses SAGE-I, SAM-II, SAGE-II and OSIRIS measurements.</p> <p>4.3 Pre-satellite era uses syntheses of different measurements</p> <p>4.4 Surface radiation measurement dataset for Agung (Dyer and Hicks, 1968) highly uncertain in the tropics (Stothers, 2001).</p>
The CMIP5-Ammann dataset ( <a href="ftp://ftp.nodc.noaa.gov/pub/data/paleo/climate_forcing/volcanic_aerosols/ammann2003b_volcanics.txt">ftp://ftp.nodc.noaa.gov/pub/data/paleo/climate_forcing/volcanic_aerosols/ammann2003b_volcanics.txt</a> )	<p>5.1 Simple model-based dataset for 13 eruption clouds 1880-2000 (<math>\text{sAOD}_{550}</math> only).</p> <p>5.2 Based on parameterisation for meridional dispersion from tropical reservoir to mid-latitudes, determined by Brewer-Dobson circulation seasonal cycle.</p> <p>5.3 12-month e-folding timescale for decay of tropical volcanic aerosol reservoir</p> <p>5.4 Peak <math>\text{sAOD}_{550}</math> for each eruption scaled to match aerosol loading from Stothers (1996); Hofmann and Rosen (1983b); Stenchikov et al. (1998), assuming <math>\text{Reff} = 0.42\mu\text{m}</math>.</p>
The post-Agung Lexington lidar dataset from Grams (1966) (see Supplementary Information)	<p>6.1 694nm backscatter ratio profiles from Lexington, Massachusetts (<math>42^{\circ}\text{N}</math>, <math>71^{\circ}\text{W}</math> Fiocco and Grams, 1964; Grams and Fiocco, 1967) (<math>\text{ext}_{550}</math> only)</p> <p>6.2 1-km dataset for 66 lidar soundings (Jan 1964 to July 1965) in Table A1 of Grams (1966).</p> <p>6.3 Backscatter ratio timeseries at 15km, 20km and 24km tabulated into ASCII file.</p> <p>6.4 Conversion to <math>\text{ext}_{550}</math> using extinction-to-backscatter ratio from Jäger and Deshler (2003).</p>
<b>Vertical profile evolution of Effective Radius (Reff) and Surface Area Density (SAD)</b>	
CMIP6-GloSSAC (Pinatubo and El Chichon) and CMIP6-AER2D (Agung)	<p>7.1 SAD for Pinatubo and El Chichon aerosol clouds from GloSSAC, using SAGE-II 3-<math>\lambda</math> method</p> <p>7.2 SAD for Agung aerosol cloud from 2D interactive stratospheric aerosol model simulations</p> <p>7.3 Volume concentration for each cloud derived from same method</p> <p>7.4 Effective radius from 3 times ratio of volume concentration to SAD</p>
<b>Vertical profile of tropical stratospheric temperature anomaly</b>	
From ECMWF reanalysis data	<p>8.1 Temperature anomaly based on difference from 5-year mean starting in year of eruption</p> <p>8.2 T-anomalies for Pinatubo and El Chichon from the ERA-interim re-analysis (Dee et al., 2011)</p> <p>8.3 For the Agung period, anomaly derived from the ERA-40 year dataset (Uppala et al., 2006)</p>

### Minor comments: Careful rewording

- a) Supplementary: the reference is missing at line 4. In general, I suggest a more careful check of the grammar of the manuscript: some phrases seem to be written in haste, and it could make for a much more enjoyable read if the style was a bit easier to understand. I offer some examples below:
- b) Lines 277-280: this phrase needs a bit of rewording, it's confusing.
- c) This again confirms that the more SO<sub>2</sub> injection leads to the faster particle growth, hence quicker removal within first few months after the eruption.
- d) Line 288: "the" lower end.
- e) Line 341: I think here you might be referring to the other Pitari et al. (2016) paper (Stratospheric Aerosols from Major Volcanic Eruptions: A Composition-Climate Model Study of the Aerosol Cloud Dispersal and e-folding Time) that discusses the effects of the QBO phase on the cloud dispersal.

--> *We agree with the reviewer. Some of the sentences were confusing and had some grammatical errors. We apologise for this. We have had a careful read and worked on the flow of the manuscript. The reference has been corrected.*

Lines 343-345: While true that both cited papers mention the low altitude of the aerosols formed after the Hudson eruption, both remark that indeed the effect of that eruption was clearly distinguishable from the one from Pinatubo. From the conclusions of Pitts and Thomason (1993): "Below 15 km, Cerro Hudson aerosols were transported poleward during September and remained a persistent feature beneath the vortex throughout the spring" I understand that the experiments shown in this paper are part of ISA-MIP and thus part of a strict protocol, but I would just not be so quick in dismissing the Hudson eruption, especially in explaining the differences shown in Fig. 2 against the CMIP6 database, that are much larger in the southern hemisphere (where the Hudson eruption had more effect). I would like to see this discussed a little bit more in the manuscript (and, as a curiosity, see how the results change if this eruption is included, but I'm not suggesting to the authors do that for this work).

--> *We agree with the reviewer that we cannot dismiss the influence of Mt. Hudson eruption, and our wording was somewhat dismissive, hence we have reworded the sentence. As GloSSAC V2 data became available, we have updated Figure 2 and, as reviewer pointed out, differences are indeed significant. Hence, we expanded discussion about Mt. Hudson eruption.*

Line 371: "the more SO<sub>2</sub> is injected"? and then, "within the first few months"

--> *We reworded it as:*

*“This again confirms that the more SO<sub>2</sub> injection leads to the faster particle growth, hence quicker removal within the first few months after the eruption.”*

Line 375: the first three months

--> Done.

**Additional comments added after the original upload of the above reply to reviewers**

*Shortly after uploading our replies to the reviewers (including AC1 above), and when finalising the revised manuscript, we discovered two subtle but important mistakes in the Python code used to generate the figures in the ACP-Discussions manuscript:*

- 1) *Figure 4: Typo in the code used to calculate effective radius: assigned the accumulation-soluble mode H<sub>2</sub>SO<sub>4</sub> mmr to accumulation-insoluble H<sub>2</sub>SO<sub>4</sub> mmr.*

*A subtle typo in the code used to calculate effective radius caused an error in the initial assignment of modal H<sub>2</sub>SO<sub>4</sub> component mass mixing ratios. The typo caused the calculation of total particle volume (PVOL) to double-count the accumulation-soluble mode H<sub>2</sub>SO<sub>4</sub> mass mixing ratios (mmr), the accumulation-insoluble H<sub>2</sub>SO<sub>4</sub> mode mmr not used in the calculations as a consequence. Specifically, the excerpt of code:*

```
H2SO4_nucsol_mmr=nc_fid.variables['NUCLEATION_MODE__SOLUBLE__H2SO4_MM'R'][:]  
H2SO4_Aitsol_mmr=nc_fid.variables['AITKEN_MODE__SOLUBLE__H2SO4_MM'R'][:]  
H2SO4_accsol_mmr=nc_fid.variables['ACCUMULATION_MODE__SOL__H2SO4_MM'R'][:]  
H2SO4_corsol_mmr=nc_fid.variables['COARSE_MODE__SOLUBLE__H2SO4_MM'R'][:]  
H2SO4_accins_mmr=nc_fid.variables['ACCUMULATION_MODE__SOL__H2SO4_MM'R'][:]
```

*should have been:*

```
H2SO4_nucsol_mmr=nc_fid.variables['NUCLEATION_MODE__SOLUBLE__H2SO4_MM'R'][:]  
H2SO4_Aitsol_mmr=nc_fid.variables['AITKEN_MODE__SOLUBLE__H2SO4_MM'R'][:]  
H2SO4_accsol_mmr=nc_fid.variables['ACCUMULATION_MODE__SOL__H2SO4_MM'R'][:]  
H2SO4_corsol_mmr=nc_fid.variables['COARSE_MODE__SOLUBLE__H2SO4_MM'R'][:]  
H2SO4_accins_mmr=nc_fid.variables['ACCUMULATION_MODE__INS__H2SO4_MM'R'][:]
```

*For the major volcanic aerosol cloud simulations analysed here, the majority of sulphuric acid mass is in that double-counted accumulation-soluble mode.*

*Hence the typo caused the particle volume PVOL, used in the calculation of the model’s effective radius (=3\*PVOL/SAREA) to be much higher.*

*This affected the effective radius values shown in Figures 4 a), b), d), e) in the ACPD article to be much higher than their true values.*

2) Figures 2d), 8d), 11d): Error in sAOD calculated for CMIP6 dataset (depth error).

*The stratospheric AOD values shown for the CMIP6 representations of the Pinatubo, El Chichon and Agung aerosol in Figures 2d, 8d, 11d of the ACPD article are factor 2 too high, due to an error in the depth used in the calculations.*

*The depth error arises within our code to integrate to sAOD the altitude-resolved aerosol extinction dataset provided with the CMIP6 volcanic aerosol dataset. When calculating the sum over vertical levels, the depth assigned when integrating the aerosol extinction to stratospheric Aerosol Optical Depth (sAOD) was set at 1.0 km rather than 0.5 km, calculated sAOD was then a factor of 2 too high.*

*We apologise for both bugs. Whereas the error 1) was more subtle, and the  $R_{eff}$  from the model being too high was not obvious, we should have realised that the CMIP6 sAOD values shown in those figures were a factor-2 too high. Even though there is no documentation paper for the pre-satellite part of the CMIP6 dataset (CMIP6-AER2D) sAOD, we should still have realised this error when preparing the manuscript. We are relieved to have found this error during the review process and in the revised manuscript, the Figures 2d, 8d and 11d show the correct  $sAOD_{525}$  values.*

*The typo explained in 1) is now remedied, and the simulated  $R_{eff}$  values shown in Figures 4c) to f) of the revised manuscript represent the model predictions correctly.*

*We also added the two extra panels requested by Reviewer 2 to additionally show the 20Tg simulation  $R_{eff}$  field at 25km (Figure 4a) and 20km (Figure 4b).*

*Note that the  $R_{eff}$  figure in the Supplementary Material (Figure S6) has also been updated since the ACPD article to show the correct values. There only the 10Tg and 20Tg runs are shown to match the runs used in Dhomse et al. (2014), enabling comparison with the corresponding figure in that paper.*

*With these changes to the simulated  $R_{eff}$  values in Figure 4 and Figure S6, the Section 4.1 text analysing the  $R_{eff}$  variations (lines 389-419 in the ACPD article) has been re-written to:*

*"Next, we evaluate the meridional, vertical and temporal variations in effective radius ( $R_{eff}$ ) in the Pinatubo UM-UKCA datasets. The particle size variations in these interactive simulations of the Pinatubo cloud reflect the chemical and microphysical processes resolved by the chemistry-aerosol module, in association with the stratospheric circulation and dynamics occurring in the general circulation model. We analyse these model-predicted size variations also alongside those in the benchmark observation-based  $R_{eff}$  dataset from CMIP6-GloSSAC, which applies the 3-lamda size retrieval from*

the 453nm, 525nm and 1020nm aerosol extinction measurements from SAGE-II (Thomason et al., 1997a, 2018).

Figure 4 shows zonal mean  $Reff$  at 25km, within the altitude range of the volcanic  $SO_2$  injection, and at 20km, underneath the main volcanic cloud, results shown from 3-member means from the 10, 14 and 20Tg  $SO_2$  emission runs (Pin10, Pin14 and Pin20). For comparability with the equivalent Figure from Dhomse et al. (2014), we also show in the Supplementary Material (Figure S6) the updated comparison to the Bauman et al. (2003)  $Reff$  dataset, for the corresponding Pin10 and Pin20 runs. Overall, the model captures the general spatio-temporal progression in the  $Reff$  variations seen in the GloSSAC dataset. However, whereas the 10Tg and 14Tg simulations agree best with the HIRS-2 sulphur-burden (Figure 1) and the GloSSAC sAOD and extinction (Figures 2 and 3), the magnitude of the  $Reff$  enhancement is best captured in the 20Tg run (Pin20). The comparisons suggest the low bias in simulated  $Reff$  seen in the previous UM-UKCA Pinatubo study (Dhomse et al., 2014) continues to be the case here. However, this low-bias in particle size/growth may simply be reflecting the required downward-adjustment of the Pinatubo  $SO_2$  emission, a larger  $Reff$  enhancement in the 20Tg simulation clearly apparent. It is possible that the two-moment modal aerosol dynamics in GLOMAP-mode may affect its predicted  $Reff$  enhancement. However, the model requirement for reduced  $SO_2$  emission is attributed to likely be due to a missing, or poorly resolved, model loss pathway, such as accommodation onto co-emitted volcanic ash. The sustained presence of ash within the Pinatubo cloud (e.g. Winker and Osborne, 1992) will likely have altered particle size and growth rates in the initial months after the eruption.

In the tropics, where  $Reff$  increases are largest, the timeseries of  $Reff$  is noticeably different in the core of the tropical reservoir ( $10^{\circ}S$  to  $10^{\circ}N$ ) to that in the edge regions ( $10^{\circ}N$ - $20^{\circ}N$  and  $10^{\circ}S$ - $20^{\circ}S$ ), at both 20km and 25km. The  $Reff$  increases in these edge regions occur when tropics to mid-latitude transport is strongest, in phase with the seasonal cycle of the Brewer-Dobson circulation, which tends to transport air towards the winter pole (Butchart, 2014). The  $Reff$  increases are due primarily to particle growth from coagulation and condensation, and the simulations also illustrate how the simulated Pinatubo cloud comprises much smaller particles at 25km than at 20km. The 25km level is in the central part of the Pinatubo cloud, particles there being younger (and smaller), because the oxidation of emitted volcanic  $SO_2$  that occurs at that level, triggers extensive new particle formation in the initial months after the eruption (e.g. Dhomse et al., 2014). By contrast, at the 20km level, particles there will almost exclusively have sedimented from the main cloud, and therefore be larger. There is a slow but sustained increase in average particle size in the equatorial core of the tropical Pinatubo cloud, with the 20km level reaching peak  $Reff$  values only during mid-1992, in contrast to the peak S-burden and  $sAOD_{550}$ , which have already peaked at this time, being in decay phase since the start of 1992 (see Figures 1 and 2).

Whereas the simulated peak  $Reff$  enhancement occurs by mid-1992 in the tropics, the peak  $Reff$  in NH mid-latitudes occurs at the time of

peak meridional transport, the  $Reff$  variation there reflecting the seasonal cycle of the Brewer-Dobson circulation, as also seen in the tropical reservoir edge region. The different timing of the volcanic  $Reff$  enhancement in the tropics and mid-latitudes is important when interpreting or interpolating the in-situ measurement record from the post-Pinatubo OPC soundings from Laramie (Deshler et al., 2003). Russell et al. (1996) show the  $Reff$  values derived from Mauna Loa ground-based remote sensing are substantially larger than those from the dust-sonde measurements at Laramie. The interactive Pinatubo simulation here confirm this expected meridional gradient in effective radius, with the chemical, dynamical and microphysical processes also causing a vertical gradient in the tropical to mid-latitude  $Reff$  ratio. The current ISA-MIP activity (Timmreck et al., 2018) brings a potential opportunity to identify a consensus among interactive stratospheric aerosol models for the expected broad-scale spatio-temporal variations in uncertain volcanic aerosol metrics such as effective radius."

*With the 1km-depth error in the integration of the CMIP6 aerosol extinction, and the subsequent correction to the sAOD shown for CMIP6-GloSSAC/CMIP6-AER2D in Figures 2d, 8d and 11d, there have also been some minor changes to interpret the evaluation of the UM-UKCA volcanic simulations. The revisions here are only minor changes in emphasis re: the comparisons to GloSSAC sAOD, and since the text is mainly analysing the sAOD variation, these changes are only minor.*

*The text changes for this CMIP6 sAOD correction are the lines 371-415, 562-583 and 623-631 of the revised (lines 446-491, 672-694 and 735-755 in a tracked change version) manuscript, corresponding to lines 316-357, 484-504 and 542-563 of the ACP Discussions article*

## **## Replies are in blue colour and italics**

Review of “Evaluating the simulated radiative forcings, aerosol properties and stratospheric warmings from the 1963 Agung, 1982 El Chichón and 1991 Mt Pinatubo volcanic aerosol clouds” by Sandip S. Dhomse et al.

### **Anonymous Reviewer #2**

This manuscript evaluates UM-UKCA simulations of the Agung, El Chichon, and Mt. Pinatubo eruptions and presents conclusions on the SO<sub>2</sub> injection amount that provides the best comparison with observations. Overall, I think this is an interesting and well written manuscript. The evaluation is detailed and well presented, the graphs are mostly clear, and the discussion is well structured and relevant. The introduction is informative and gives a good overview of modeling and observational constraints. I would see this manuscript more fitting to GMD, rather than ACP, but in any case I think this manuscript is publishable after minor changes.

### **Comments**

Line 60: it is correct that the stratospheric aerosol load was enhanced in both hemispheres, but one also needs to account for the Cerro Hudson eruption that increased the aerosols in the southern hemisphere shortly after the Pinatubo eruption. There is a comment about this later in the manuscript, but I think it would be useful to mention this here, too.

--> *We prefer to keep this paragraph as an overview of the main differences between the 3 eruption clouds. As also suggested by Reviewer #1, we modified the discussion to mention that the Cerro Hudson aerosol cloud may have contributed to the model - GloSSAC sAOD differences in the Southern Hemisphere. However, as we explain in the manuscript, SAGE-II measurements (Pitts and Thomason, 1993) and lidar measurements from Aspendale, Australia (Barton et al., 1992) clearly show that the Hudson aerosol was only a minor contributor to the total optical depth over the two volcanic aerosol clouds. We have instead modified the text to say:*

“One thing to note is that our simulations do not include the source of volcanic aerosol from the August 1991 Cerro Hudson eruption in Chile. However, measurements from SAGE II \citet{Pitts1993} and ground-based lidar \citet{Barton1992} indicate that the Hudson aerosol cloud only reached to around 12 km, with the Pinatubo cloud by far the dominant contributor to SH mid-latitude sAOD. So, although we have not included the Mt. Hudson aerosol in our simulations, we argue this was only a minor contributor to the differences between model and GloSSAC V2 sAOD, and does not explain why 20Tg SO<sub>2</sub> injection (\pind) shows best agreement in the SH.”

Line 160: 10 years of spin-up might not be enough for some slow adjusting variables such as age of air. Did the authors check that the stratosphere was indeed at equilibrium?

*Yes, we analysed age of air and long-lived tracers in each 20-year timeslice run to check that the model was fully spun up. In the revised manuscript we added a sentence to explain the exact procedure we followed, that paragraph now reading:*

*"For each 20-year time-slice run, we analysed the stratospheric sulphur burden, ozone layer and the distributions of age of air and selected long-lived tracers, to check that the model had fully adjusted to the GHG and ODS setting. We then analysed timeseries of the tropical zonal wind profile, to then identify three different model years that gave QBO transition approximately matching that seen in the ERA-interim re-analysis \citep{Dee2011}, the initialisation fields for those years then used to re-start the three ensemble member transient runs. We show the QBO evolution for each Pinatubo simulation in the Supplementary Material (Figure S1)."*

Line 163: Three ensemble members is not many. Jones et al (2016, doi:10.1002/2016JD025001) showed that the dispersal is highly sensitive to the initial conditions. It would be useful to add, at least in the supplementary material, results from each of the ensemble members, to understand how the latitudinal dispersal varies within an ensemble.

*--> We thank the reviewer for pointing this out. We agree that some readers might be interested in this comparison. We note that the SO<sub>2</sub> injection altitude in Jones et al., (2016) is closer to the tropopause than in our simulations, which we think may explain why they observe such large differences in sAOD evolution. We also note that the interactive stratospheric aerosol simulations in Jones et al. (2016) used a simpler (single-moment) aerosol scheme, so sulphate aerosol particles form immediately at the assumed size as the SO<sub>2</sub> oxidises. By contrast, in our aerosol microphysics module, the particles grow from initial nanometre sizes according to the timescales of the microphysical processes (coagulation and condensation). That particles form immediately at radiation-interacting sizes might also have contributed to the larger variation between ensemble members in Jones et al. (2016). We have added to the Supplementary Material an extra figure showing the sAOD evolution for each ensemble member.*

Line 163: The different injections all have the same altitude, but the injection altitude is also a degree of freedom. The chosen injection altitudes are all above the tropopause, but a larger injection with a lower boundary in the UTLS could deliver similar results. I understand that the setup of this experiment was dictated by SSiRC, but it would be interesting to comment on the importance of the vertical distribution of the injection.

--> *We agree that interactive stratospheric aerosol simulations of volcanic aerosol clouds are sensitive to the assumed injection height, and this is part of the rationale for the HErSEA experiments within ISA-MIP. This sensitivity to injection height is discussed extensively in Timmreck et al., (2018) and Marshall et al., (2018) (<https://doi.org/10.1029/2018JD028675>).*

*The reviewers is incorrect in stating that setup of the experiment was dictated by SSiRC, the rationale for the experiment is explained clearly in the HErSEA section of the Timmreck et al. (2018) paper. The HErSEA design involves three alternative injection height simulations, which we have carried with UM-UKCA, but here we only show one of the three injection height “eruption realisations” included in the HErSEA design.*

Line 165: Not sure what you mean with “for simplicity”. For simplicity of set up or for simplicity of analyzing the results, as it reduces the degrees of freedom?

--> *Good point. Indeed simplicity was referring to terms of model setup as well as our attempt to avoid any complicated ozone chemistry feedback mechanism. However, to avoid the confusion we have deleted “For simplicity” as our approach is focussed on the aerosol evolution.*

Line 225: It is not really correct that satellite measurements constrain particle size. Some satellite instrument provide the Angstrom coefficient, which is a proxy (not a measurement) for size. The Angstrom coefficient depends on the size of the particle but also on the composition of the particle and hydration.

--> *Whilst we agree that in-situ measurements are the primary ground-truth for evaluating stratospheric aerosol particle size distribution, the multi-wavelength algorithm for particle surface area density and particle volume concentration used in the GloSSAC-derived effective radius (Thomason et al., 1997), including the improvement to now incorporate HALOE data (Thomason, 2012), does provide additional constraints for the global variation in particle size. This is different to the Angstrom coefficient, which is based on only 2 wavelengths.*

*We have re-worded that paragraph slightly to instead read:*

“In the Pinatubo case, satellite measurements are able to provide additional constraints for the particle size evolution, with particle effective radius derived from the volume concentration and surface area density SAGE-II extinction at multiple wavelengths (Thomason et al., 1997; SPARC ASAP report, 2006). Hence for Pinatubo, we also compare model-simulated effective radius to that provided with the GloSSAC dataset, which underpins each climate model’s specified multi-wavelength aerosol optical properties in the Pinatubo forcings in CMIP6 historical integrations.”

Line 250: Mann et al (2019b) and (2020) are conference abstracts. Does ACP allow them as references?

-->*Yes, we followed ACP manuscript preparation guidelines for authors ([https://www.atmospheric-chemistry-and-physics.net/for\\_authors/manuscript\\_preparation.html](https://www.atmospheric-chemistry-and-physics.net/for_authors/manuscript_preparation.html)).*

Line 277: Larger injections produce a stronger upwelling (which push toward a longer S lifetime) and larger particle radii (which push toward shorter e-folding time). Do your result imply that the net effect is driven by the particle size, rather than the changes in upwelling?

-->*We agree with the reviewer that both effects are important, but although the result confirms the residence time occurs at the time of maximum effective radius, since the stronger upwelling is also linked to particle size changes, we do not feel the results support such a conclusive statement as the reviewer suggests.*

Line 295: Is there a published paper or report that documents the changes brought up by increasing the resolution? Maybe something was published when the model with higher resolution was released?

-->*Good point. The UK Met Office publishes documentation papers in GMD describing each successive Global Atmosphere configuration, with comparisons of climatologies of a range of different metrics and, for example, Walters et al. (2014) compare GA4, the physical model used in this study to the previous GA3 version.*

Line 306: How is stratospheric AOD calculated? Is aerosol extinction integrated above the tropopause or above a fixed altitude?

-->*Yes, aerosol extinctions are integrated for all the levels above the tropopause.*

Line 310: I'm confused by this. Are the authors referring to Fig.1, when they write that Pin20 best matches the satellite observed SO<sub>2</sub> estimates? Pin20 is the one that compare the worst with HIRS.

-->*The sentence is referring to the 14-23 Tg range from Guo et al. (2004), we do not compare to SO<sub>2</sub>, but the emission amount of 20 Tg is in the upper-mid-range from the TOMS/TOVS satellite measurements. We are aware that Pin20 compares worst with HIRS derived SO<sub>4</sub> burden, and this point is discussed clearly in the text.*

Line 313: I am not sure it is fair to say that Pin10 has the best agreement. All of them, including Pin10, overestimate the peak sAOD in the tropics. 18 months after the eruption Pin20 seems actually to do better. A similar statement requires a metric such as the globally averaged root mean square error. I generally find the qualitative comparison a weak point of this manuscript. It is very difficult to judge which simulation is performing best just by looking at the figures.

--> As the reviewer notes the 10, 14 and 20 Tg simulations all overestimate the peak sAOD in the tropics, but Pin10 clearly has a lower high bias than the other scenarios, and that sense Pin10 has best agreement. We note in the text that the Pin20 run compares best in the Southern Hemisphere.

Line 344: Cerro Hudson is at 45S, 12 km could be above the tropopause.

--> Whilst we agree that the Hudson volcanic aerosol cloud reached the lowermost stratosphere, we just try to reiterate the point we make on line 344 that the measurements in the cited papers (e.g. Fig 1 of Pitts and Thomason, 1992) which demonstrate that Pinatubo was by far the dominant contributor to the stratospheric AOD, even when the Hudson cloud was at its maximum optical depth.

Line 390: I think Pin20 should be included in Fig. 4. Even if high biased, it is interesting to see how the effective radius scales with injection burden.

--> *Done*

Line 392: I am confused by this sentence. Pin20 is not shown, and between Pin14 and Pin10 I don't see any clear difference. There is a need of some kind of metric, such as mean error. Judging from the current plot, both simulations seems to perform pretty poorly when compared to the CMIP6 dataset (if that is a valuable benchmark).

--> *We could have calculated a mean bias from the CMIP6 effective radius, but there is a sufficient variation among different effective radius datasets, with a substantial uncertainty, and for this reason we prefer not to calculate and evaluate metrics to just one dataset.*

Line 405: I am not sure where to look to see this. Please specify latitude and months of the part of the plot that you are commenting on.

--> As suggested by the reviewer, we now have additional panel for Pin20 in Figure 4, so

"At 25km, the model simulations are somewhat counter-intuitive. Initially, they show decrease in Reff, likely due to this central part of the volcanic cloud being younger (and smaller) particles formed as the oxidation of the volcanic SO2 triggers extensive new particle formation,"

is revised to instead read:

"The Reff increase is due to particle growth from coagulation and condensation, and the simulations illustrate much slower temporal increase in size at 25km than at 20km. The 25km level is in the central part of the volcanic cloud, particles there being younger (and smaller) as the oxidation of the volcanic SO2 continues to trigger extensive new particle formation. By contrast, at the 20km

level, particles there will almost exclusively have sedimented from the main cloud, and therefore at larger particle sizes. This explains why at 20km, below the altitude at which the volcanic plume detrains the SO<sub>2</sub> (injection height range is 21-23 km) the effective radius shows a steady increase, as relatively larger particles sediment to these altitudes as the tropical volcanic aerosol reservoir progresses."

Line 598: Figure 13, not 12, right? Also, take out either "as" or "hence"

--> *Thanks for spotting this, we removed "hence".*

Figure 1: I think "blue line" should be "solid lines", otherwise I do not understand which lines I am supposed to look at.-

--> *This was an error in the caption, corrected to "Pin00 (aqua), Pin10 (blue), Pin14 (green), Pin20 (red)". Apologies for the confusion.*

Figure 2: I find this kind of graph (Fig 2, 5, 8, 7, etc) difficult to interpret. Next to the AOD, there should also be a panel with the absolute or relative difference between simulations and datasets. You could build a 3x3 table of graphs showing the difference between each of the three ensembles and each of the 3 datasets.

--> *Although it would be possible to construct the difference plot suggested, partly because of the differences between the observational datasets, and partly because it enables visual inspection of the patterns of variation in each dataset, we prefer to show side-by-side comparisons of the predicted metric rather than bias plots.*

Figure 3: just to be clear, the variability among ensemble members is the ensemble spread, right? Min to max values per each month.

--> *Yes. We consider the term "variability among ensemble members" more scientifically descriptive.*

Fig. 10: seeing the colors in panel d) is difficult, as lines become dense right where the warming happens. It would be better to make the lines light grey or change the color table to something with more diversity. Also, why not include the mean QBO also in the simulation graphs? Does the QBO change between the experiments with and without eruptions?

--> *We reduced the contour interval lines to 5 m/s, reduced line thickness and plotted contour lines with thicker black line to enhance the clarity.*

### **Minor comments and typos.**

--> *Revised manuscript has been modified to add all the minor and technical corrections.*

**Additional comments added after the original upload of the above reply to reviewers**

*Shortly after uploading our replies to the reviewers (including AC2 above), and when finalising the revised manuscript, we discovered two subtle but important mistakes in the Python code used to generate the figures in the ACP-Discussions manuscript:*

- 1) *Figure 4: Typo in the code used to calculate effective radius: assigned the accumulation-soluble mode H<sub>2</sub>SO<sub>4</sub> mmr to accumulation-insoluble H<sub>2</sub>SO<sub>4</sub> mmr*

*A subtle typo in the code used to calculate effective radius caused an error in the initial assignment of modal H<sub>2</sub>SO<sub>4</sub> component mass mixing ratios. The typo caused the calculation of total particle volume (PVOL) to double-count the accumulation-soluble mode H<sub>2</sub>SO<sub>4</sub> mass mixing ratios (mmr), the accumulation-insoluble H<sub>2</sub>SO<sub>4</sub> mode mmr not used in the calculations as a consequence. Specifically, the excerpt of code:*

```
H2SO4_nucsol_mmr=nc_fid.variables['NUCLEATION_MODE__SOLUBLE__H2SO4_MM'R'][:]
H2SO4_Aitsol_mmr=nc_fid.variables['AITKEN_MODE__SOLUBLE__H2SO4_MM'R'][:]
H2SO4_accsol_mmr=nc_fid.variables['ACCUMULATION_MODE__SOL__H2SO4_MM'R'][:]
H2SO4_corsol_mmr=nc_fid.variables['COARSE_MODE__SOLUBLE__H2SO4_MM'R'][:]
H2SO4_accins_mmr=nc_fid.variables['ACCUMULATION_MODE__SOL__H2SO4_MM'R'][:]
```

*should have been*

```
H2SO4_nucsol_mmr=nc_fid.variables['NUCLEATION_MODE__SOLUBLE__H2SO4_MM'R'][:]
H2SO4_Aitsol_mmr=nc_fid.variables['AITKEN_MODE__SOLUBLE__H2SO4_MM'R'][:]
H2SO4_accsol_mmr=nc_fid.variables['ACCUMULATION_MODE__SOL__H2SO4_MM'R'][:]
H2SO4_corsol_mmr=nc_fid.variables['COARSE_MODE__SOLUBLE__H2SO4_MM'R'][:]
H2SO4_accins_mmr=nc_fid.variables['ACCUMULATION_MODE__INS__H2SO4_MM'R'][:]
```

*For the major volcanic aerosol cloud simulations analysed here, the majority of sulphuric acid mass is in that double-counted accumulation-soluble mode.*

*Hence the typo caused the particle volume PVOL, used in the calculation of the model's effective radius (=3\*PVOL/SAREA) to be much higher.*

*This caused the effective radius values shown in Figures 4 a), b), d), e) in the ACPD article to be much higher than their true values.*

- 2) *Figures 2d), 8d), 11d): Error in sAOD calculated for CMIP6 dataset (depth error).*

*The stratospheric AOD values shown for the CMIP6 representations of the Pinatubo, El Chichon and Agung aerosol in Figures 2d, 8d, 11d of the ACPD article are factor 2 too high, due to an error in the depth used in the calculations.*

*The depth error arises within our code to integrate to sAOD the altitude-resolved aerosol extinction dataset provided with the CMIP6 volcanic aerosol dataset.*

*When calculating the sum over vertical levels, the depth assigned when integrating the aerosol extinction to stratospheric Aerosol Optical Depth (sAOD) was set at 1.0km rather than 0.5km, calculated sAOD then a factor of 2 too high.*

*We apologise for both bugs. Whereas the error 1) was more subtle, and the  $Reff$  from the model being too high was not obvious, we should have realised that the CMIP6 sAOD values shown in those figures were a factor-2 too high. Even though there is no documentation paper for the pre-satellite part of the CMIP6 dataset (CMIP6-AER2D) sAOD, we should still have realised this error when preparing the manuscript. We are relieved to have found this error during the review process and in the revised manuscript, the Figures 2d, 8d and 11d show the correct  $sAOD_{525}$  values.*

*The typo explained in 1) is now remedied, and the simulated  $Reff$  values shown in Figures 4c) to f) of the revised manuscript represent the model predictions correctly.*

*We also added the two extra panels requested by Reviewer 2 to additionally show the 20Tg simulation  $Reff$  field at 25km (Figure 4a) and 20km (Figure 4b).*

*Note that the  $Reff$  Figure in the Supplementary Material (Figure S6) has also been updated from the ACPD article to show the correct values. There only the 10Tg and 20Tg runs are shown to match the runs used in Dhomse et al. (ACP, 2014), enabling comparison with the corresponding figure in that paper.*

*With these changes to the simulated  $Reff$  values in Figure 4 and Figure S6, the Section 4.1 text analysing the  $Reff$  variations (lines 389-419 in the ACPD article) has been re-written to:*

“Next, we evaluate the meridional, vertical and temporal variations in effective radius ( $Reff$ ) in the Pinatubo UM-UKCA datasets. The particle size variations in these interactive simulations of the Pinatubo cloud reflect the chemical and microphysical processes resolved by the chemistry-aerosol module, in association with the stratospheric circulation and dynamics occurring in the general circulation model. We analyse these model-predicted size variations also alongside those in the benchmark observation-based  $Reff$  dataset from CMIP6-GloSSAC, which applies the 3- $\square$  size retrieval from the 453nm, 525nm and 1020nm aerosol extinction measurements from SAGE-II (Thomason et al., 1997a, 2018).

Figure 4 shows zonal mean  $Reff$  at 25km, within the altitude range of the volcanic  $SO_2$  injection, and at 20km, underneath the main volcanic cloud, results shown from 3-member means from the 10, 14 and 20Tg  $SO_2$  emission runs (Pin10, Pin14 and Pin20). For comparability with the equivalent Figure from Dhomse et al. (2014), we also show in the Supplementary Material (Figure S6) the updated comparison to the Bauman et al. (2003)  $Reff$  dataset, for the corresponding Pin10 and Pin20 runs. Overall, the model captures the general spatio-temporal progression in the  $Reff$  variations seen in

the GloSSAC dataset. However, whereas the 10Tg and 14Tg simulations agree best with the HIRS-2 sulphur-burden (Figure 1) and the GloSSAC sAOD and extinction (Figures 2 and 3), the magnitude of the  $Reff$  enhancement is best captured in the 20Tg run (Pin20). The comparisons suggest the low bias in simulated  $Reff$  seen in the previous UM-UKCA Pinatubo study (Dhomse et al., 2014) continues to be the case here. However, this low-bias in particle size/growth may simply be reflecting the required downward-adjustment of the Pinatubo  $SO_2$  emission, a larger  $Reff$  enhancement in the 20Tg simulation clearly apparent. It is possible that the two-moment modal aerosol dynamics in GLOMAP-mode may affect its predicted  $Reff$  enhancement. However, the model requirement for reduced  $SO_2$  emission is attributed to likely be due to a missing, or poorly resolved, model loss pathway, such as accommodation onto co-emitted volcanic ash. The sustained presence of ash within the Pinatubo cloud (e.g. Winker and Osborne, 1992) will likely have altered particle size and growth rates in the initial months after the eruption.

In the tropics, where  $Reff$  increases are largest, the timeseries of  $Reff$  is noticeably different in the core of the tropical reservoir ( $10^{\circ}S$  to  $10^{\circ}N$ ) to that in the edge regions ( $10^{\circ}N$ - $20^{\circ}N$  and  $10^{\circ}S$ - $20^{\circ}S$ ), at both 20km and 25km. The  $Reff$  increases in these edge regions occur when tropics to mid-latitude transport is strongest, in phase with the seasonal cycle of the Brewer-Dobson circulation, which tends to transport air towards the winter pole (Butchart, 2014). The  $Reff$  increases are due primarily to particle growth from coagulation and condensation, and the simulations also illustrate how the simulated Pinatubo cloud comprises much smaller particles at 25km than at 20km. The 25km level is in the central part of the Pinatubo cloud, particles there being younger (and smaller), because the oxidation of emitted volcanic  $SO_2$  that occurs at that level, triggers extensive new particle formation in the initial months after the eruption (e.g. Dhomse et al., 2014). By contrast, at the 20km level, particles there will almost exclusively have sedimented from the main cloud, and therefore be larger. There is a slow but sustained increase in average particle size in the equatorial core of the tropical Pinatubo cloud, with the 20km level reaching peak  $Reff$  values only during mid-1992, in contrast to the peak S-burden and  $sAOD_{550}$ , which have already peaked at this time, being in decay phase since the start of 1992 (see Figures 1 and 2).

Whereas the simulated peak  $Reff$  enhancement occurs by mid-1992 in the tropics, the peak  $Reff$  in NH mid-latitudes occurs at the time of peak meridional transport, the  $Reff$  variation there reflecting the seasonal cycle of the Brewer-Dobson circulation, as also seen in the tropical reservoir edge region. The different timing of the volcanic  $Reff$  enhancement in the tropics and mid-latitudes is important when interpreting or interpolating the in-situ measurement record from the post-Pinatubo OPC soundings from Laramie (Deshler et al., 2003). Russell et al. (1996) show the  $Reff$  values derived from Mauna Loa ground-based remote sensing are substantially larger than those from the dust-sonde measurements at Laramie. The interactive Pinatubo simulation here confirm this expected meridional gradient in effective radius, with the chemical, dynamical and microphysical processes also causing a vertical gradient in the tropical to mid-

latitude Reff ratio. The current ISA-MIP activity (Timmreck et al., 2018) brings a potential opportunity to identify a consensus among interactive stratospheric aerosol models for the expected broad-scale spatio-temporal variations in uncertain volcanic aerosol metrics such as effective radius.

*With the 1km-depth error in the integration of the CMIP6 aerosol extinction, and the subsequent correction to the sAOD shown for CMIP6-GloSSAC/CMIP6-AER2D in Figures 2d, 8d and 11d, there have also been some minor changes to interpret the evaluation of the UM-UKCA volcanic simulations. The revisions here are only minor changes in emphasis re: the comparisons to GloSSAC sAOD, and since the text is mainly analysing the sAOD variation, these changes are only minor.*

*The text changes for this CMIP6 sAOD correction are the lines 371-415, 562-583 and 623-631 of the revised (lines 446-491, 672-694 and 735-755 in a tracked change version) manuscript, corresponding to lines 316-357, 484-504 and 542-563 of the ACP Discussions article*

# Evaluating the simulated radiative forcings, aerosol properties and stratospheric warmings from the 1963 Mt Agung, 1982 El Chichón and 1991 Mt Pinatubo volcanic aerosol clouds

Sandip S. Dhomse<sup>1,2</sup>, Graham W. Mann<sup>1,3</sup>, Juan Carlos Antuña Marrero<sup>4</sup>, Sarah E. Shallcross<sup>1</sup>, Martyn P. Chipperfield<sup>1,2</sup>, Kenneth S. Carslaw<sup>1</sup>, Lauren Marshall<sup>1,5</sup>, N. Luke Abraham<sup>5,6</sup>, and Colin E. Johnson<sup>3,7</sup>

<sup>1</sup>School of Earth and Environment, University of Leeds, Leeds, UK

<sup>2</sup>National Centre for Earth Observation, University of Leeds, Leeds, UK

<sup>3</sup>National Centre for Atmospheric Science (NCAS-Climate), University of Leeds, UK

<sup>4</sup>Department of Theoretical Physics, Atomic and Optics, University of Valladolid, Valladolid, Spain

<sup>5</sup>Department of Chemistry, University of Cambridge, Cambridge, UK

<sup>6</sup>National Centre for Atmospheric Science, University of Cambridge, UK

<sup>7</sup>Met Office Hadley Centre, Exeter, UK

**Correspondence:** Sandip Dhomse (s.s.dhomse@leeds.ac.uk), Graham Mann (g.w.mann@leeds.ac.uk)

**Abstract.** ~~Accurate quantification of the effects of volcanic eruptions~~ Accurately quantifying volcanic impacts on climate is a key requirement for ~~better robust~~ attribution of anthropogenic climate change. Here we use the UM-UKCA composition-climate model to simulate the global dispersion of the volcanic ~~aerosol~~ aerosol clouds from the three largest eruptions of the 20th century: 1963 Mt Agung, 1982 El Chichón and 1991 Mt Pinatubo. The model has interactive stratospheric chemistry and aerosol microphysics, with coupled aerosol-radiation interactions for realistic composition-dynamics feedbacks. Our simulations align with the design of the Interactive Stratospheric Aerosol Model Intercomparison (ISA-MIP) "Historical Eruption SO<sub>2</sub> Emissions Assessment". For each eruption, we perform 3-member ensemble model experiments ~~with for~~ upper, mid-point and lower estimates ~~for of~~ SO<sub>2</sub> emission, each initialised to a meteorological state to match the observed phase of the quasi-biennial oscillation (QBO) at the times of the eruptions. We assess how each eruption's emitted SO<sub>2</sub> ~~evolves translates~~ into a tropical reservoir of volcanic aerosol and analyse the subsequent dispersion to mid-latitudes.

We compare the simulations to ~~the three different~~ volcanic forcing datasets ~~used in historical integrations for the two most recent Coupled Model Intercomparison Project (CMIP) assessments: the Global (e.g. Space-based Stratospheric Aerosol Climatology (GloSSAC) for CMIP6, and the~~ Sato et al. (1993) and Ammann et al. (2003) ~~datasets used in CMIP5~~. <sup>15</sup> ~~We also~~ that are used in historical integrations for the two recent Coupled Model Intercomparison Project (CMIP) assessments. We assess the vertical extent of the volcanic aerosol clouds by comparing ~~simulated extinction~~ to Stratospheric Aerosol and Gas Experiment II (SAGE II) v7.0 satellite aerosol ~~data extinction measurements~~ (1985-1995) for Pinatubo and El Chichón, and to 1964-65 northern hemisphere ground-based lidar measurements for Agung. As an independent test for the simulated volcanic forcing after Pinatubo, we also compare to the shortwave (SW) and longwave

20 (LW) ~~Top-of-the-Atmosphere~~ top-of-the-atmosphere flux anomalies measured by the Earth Radiation Budget Experiment (ERBE) satellite instrument.

For the Pinatubo simulations, an injection of 10 to 14 Tg SO<sub>2</sub> gives the best match to the High Resolution Infrared Sounder (HIRS) satellite-derived global stratospheric sulphur burden, with good agreement also to SAGE II mid-visible and near-infrared extinction measurements. This 10-14 Tg range of emission also generates a heating of the tropical stratosphere that is comparable with the temperature anomaly ~~seen~~ present in the ERA-Interim reanalyses. For El Chichón-Chichón, the simulations with 5 Tg and 7 Tg ~~SO<sub>2</sub>-SO<sub>2</sub>~~ emission give best agreement with the observations. However, ~~these runs for first few months these simulations~~ predict a much deeper volcanic cloud than ~~present in the CMIP6 data, with much higher aerosol extinction than the GloSSAC data up to October 1984, but represented in the GloSSAC dataset that is largely based on an interpolation between Stratospheric Aerosol Measurements (SAM-II) satellite and aircraft measurements. In contrast, these simulations show much better agreement during the later SAGE II period - after October 1984.~~ For 1963 Agung, the 9 Tg simulation compares best to the forcing datasets with the model capturing the lidar-observed signature of ~~the altitude of~~ peak extinction descending from 20 km in 1964 to 16 km in 1965.

Overall, our results indicate that the downward adjustment to ~~previous~~ SO<sub>2</sub> emission ~~estimates for Pinatubo as suggested found to be required~~ by several interactive modelling studies ~~when simulating Pinatubo~~, is also needed ~~for when simulating~~ the Agung and El Chichón aerosol clouds. This strengthens the hypothesis that interactive stratospheric aerosol models may be missing an important removal or redistribution process (e.g. effects of co-emitted ash) which changes how the tropical reservoir of volcanic aerosol evolves in the initial months after an eruption. Our ~~analysis identifies model comparisons also identify~~ potentially important inhomogeneities in the CMIP6 dataset for all three ~~eruption~~ periods that are hard to reconcile with variations predicted ~~by in~~ the interactive stratospheric aerosol ~~model simulations~~. We also highlight large differences between the CMIP5 and CMIP6 volcanic aerosol datasets for the Agung and El Chichón periods. Future research should aim to reduce this uncertainty by reconciling the datasets with additional stratospheric aerosol observations.

## 1 Introduction

Quantifying the effects of volcanic eruptions on the climate system is challenging due to ~~significant and complex coupling complex coupling pathways~~ between various atmospheric processes (Cadle and Grams, 1975; Turco et al., 1982; Robock, 2000). ~~Major~~ All major volcanic eruptions directly inject large amounts of SO<sub>2</sub> into the stratosphere, leading to an abrupt enhancement of the stratospheric aerosol layer. The ~~volcanic aerosol cloud then causes~~ principal effect of volcanic aerosol clouds is to increase backscatter of incoming solar radiation, thereby cooling the Earth's surface. Major volcanic aerosol clouds can also cause a range of other composition responses, which together with the direct aerosol effects, ~~initiates~~ initiate a complex system of radiative, dynamical and chemical interactions. ~~The principal effect of the volcanic aerosol cloud is to greatly increase backscatter of incoming solar radiation, thereby cooling the Earth's surface.~~ As aerosol particles in the volcanic cloud grow larger, they also absorb outgoing longwave (LW) radiation, which off-

sets some of the shortwave (SW) ~~cooling, also warming~~ surface cooling, and also causes a warming of the lower stratosphere (e.g. Angell, 1997a; Free et al., 2009). ~~This aerosol-induced stratospheric heating tends to occur When this volcanic-aerosol-induced heating occurs~~ within the tropical reservoir of volcanic aerosol, which then enhances stratospheric reservoir (e.g. Dyer, 1974; Grant et al., 1996), the effect causes an increase in the upwelling in the lowermost tropical stratosphere. ~~Also, tropical warming alters the tropics-to-pole~~ Such tropical stratospheric warmings also alter the meridional temperature gradient in the stratosphere, which in turn can modify the vertical propagation (and breaking) of the large planetary and synoptic-scale waves that drive the ~~stratospheric~~ Brewer-Dobson circulation (e.g. Poberaj et al., 2011; Bittner et al., 2016), with ~~additional ozone changes caused by~~ decreased tropical ozone and additional ozone transport to mid-latitudes caused by the enhanced upwelling (e.g. Kinne et al., 1992; Dhomse et al., 2015). These indirect (circulation-driven) ozone changes ~~also combine with~~ ~~combine with direct~~ chemical ozone loss from the increased aerosol surface area available for heterogeneous chemistry (e.g. Prather, 1992; Solomon, 1999), and ~~from also~~ photochemical ozone changes (e.g. Bekki et al., 1993).

~~Tropical eruptions~~ Eruptions that inject SO<sub>2</sub> directly into the ~~tropical~~ stratosphere cause relatively prolonged surface cooling ~~as this region is the, because a~~ long-lived ~~reservoir for the volcanic aerosol~~ (Dyer, 1974) that forms within the ~~tropical pipe region~~ "reservoir" of volcanic aerosol forms (Dyer, 1974; Grant et al., 1996), with particles in the volcanic cloud remaining within the "tropical pipe" due to a prevailing and sustained upwelling (Plumb, 1996). At the edge of the tropical pipe, ~~strong meridional gradients in wind shear reduce tropics-to-mid-high-latitude transport and the~~ ~~subtropical-barrier~~ reduces transport to mid-latitudes, slowing subsequent removal via stratosphere-troposphere exchange (STE) (Holton et al., 1995). The (Holton et al., 1995). Since the intensity of incoming solar radiation ~~maximises is highest~~ at low latitudes, hence a tropical volcanic aerosol ~~increases~~ ~~cloud~~ also has greatest solar dimming efficacy. The three largest tropical eruptions over the past century are Mt. Agung (March 1963), El Chichón (April 1982) and Mt. Pinatubo (June 1991). The ~~extents~~ ~~extent~~ to which these eruptions cool the Northern and Southern Hemispheres differ substantially depending ~~to a large extent~~ on the dispersion pathways of ~~these~~ ~~the resulting~~ volcanic aerosol clouds from the tropical reservoir. For El Chichón and Agung, the volcanic aerosol dispersed mostly to the hemisphere of the volcano (e.g. Dyer, 1970; McCormick and Swissler, 1983), whereas for Pinatubo the cloud dispersed to both hemispheres (e.g. Trepte et al., 1993).

Major eruptions are known to cause dominant ~~cooling~~ signatures within decadal ~~surface temperature~~ ~~global mean~~ ~~surface temperature (GMST)~~ trends (e.g. Santer et al., 2001, 2014). ~~However, the uncertainty within volcanic forcings such as Agung has only recently become recognised (Marotzke and Forster, 2015)~~ The abruptness and dominant magnitude of major volcanic forcings, compared to the slower variations in all other external forcings, means even a small relative uncertainty in their global dimming impact will introduce important variations in the decadal GMST tends (e.g. Marotzke and Forster, 2015). There has been a substantial change in the volcanic forcing from 1963 Agung between CMIP5 and CMIP6 (Niemeier et al., 2019), and the effects that this change may have caused within CMIP5 and CMIP6 historical simulations is starting to become recognised (e.g. Mann et al., 2020). Even with the greater amount of observational data after the most recent major eruption (Pinatubo), the magnitude of the peak stratospheric aerosol optical depth (~~AOD~~<sup>s</sup>~~AOD~~) remains highly uncertain

from 0.3 at 0.25 - 0.45 (e.g. Russell et al., 1996) (e.g. Russell et al., 1996; Kovilakam et al., 2020). Global tropospheric cooling estimates from Pinatubo are even more uncertain, ranging from 0.2 K - 0.5 K (Soden et al., 2002; Carty et al., 90 Folland et al., 2018). The modern satellite era has provided a wealth of information about the progression of volcanic aerosol clouds, but space-borne remote sensing measurements can sometimes have significant uncertainties. Limb-sounding satellite instruments, such as After the 1991 Pinatubo eruption, the unprecedented optical thickness of the volcanic aerosol cloud caused retrieval problems for several limb-sounding satellite instruments. For example, the Stratospheric Aerosol and Gas Experiment (SAGE) and Microwave Limb Sounder (MLS), have large retrieval errors in the 95 presence of volcanically enhanced aerosol loading (SAGE-II) instrument that provides the benchmark dataset for Pinatubo, was only able to measure aerosol extinction in the upper parts of the tropical volcanic cloud (e.g. Thomason, 1992). Nadir-sounding satellite measurements such as the Advanced Very High Resolution Radiometer (AVHRR) provide important information for the dispersion of the El Chichón (Robock and Matson, 1983) and Pinatubo (e.g. Long and Stowe, 1994) aerosol clouds, but are not able to determine their vertical distribution.

100 Another important uncertainty for Pinatubo's effects is the lower stratospheric warming, with observational estimates of this effect in the tropical lower stratosphere after Pinatubo eruption in the range 2 K to 4 K (SPARC, 2010, Chap. 8) magnitude and longevity of the warming of the lower stratosphere. Within the CCMVal-2 hindcast integrations (SPARC, 2010, Chap. 8), chemistry-climate model show about 0.5 to 3 K warming at 50 hPa, with the temperature anomaly from the ERA-interim reanalysis, (Dee et al., 2011) suggesting ~1 K warming. The magnitudes of the lower stratospheric warmings for the El 105 Chichón and Agung eruptions are even more uncertain (e.g. Free et al., 2009; Driscoll et al., 2012; DallaSanta et al., 2019). Such large uncertainties in stratospheric warming. The large diversity in the CCMVal-2 warming anomalies are mostly due to differences in the methods used to attribute the volcanic influence, accounting for the phase progression in the methodologies used to estimate the volcanic heating, differences in vertical resolution and stratospheric circulation, meaning the effects from the quasi-biennial oscillation (QBO) (Angell, 1997a; Sukhodolov et al., 2018), phase propagation 110 (Angell, 1997a; Sukhodolov et al., 2018), and influences from 11-year solar flux variability, (e.g. Lee and Smith, 2003; Dhomse et al., 2011, 2013) are resolved differently. The attribution of volcanically forced warming is also complicated by the inherent coupling with changes in tropical upwelling due volcanic aerosol induced heating (e.g. Young et al., 1994; McCormick et al., 1995; Aquila et al., 2013), the associated fact that the increased tropical upwelling caused by the aerosol-induced heating subsequently leads to 115 changes to the volcanic aerosol cloud itself (e.g. Young et al., 1994; McCormick et al., 1995; Aquila et al., 2013), a partial offset of the warming also caused by a circulation-driven chemical changes reduction in tropical ozone (e.g. Kinne et al., 1992; Dhomse et al., 2015).

Climate models are important research tools. Model simulations are the benchmark method to understand past climate change and attribute the impacts of individual external forcings within observed temperature trends. All climate models variations seen within observed surface temperature trends (e.g. Hegerl and Zwiers, 2011) to natural and anthropogenic 120 external forcings. Whereas all climate models participating in the 5th and 6th Coupled Model Intercomparison Project (CMIP5 and CMIP6) include interactive aerosol modules for tropospheric aerosol radiative effects, yet very few use these schemes for volcanic forcing to simulate the effects of volcanic eruptions. Instead, Coupled Model Intercomparison

Project (CMIP) historical integrations with climate models the climate models performing historical integrations use pre-scribed volcanic aerosol datasets to mimic climatic effects of the forcings from past eruptions. In CMIP5, most climate 125 models used the NASA Goddard Institute for Space Studies (GISS) volcanic forcing dataset (Sato et al., 1993, hereafter, Sato data), constructed from (Sato et al., 1993, hereafter, the Sato dataset) that is constructed from SAGE-I, SAM-II and SAGE-II aerosol extinction measurements, combined with an extensive synthesis of observational data, originally for 1850-1990, that is often updated to include later eruptions pre-satellite-era observational datasets (see <https://data.giss.nasa.gov/modelforce/strataer>). The Sato dataset consists of zonal-mean stratospheric AOD at 550 nm (sAOD<sub>550</sub>) and column effective radius (Reff). The CMIP5 modelling groups used different approaches to apply this the 550 nm information across the spectral wavebands of their model's radiative transfer module models' radiative transfer modules and to redistribute the total stratospheric aerosol optical thickness into their model vertical levels (e.g. Driscoll et al., 2012).

130 Stenchikov et al. (1998) also constructed a forcing dataset for Pinatubo that included the variation in the forcings aerosol optical properties across wavebands in the SW and LW, combining SAGE-II and Stratospheric Aerosol Measurement (SAM) II (McCormick, 1987) aerosol extinctions. They combined SAGE-II and SAM-II (McCormick, 1987) aerosol extinction, 135 as well as infra-red aerosol extinction data from the Improved Stratospheric and Mesospheric Sounder (ISAMS) (Lambert et al., 1993; Grainger et al., 1993; Lambert et al., 1997) and the Cryogenic Limb Array Etalon Spectrometer (CLAES) (Roche et al., 1993). They also compared and/or calibrated to AVHRR, lidar and balloon-balloon-borne particle counter observations.

140 Since then, Over the past two decades a large number of chemistry-climate models (CCMs) have been developed, and applied to improve our understanding of past stratospheric change. Several co-ordinated hindcast integrations with the CCMs were designed and carried out CCM hindcast integrations have been performed via activities such as CCMVal (Eyring et al., 2005, 2008; Morgenstern et al., 2010) and CCM3 (Eyring et al., 2013; Morgenstern et al., 2017), with each of the models using different methods to include stratospheric heating from volcanic aerosol clouds, so as to represent 145 volcanically-forced changes in stratospheric trace species. Some CCMs prescribed pre-calculated zonal mean heating rate anomalies (e.g. Schmidt et al., 2006), whilst either derived the others applied radiative heating from prescribed aerosol datasets, either the 2-D GISS sAOD<sub>550</sub> data set or from a 3-D prescribed aerosol surface area density (SAD). SPARC (2010, Chap. 8) presented a detailed analysis of lower stratospheric warming in analysed lower stratospheric 150 temperatures following the Pinatubo eruption across different models participating in the CCMVal-2 simulations following Pinatubo eruptions, that showed activity. They showed that CCMVal-2 models show a broad range in the simulated lower stratospheric warming (from 0 to 4 K temperature anomalies (0.5 to 3 K at 50 hPa) with SAD-derived warming tending to over-predict the effect be higher than the ~1 K anomaly suggested by ERA-interim reanalysis data.

155 Another important The other volcanic forcing dataset used in CMIP5 is that from Ammann et al. (2003, hereafter, Ammann data), which was produced via a simple Ammann et al. (2003, hereafter, Ammann dataset), which is based on a parameterisation for the dispersion of the volcanic aerosol from a specified number of major tropical eruptions meridional dispersion of volcanic aerosol clouds to mid-latitudes, as determined by the seasonal cycle in the Brewer-Dobson circulation. The Brewer-Dobson circulation and an assumed 12-month decay timescale for the tropical reservoir. The dataset specifies the

forcing for all major tropical eruptions in the 20th century, but does not resolve the effect of the QBO phase in modulating the inter-hemispheric dispersion pathways. The peak aerosol optical depth for each eruption was is scaled to match estimates of maximum aerosol loading from Stothers (1996); Hofmann and Rosen (1983b); Stenchikov et al. (1998) (Stothers, 1996; Hofmann and Rosen, 1983b; Stenchikov et al., 1998) assuming a fixed particle size distribution ( $R_{eff} = 0.42 \text{ micron } \mu\text{m}$ ).

Recently, Arfeuille et al. (2014) created the most up-to-date volcanic forcing dataset to enable For the latest historical simulations in CMIP6 (e.g. Eyring et al., 2016), a single volcanic aerosol dataset was provided for the full 1850-2016 period. This dataset is split into two parts, depending on the availability of satellite data. For 1850-1979 it is based on a simulation of a 2-D interactive stratospheric aerosol model (AER2D) [hereafter CMIP6-AER2D] Arfeuille et al. (2014). For the satellite era (after 1979), the dataset is provided as the Global Space-based Stratospheric Aerosol Climatology (GloSSAC) dataset (Thomason et al., 2018) . The combined forcing dataset is designed to enable chemistry-climate models to include aerosol-radiation interactions (aerosol optical properties) consistently with the additional heterogenous chemistry occurring on volcanic aerosol particles. This comprises three datasets, two for SW and LW along with a prescribed surface area density for heterogeneous chemistry. The aerosol optical properties , for each model to map the aerosol onto the wavebands datasets are tailored for each climate model; the provided properties are mapped onto the model's SW and LW wavebands used in the radiative transfer module of the host climate model (see Luo, 2016). For the heterogeneous chemistry, a third dataset of SAD was provided, the original version known as the 4 dataset. An updated version of this dataset (3 dataset) was produced specifically for the CMIP6 simulations (see ). All three datasets were generated from simulations with a 2-D interactive stratospheric aerosol microphysics model (AER), including 26 separate eruptions for the 1600-2013 time period. (see Luo, 2016) .

Here we analyse volcanic forcing major volcanic experiments with the Unified Model interactive stratospheric aerosol configurations of the Unified Model - United Kingdom Chemistry and Aerosol (UM-UKCA) composition-climate model, which has interactive stratosphere-troposphere chemistry and aerosol microphysics. The model experiments simulate the volcanic aerosol clouds, and associated radiative forcings, from the three largest tropical eruptions over the past century: Mt. Agung (March 1963), El Chichón (April 1982) and Mt. Pinatubo (June 1991). Aligning with the design of the Interactive Stratospheric Aerosol Model Inter-comparison Project (ISA-MIP) co-ordinated multi-model "Historical Eruption SO<sub>2</sub> Emissions Assessment" (Timmreck et al., 2018), we have carried out the experiments consist of 3-member ensembles of simulations with each of upper, low lower and mid-point best estimates for estimates of the SO<sub>2</sub> injection for emitted from each eruption. Simulated We then compare the simulated aerosol properties of the volcanic aerosol plume are compared to range of observation-based clouds to a range of observational datasets.

The In addition to the aerosol cloud, the UM-UKCA experiments includes the online radiative effects from both tropospheric as well as stratospheric volcanic experiments include the effects on the stratospheric ozone layer. The GLOMAP-mode aerosol microphysics scheme (Mann et al., 2010; Dhomse et al., 2014) also simulates the tropospheric aerosol layer (Yoshioka et al., 190 with the stratosphere-troposphere chemistry scheme (Archibald et al., 2020) predicting tropospheric ozone and oxidising capacity consistent with the corresponding decade's composition-climate setting. There have been several improvements to the aerosol simulated with same interactive aerosol microphysics module. There several important improvements in

aerosol-microphysics module since ~~the~~ our original Pinatubo analysis presented in Dhomse et al. (2014), ~~that~~ and these are discussed in ~~?Marshall et al. (2018, 2019); Yoshioka et al. (2019)~~ Brooke et al. (2017); Marshall et al. (2018, 2019).

195 Section 3 provides the specifics of the model experiments, with ~~section~~ Section 4 describing the observational datasets. Model results are given in Section 5. Key findings and conclusions are presented in Section 6.

## 2 Model Experiments

We use the Release Job 4.0 (RJ4.0) version of the UM-UKCA composition-climate model (Abraham et al., 2012), which couples the Global Atmosphere 4.0 configuration (Walters et al., 2014, GA4) of the UK Met Office Unified Model (UM v8.4)

200 general circulation model with the UK Chemistry and Aerosol chemistry-aerosol sub-model (UKCA). The GA4 atmosphere model has a horizontal resolution of  $1.875^\circ \times 1.25^\circ$  (N96) with 85 vertical levels from the surface to about 85 km. The RJ4.0 configuration of UM-UKCA adapts GA4 with aerosol radiative effects from the interactive GLOMAP aerosol microphysics scheme and ozone radiative effects from the whole-atmosphere chemistry that is a combination of the detailed stratospheric chemistry and simplified tropospheric chemistry schemes (~~Morgenstern et al., 2009; O'Connor et al., 2014~~) (Morgenstern et al., 2009; O'Connor et al., 2014)

205 The experiment design is similar to that in Dhomse et al. (2014), but with the volcanic aerosol radiatively coupled to the dynamics ~~, as in Mann et al. (2015),~~ for transient atmosphere-only ~~free-running~~ free-running simulations. Briefly, the model uses the GLOMAP aerosol microphysics module, ~~the scheme configured to be and the chemistry scheme~~ applied across the troposphere and stratosphere ~~with stratosphere-troposphere chemistry, Greenhouse gases (GHGs, Greenhouse gas (GHG)~~ and ozone-depleting substance (ODS) concentrations are from Ref-C1 simulation recommendations in the Chemistry-Climate Model Initiative (CCMI-1; Eyring et al. (2013); Morgenstern et al. (2017)) activity. Simulations are performed in atmosphere-only mode, and we use CMIP6 recommended sea-surface temperatures and sea-ice concentration that are obtained from <https://esgf-node.llnl.gov/projects/cmip6/>. The main updates since Dhomse et al.

210 (2014) are: i) updated dynamical model (from HadGEM3-A r2.0 to HadGEM3 Global Atmosphere 4.0), hence improved vertical and horizontal resolution (N48L60 vs N96L85, (Walters et al., 2014)), ii) coupling between aerosol and radiation

215 scheme (Mann et al., 2015), iii) additional sulphuric particle formation pathway via heterogeneous nucleation on transported meteoric smoke particle cores ~~(?)~~ (Brooke et al., 2017). The atmosphere-only RJ4.0 UM-UKCA model ~~applied here is the identical model used here is identical~~ to that applied in Marshall et al. (2018) and Marshall et al. (2019), with the former run in pre-industrial setting for the VolMIP interactive Tambora experiment (see Zanchettin et al., 2016) and the latter in year-2000 timeslice mode for ~~the a~~ perturbed injection-source-parameter ensemble ~~analysed there~~ analysis.

220 Prior to each of the eruption experiments, we first ran 20-year time-slice simulations with GHGs and ODSs for the corresponding decade (1960 for Agung, 1980 for El Chichón and 1990 for Pinatubo), to allow enough time for the stratospheric circulation and ozone layer to adjust ~~each to the~~ composition-climate setting for that time period. Tropospheric aerosol and chemistry (primary and precursor) emissions were also set to interactively simulate the tropospheric aerosol layer and oxidising capacity for the corresponding decade. ~~Discarding the first 10 years as spin-up, we then analysed the~~

225 ~~QBO behaviour in the second 10 years, selecting initialisation fields from~~ For each 20-year time-slice run, we analysed

the evolution of stratospheric sulphur burden, ozone, age-of-air and selected long-lived tracers, to check that the model had fully adjusted to the GHG and ODS settings for a given time period. We then analysed timeseries of the tropical zonal wind profile to identify three different model years that then ensure each ensemble member approximately matches the post-eruption QBO state gave a QBO transition approximately matching that seen in the ERA-interim re-analysis (Dee et al., 2011). The initialisation fields for those years was then used to re-start the three ensemble member transient runs. The QBO evolution for each Pinatubo simulation is shown in the Supplementary Material (Figure S1).

For each eruption then, a total of nine different volcanically-perturbed simulations were performed, three different "approximate QBO progressions" for each SO<sub>2</sub> "approximate QBO progressions" for each SO<sub>2</sub> emission amount (see Table 1). The 9 corresponding control simulations had identical pre-eruption initial conditions and emissions, except the Pinatubo/El Chichon/Agung SO<sub>2</sub> that the relevant volcanic emission was switched off. For simplicity the simulations do not use the simulated aerosol in Note that simulated aerosol are not included the calculation of heterogeneous chemistry; the control simulations use climatological uses climatological background SAD values in the stratosphere (mean 1995–2006) while the other simulations use include effects of associated heterogeneous chemistry via time-varying SAD from Arfeuille et al. (2013) Arfeuille et al. (2014) .

### 240 3 Evaluation Datasets

To provide additional context for the UM-UKCA simulated aerosol properties volcanic aerosol clouds, we compare primarily to the mid-visible and near-infrared extinction from CMIP6 volcanic forcing data set, obtained from (last access: January 25, 2020) (Luo, 2016) . Aerosol properties are derived using the simulations to three different observation-based volcanic forcing datasets, as well as several individual stratospheric aerosol measurement datasets (see Table 2).

245 The primary evaluation dataset for this study are the two parts of the volcanic aerosol dataset provided for the co-ordinated CMIP6 historical integrations (Eyring et al., 2016) . For 1979 onwards, we use CMIP6 recommended GloSSAC (Thomason et al. (2018) , hereafter referred to as CMIP6-GloSSAC) dataset. CMIP6-GloSSAC is a best-estimate aerosol extinction dataset from various satellite instruments: SAGE I, Stratospheric Aerosol Measurement (SAM), SAGE II, the latest version of the SAGE-II dataset and, for the Pinatubo period, the infra-red aerosol extinction measurements from the Halogen Occultation Experiment (HALOE) , Optical Spectrograph and InfraRed Imager System (OSIRIS), Cloud Aerosol Lidar and Infrared Pathfinder Satellite Observation (CALIPSO) and and Cryogenic Limb Array Etalon Spectrometer (CLAES) measurements.

250 For the pre-satellite era (1850–1979), volcanic aerosol properties in CMIP6 data are constructed using results from the AER 2-D aerosol model (Arfeuille et al., 2014) , considering injection heights in the literature and from plume-rise model, and from comparing to other forcing datasets, ice core sulphate deposition and ground-based solar radiation measurements within Sato et al. (1993) and Stothers (2001) . Although the CMIP6 dataset consists primarily of the three parts explained in Introduction section (waveband-mapped aerosol optical properties in the SW and LW, plus surface area density), additional datasets are also provided, including monthly zonal mean log-normal aerosol size distribution

260 properties such as mean radius, volume density and extinctions at 550 nm. These datasets are provided at 0.5 km vertical resolution between 5 km and 40 km).

265 For 1979–2016, the CMIP6 dataset is replaced with the most up-to-date the Global Space-based Stratospheric Aerosol Climatology data known as the GloSSAC dataset () described in (Thomason et al., 2018). GloSSAC combines stratospheric aerosol information from several different satellite instruments: SAGE I and II, HALOE, OSIRIS, CALIPSO and CLAES. Measurements from other space instruments and in-situ (ground-based, air and balloon-borne) instruments are also 270 Lidar measurements from Hawaii, Cuba and Hampton, Virginia are used to fill gaps in the the gap in the post-Pinatubo part of the dataset where none of these datasets were was able to measure the full extent of the volcanic cloud. The v1.1 GloSSAC dataset used here is obtained from the NASA Atmospheric Science Data Center (last access March 10, 2020). During the El Chichón For the El Chichón period, GloSSAC airborne lidar surveys between SAGE-1 and SAGE-II period are used. Here we use latest version (V2) of the CMIP6-GloSSAC; key differences between CMIP6-GloSSAC V1 and V2 data are described in Kovilakam et al. (2020).

275 With the El Chichón eruption occurring between the SAGE-I and SAGE-II instruments, CMIP6-GloSSAC is largely based on SAGE I (January 1979–November 1981) and SAM II (1978–1993) extinction combining the SAM-II extinction measurements at 1000 nm, and the 550 nm (1978–1993), with a 550 nm extinction derived from applying fit to the variation in 550:1020 colour ratio that is derived from SAGE-II measurements. One limitation is that the SAM-II from the SAGE-II period. The SAM-II instrument only measures at high-latitudes. After the with the period after the El-Chichón eruption (SAGE gap period, April 1982–October 1984) data is primarily constructed based on linearly interpolating between data from constructed via linear interpolation. CMIP6-GloSSAC also uses lidar measurements from the NASA Langley lidar (Hampton, USA) and the 5 aircraft missions after El Chichón: July 1982 (13°N to 40°N), October and November 1982 (45°S to 44°N), January and February 1983 (28°N to 80°N), May 1983 (59°S to 70°N), and January 1984 (40°N to 280 68°N).

285 For the Pinatubo period, GloSSAC data follows the method described in SPARC (2006, chapter 2), combining SAGE II, CMIP6-GloSSAC is an updated version of the gap-filled dataset described in SPARC (2006, Chapter 4), combining SAGE-II aerosol extinction (in the solar part of the spectrum), with HALOE and CLAES measurements. GloSSAC also utilized backscatter-sonde measurements from Lauder, New Zealand (Rosen et al., 1994), aerosol extinction in the infra-red (see Thomason et al., 2018). For the period where the SAGE-II signal was saturated (e.g. Thomason, 1992), CMIP6-GloSSAC applies an improved gap-fill method in mid-latitudes, but in the tropics is still based on the composite dataset from SPARC (2006, pages 140–147), combining with ground-based lidar measurements from Mauna Loa, Hawaii (19.5°N, (Barnes and Hofmann, 1997)) from the NASA Langley lidar at Hampton, USA, and and, after January 1992, also with lidar measurements from Camaguey, Cuba (23°N, see Antuña, 1996)).

290 For the period 1984 to 2005, the SAD provided is derived from the SAGE-II multi-wavelength aerosol extinction (Thomason et al., 2008), known as the  $4\lambda$  dataset as it uses all 4 aerosol extinction channels (386 nm, 453 nm, 525 nm and 1020 nm). The updated version provided for CMIP6 (the  $3\lambda$  dataset) uses only 3 channels as the 386 nm aerosol extinction are excluded due to a higher uncertainty.

For the pre-satellite part of the CMIP6 historical period (1850–1979), the volcanic aerosol properties dataset is constructed using results from the 2-D interactive stratospheric aerosol model (CMIP6-AER2D) and is obtained via [ftp://iacftp.ethz.ch/pub\\_read/luo/CMIP6/](ftp://iacftp.ethz.ch/pub_read/luo/CMIP6/) (last access: January 25, 2020) (Luo, 2016). Each of the volcanic aerosol clouds within the interactive 2-D simulations was formed from individual volcanic SO<sub>2</sub> emissions. Each eruption's mass emission and injection height was based on literature estimates, considering also plume-rise model information, and from comparison and calibration to ice core sulphate deposition and ground-based solar radiation measurements (Arfeuille et al., 2014).

Each of these two parts of the CMIP6 dataset (CMIP6-GloSSAC and CMIP6-AER2D) primarily consists of the three parts explained in the Introduction (waveband-mapped aerosol optical properties in the SW and LW, plus surface area density). A 2-D monthly zonal-mean monochromatic aerosol extinction dataset at 550 nm is provided for the full 1850–2014 period, also with monthly zonal-mean effective radius, particle volume concentrations and single-mode log-normal mean radii values. For the CMIP6-GloSSAC part of the dataset, aerosol extinction is also provided at 1020 nm wavelength.

As an extra constraint for the simulated Agung aerosol cloud, observational data not readily available we have recovered an important additional observational dataset, which until now has only been available in tables within the appendix of a PhD thesis (Grams, 1966). The dataset provides an important observational constraint to evaluate the progression in the vertical extent of the simulated Agung aerosol cloud. Hence we digitised the observations from optical radar. This dataset is the 694 nm backscatter ratio observations from 66 nights of lidar measurements at Lexington, Massachusetts (42°44' N, 71°15' W Grams and Fiocco, 1967). These aerosol backscatter (42°44' N, 71°15' W, Fiocco and Grams, 1964; Grams and the periods January to May 1964 (23 profiles), and October 1964 to July 1965 (43 profiles). To enable comparison to the model-predicted 550 nm extinction, the aerosol backscatter ratio observations at 694 nm are converted to extinction at 532 nm aerosol extinction at 532 nm, as described in supplementary material. the Supplementary Material. Note that the Lexington measurements used here are an initial version of a 532 nm extinction profile dataset being prepared for submission to the Earth System Science Datasets journal (Antuna Marrero et al., in prep.).

For the To evaluate simulated stratospheric aerosol optical depth (sAOD) comparison, we use we provide three different observation-based datasets to provide greater context for the comparisons. For the CMIP6 extinctions at 550 nm are integrated dataset, we derive sAOD<sub>550</sub> by vertically integrating CMIP6-GloSSAC/CMIP6-AER2D 550 nm extinction for all the levels above the tropopause to calculate sAOD<sub>550</sub>. As mentioned earlier, the most widely used volcanic forcing data is from Sato et al. (1993) and is obtained from . Another important . For the other two volcanic forcing datasets (Sato et al., 1993; Ammann et al., 2003), the sAOD<sub>550</sub> evaluation dataset is based on a combination of simple representation of the dispersion and an assumption of the size distribution by Ammann et al. (2003), and is obtained via . The is specified in the data files, as the primary aerosol metric provided (see Table 2). To analyse the lower stratospheric warming following each eruption is estimated by comparing we show the model temperature differences between control and sensitivity simulations alongside the 5-year temperature anomalies anomaly from the ERA-Interim reanalysis data (ERA-Int, available from [www.ecmwf.int](http://www.ecmwf.int)). ERA-int data is available since 1979, hence for the Dee et al., 2011), and overplot the progression of the re-analysis tropical zonal wind profile to indicate the QBO transitions through

each period. For the Agung comparison, we use ERA40ERA-40, an earlier version of ECWMF reanalysis datasets: 40-year ECWMF reanalysis dataset (Uppala et al., 2005)

## 330 4 Results and Discussion

The temporal radiative forcing signature from a major tropical eruption is primarily determined by the evolution of the volcanic aerosol cloud in the stratosphere. An initial "tropically confined phase" sees zonally-dispersing SO<sub>2</sub> and ash plume transforming to layered aerosol cloud. Meridional transport in the subsequent "dispersion phase" then leads to a hemispheric or global cloud of mainly aqueous sulphuric acid droplets. The efficacy of such volcanic clouds' solar 335 dimming, and the extent of any offset via long-wave aerosol absorption, is strongly linked to how large the sulphuric aerosol particles grow (their size distribution) as this large-scale dispersion progresses (e.g Lacis et al., 1992).

In the following subsections we assess, for each eruption, the simulated volcanic aerosol cloud for the upper, lower and mid-point /best estimate SO<sub>2</sub> emissions and compare to available observational constraints. Our focus here is primarily 340 on aerosol optical properties, evaluating mid-visible stratospheric AOD, but also and aerosol extinction, in both the mid-visible and near-infra-red, to understand how the altitude and vertical extent of the cloud varies for each eruption. In each case, we also compare the lower stratospheric warming with the temperature anomaly from the ERA-Interim/ERA-40 reanalyses.

### 4.1 Mt. Pinatubo aerosol cloud

In the Pinatubo case, satellite measurements are able to constrain provide an additional constraint for the particle size evolution (in terms of effective radius), and hence here, with particle effective radius derived from the volume concentration 345 and surface area density SAGE-II extinction at multiple wavelengths (Thomason et al., 1997a; SPARC, 2006). Hence for Pinatubo, we also compare model-simulated effective radius to that provided with the CMIP6-CMIP6-GloSSAC dataset, which underpins each model climate model's specified multi-wavelength aerosol optical properties in the Pinatubo forcings 350 in CMIP6 historical integrations. With Pinatubo by far the dominant external forcing in the 1990s, we also compare simulated SW and LW forcings to the Earth Radiation Budget Experiment (ERBE) satellite data to gain direct insight into how the different SO<sub>2</sub> emission simulations evolve in terms of top-of-the-atmosphere (TOA) radiative forcings.

Baran and Foot (1994) analysed satellite observations of the Pinatubo aerosol cloud from the High-resolution Infrared Radiation Sounder (HIRS), converting the measured LW aerosol optical properties into a timeseries of global aerosol burden. In Dhomse et al. (2014), we used this observed global burden dataset to evaluate the models model's simulated 355 aerosol cloud, translating the peak global burden of 19 to 26 Tg from the HIRS measurements into a 3.7 to 6.7 Tg range for stratospheric sulphur, assuming the particles were 75% by weight aqueous sulphuric acid solution droplets. We identified an important inconsistency in the models model's predictions, when also considering satellite observations of volcanic SO<sub>2</sub>. The satellite measurements of SO<sub>2</sub> show that 7 to 11.5 Tg of sulphur was present in the stratosphere in the for few days after the eruption (14 to 23 Tg of SO<sub>2</sub>, Guo et al. (2004a)), so only around 50% of the emitted sulphur

360 remained present at peak volcanic aerosol loading. In contrast, the model simulations showed that 90% of the sulphur emitted remained in the volcanic aerosol cloud at its peak global mass burden. This inconsistency was also found in other interactive Pinatubo stratospheric aerosol model studies (Sheng et al., 2015a; Mills et al., 2016), with number of models finding best agreement with observations for 10 to 14 Tg emitted  $\text{SO}_2$  (5 to 7 Tg of sulphur), which is less than the lower bound from the TOMS/TOVS measurements. In Dhomse et al. (2014), we suggested the models may be missing some  
365 process or influence, which acts to redistribute the sulphur within the volcanic cloud, causing it then to be removed more rapidly.

Figure 1a shows the timeseries of global stratospheric aerosol sulphur burden from ~~current Pinatubo simulations compared to the present study's Pinatubo simulations, comparing also~~ to the previous ~~model~~ interactive Pinatubo UM-UKCA simulations with 20 and 10 Tg  $\text{SO}_2$  injection as presented in Dhomse et al. (2014). The 20, 14 and 10 Tg  $\text{SO}_2$  Pinatubo clouds  
370 generate peak ~~loadings~~ loading of 8.3, 5.9 and 4.2 Tg of sulphur, translating into conversion efficiencies of 83, 84 and 84%, respectively. This continuing discrepancy with the satellite-derived 50% conversion efficiency might be due to accommodation onto co-emitted ash particles. Recently we have re-configured the UM-UKCA model to enable new simulations to test this hypothesis (Mann et al., 2019b). We consider the requirement to reduce ~~model-emitted~~ model-emitted  $\text{SO}_2$  to be less than that indicated by satellite measurements as an adjustment to compensate for a missing removal/redistribution  
375 process in the initial weeks after the eruption.

The simulated Pinatubo global stratospheric sulphur burden in runs **Pin10** and **Pin14** is in good agreement with the HIRS observations, both in terms of predicted peak burden, and the evolution of its removal from the stratosphere. In particular, the model captures a key variation in the HIRS measurements, namely that the removal of stratospheric sulphur was quite slow in the first year after the eruption. The volcanic aerosol cloud retained a steady 4-5 Tg of sulphur  
380 for more than 12 months after the eruption, before its removal proceeded at much faster rate in late 1992 and early 1993. The corresponding simulations from Dhomse et al. (2014) (**Pin10** and **Pin20**) show a simpler peak and decay curve, with the removal from the stratosphere proceeding much faster and earlier than the HIRS measurements indicate.

As shown in Mann et al. (2015), and other studies (Young et al., 1994; Sukhodolov et al., 2018), when interactive stratospheric aerosol simulations of the Pinatubo cloud include the heating effect from aerosol absorption of outgoing  
385 LW radiation (i.e. the radiative coupling of the aerosol to the dynamics), the resulting enhanced tropical upwelling greatly changes the subsequent global dispersion. In Mann et al. (2015), we also showed that this coupling improves the simulated tropical mid-visible and near infra-red extinction compared to the SAGE II measurements. We identified that the SAGE II measurements are consistent with the combined effects of increased upwelling and later sedimentation, highlighting the need to resolve composition-dynamics interactions ~~when interactively simulating such major volcanic aerosol clouds~~.

Here we show that this effect also leads to a quite different global sulphur burden, with the later dispersion peak in the mid-latitude sulphur becoming a greater contributor. This behaviour is explored further in Figure 1b, where we assess the e-folding timescale for the removal of stratospheric sulphur, derived by ~~applyig~~ applying a least squares regression fit on 7-month running-mean mass burden values (3 monthly means either side). We find that a Pinatubo realisation that

395 injects more sulphur produces a volcanic aerosol cloud that is removed more rapidly, the effect apparent throughout the decay period. The timing of the accelerating removal occurs consistently across the 3 runs with residence times for **Pin10**, **Pin14** and **Pin20** decreasing from 9, 6 and 4 months in May 1992, to minima of 5, 3 and 2 months in February 1993.

400 Later (in Figure 4) we assess the behaviour of model-predicted effective radius, showing that it continues to increase steadily in the tropics throughout 1992, the maximum particle size at 20 km occurring in January 1993. That the maximum effective radius occurs at exactly the same time as the minimum in e-folding time illustrates the importance for interactive stratospheric aerosol models to represent its increased size, sedimentation of particles proceeding faster as the particles grow larger. One thing to note however, is that although the different volcanic SO<sub>2</sub> amount is emitted at the same altitude, since the runs are free-running, later we show that each different emission amount causes different amounts of heating, the resulting enhancements to tropical upwelling lofting the cloud to different altitudes.

405 The predicted stratospheric sulphur burdens in **Pin10** and **Pin14** compare compares well to the observations, suggesting a 10 Tg to 14 Tg SO<sub>2</sub> emission range will produce a volcanic aerosol cloud with realistic volcanic forcing magnitude. The comparison could provide a test for other interactive stratospheric models, to identify a model-specific source parameter calibration. It should be noted that such a reduction in emissions, to values below the SO<sub>2</sub> detected (Guo et al., 2004a), is a model adjustment, likely compensating for a missing sulphur loss/re-distribution process.

410 We also note some differences in sulphur burden between [current and previous \(Dhomse et al., 2014\) Pinatubo simulations](#) [this study's interactive Pinatubo simulations and the previous equivalent simulations presented in Dhomse et al. \(2014\)](#). Firstly, the background burden in run **Pin00** is much lower (0.11 Tg) than previous simulations (0.50 Tg) and now in reasonable agreement with [other studies](#) (Hommel et al., 2011; Sheng et al., 2015b; Kremser et al., 2016), [or with and at the](#) lower end of the [ASAP report \(SPARC, 2006\)](#) ([burden range estimates in SPARC \(2006\)](#) of 0.12-0.18 for Laramie 415 OPC balloon soundings and 0.12-0.22 Tg Garmisch lidar measurements[respectively; there cited, respectively. They are reported](#) as 0.5-0.7 Tg and 0.5-0.9 Tg mass of 75% weight aqueous sulphuric acid solution, respectively). The main reason for the reduction in simulated quiescent stratospheric sulphur burden, compared to Dhomse et al. (2014), is the influence from meteoric smoke particles (MSP), forming meteoric-sulphuric particles (Murphy et al., 2014). One of the effects from simulating these particles, [in addition to alongside](#) homogeneously nucleated pure sulphuric acid particles, is 420 [also](#) to reduce the sulphur residence time, [compared to equivalent quiescent simulations with pure sulphuric particles only](#) (Mann et al., 2019a). There are also some dynamical differences in the updated simulations here, which use an improved vertical and horizontal resolution model (N96L85 rather than N48L60), that might influence stratosphere-troposphere exchange and stratospheric circulation[\(e.g. Walters et al., 2014\)](#).

425 Secondly, we also assess the simulated stratosphere into the 3rd post-eruption year (after June 1993). Although for the first two years, the [models model's](#) global stratospheric sulphur in the simulations **Pin10** and **Pin14** tracks closely with HIRS estimates (Figure 1a), the satellite-derived S-burden drops off rapidly from about 3 Tg in January 1993 to 0.5 Tg by September 1993. On the other hand, the simulated volcanic aerosol cloud does not disperse down to that value until September 1994. However, this accelerated loss of stratospheric sulphur in the HIRS data seems to be inconsistent with other satellite measurements, for example [SAGE-II](#) [SAGE-II](#) measurements (see Figure 3), as well as OPC measurements

430 (Thomason et al., 1997b) and CLAES observations (e.g. Bauman et al., 2003; Luo, 2016). This suggests that latter part of the HIRS data may be inaccurate, though it seems difficult to identify a driving mechanism for this. Each of the model experiments suggest the ~~stratosphere~~ ~~stratospheric aerosol~~ remained moderately enhanced throughout 1993 and 1994.

435 Figure 2 shows, for each eruption magnitude, the zonal mean ensemble-mean stratospheric AOD at 550 nm (sAOD<sub>550</sub>) from the UM-UKCA Pinatubo simulations (**Pin10**, **Pin14**, **Pin20**), compared to three different volcanic forcing datasets.   
~~To clarify the exact nature of the easterly QBO phase and sAOD evolution in each ensemble member are shown Supplementary Figures S2 and S3, respectively. For this period, the GloSSAC CMIP6-GloSSAC V2 data should be considered the primary one, being as it is based on the latest version of the SAGE II, as an update from the gap-filled dataset from the SPARC ASAP report (SPARC, 2006, Chapter 3) versions of each of the different satellite products (Thomason et al., 2018; Kovilakam et al., 2020) .~~

440 As in the HIRS sulphur burden comparisons (Figure 1), the **Pin20** simulation, which best matches the satellite-observed SO<sub>2</sub> estimates, strongly ~~overpredicts~~ ~~over-predicts~~ the stratospheric AOD in the tropics and ~~Northern Hemisphere (NH)~~   
~~NH~~ mid-latitudes, compared to all three reference datasets. However, whereas the lower emissions runs **Pin10** and **Pin14** both closely track the observed global column sulphur variation, run **Pin10** has best agreement with all three reference datasets for mid-visible sAOD. For this run **Pin14** is high-biased in the tropics and NH mid-latitudes. In the tropics, all  
445 three emission-magnitude ensembles are higher than the reference datasets.

450 Figure 2 illustrates the well-established global dispersion pattern for the Pinatubo aerosol cloud: initially confined to the tropical reservoir region, then dispersing to mid-latitudes, following the seasonal variation in the Brewer-Dobson circulation. The over-prediction in the tropics is a common feature among interactive stratospheric aerosol models. It is noticeable that this over-prediction is worst in the first 6-9 months after the eruption, which could indicate the source of  
455 the model's discrepancy. Whereas an overly non-dispersive tropical pipe in the model could be the cause, the timing is potentially more consistent with a missing loss pathway that is most effective in the initial months after the eruption. Co-emitted volcanic ash will also have been present within the tropical reservoir, as seen in the airborne lidar depolarisation measurements in the weeks after the eruption (Winker and Osborn, 1992), and remained present in the lowermost part of the mid-latitude aerosol cloud in both hemispheres (Young et al., 1992; Vaughan et al., 1994). The AOD high bias  
460 is consistent with the hypothesis that a substantial proportion of the emitted sulphur may have been removed from the stratosphere by accommodation onto the sedimenting ash. If this mechanism is causing such a vertical re-distribution within the tropical reservoir, it will increase the proportion of Pinatubo sulphur being removed into the troposphere via the rapid isentropic transport that occurred during the initial months in the lowermost stratosphere. Furthermore, stratospheric AOD is not a measure of sulphur, and the variations in sAOD will partly indicate changes in scattering efficiency that ~~result~~   
~~results~~ from the gradient in effective radius that ~~is discussed in later~~ ~~were apparent at the time, as discussed in this~~ section.

465 The peak mid-visible AOD from AVHRR is higher than the ~~SAGE II~~ ~~SAGE-II~~ gap-filled satellite measurements (Long and Stowe, 1994). For example, as noted in Thomason et al. (2018), the peak mid-visible stratospheric AOD in the AVHRR dataset is around 0.4, compared to 0.22 in GloSSAC. However, other possible model biases cannot be ruled out. One consideration for these free-running simulations, even with each ensemble member initialised to approximate

465 the period's QBO phase, is that nudging towards re-analysis meteorology would give more realistic representation of this initial phase of the plume dispersion (Sukhodolov et al., 2018). We chose to perform free-running simulations to allow the enhanced tropical upwelling resulting from increased LW aerosol-absorptive heating, consistent with the SO<sub>2</sub> emission, known to ~~be a exert~~ strong influence on the subsequent simulated global dispersion (Young et al., 1994).

470 In contrast to the tropics and NH mid-latitudes, where run **Pin10** agrees best with the reference datasets, run **Pin14** compares best to the Southern Hemisphere (SH) sAOD<sub>550</sub> measurements in ~~GLOSSAC~~. ~~Runs and underestimate the cloud in this region.~~ GloSSAC. This difference may be highlighting the requirement for a more accurate simulation of the QBO evolution, likely necessary to capture the Pinatubo cloud's transport to SH mid-latitudes (e.g. Jones et al., 2016; Pitari et al., 2016). One thing to note is that our simulations do not include the source of volcanic aerosol ~~formed~~ from the August 1991 ~~Mount Cerro~~ Hudson eruption in Chile. However, measurements from ~~SAGE-II~~ SAGE-II (Pitts and Thomason, 1993) and ground-based lidar (Barton et al., 1992) indicate that the Hudson aerosol cloud only reached to around 12 km, with the Pinatubo cloud by far the dominant contributor to SH mid-latitude sAOD.

475 So, although we have not included the Hudson aerosol in our simulations, hence it is possible that minor contributor from Cerro Hudson sAOD might reduce differences between Pin10 and CMIP6-GloSSAC V2 sAOD. Overall, the sAOD<sub>550</sub> comparisons confirm the findings from Figure 1 that for UM-UKCA, consistent with other global microphysics models (Sheng et al., 2015a; Mills et al., 2016), Pinatubo aerosol properties are better simulated (acknowledging the discrepancy in the SH) with a 10 Tg to 14 Tg range in volcanic SO<sub>2</sub> emission.

480 Although Figure 2 suggests significant differences among the volcanic forcing datasets for the Pinatubo period, the ~~GLOSSAC-CMIP6-GloSSAC~~ data is the reference dataset while the ~~1991-4 period in Sato data~~ 1991-94 period in the Sato dataset is mostly based on an earlier version of the ~~SAGE-II~~ SAGE-II data. The GloSSAC data have been compared 485 extensively with lidar measurements (Antuña et al., 2002; Antuña, 2003), and combined for the gap-filled dataset (SPARC, 2006) with improvements in the ~~SAGE-II~~ SAGE-II aerosol extinction retrieval algorithm (version 7).

490 For historical climate integrations in CMIP5, some models used the Sato forcing dataset whilst others used Ammann and their differences affect interpretation of volcanic impacts among the models (Driscoll et al., 2012). For CMIP6, all models have harmonised to use the same forcing dataset, with a dedicated VolMIP analysis to compare the climate response in each model and with the ~~GloSSAC-CMIP6-GloSSAC~~ Pinatubo forcing applied to the pre-industrial control (Zanchettin et al., 2016).

495 After comparing the total sulphur burden and sAOD, Figure 3 shows UM-UKCA simulated mid-visible extinction at 3 different altitudes in the lower stratosphere, to evaluate the simulated vertical extent of the Pinatubo cloud through the global dispersion phase. For the tropics, extinction comparisons are shown at 24 km, 28 km and 32 km, whereas for SH (35°S-60°S) and NH (35°N-60°N) mid-latitudes the chosen levels are 20 km, 24 km and 28 km, to account for the higher tropical tropopause. Simulated extinctions are compared with raw SAGE v7.0 data (Damadeo et al., 2013) as well as the gap-filled ~~GloSSAC product~~ (Thomason et al., 2018) extinction from CMIP6-GloSSAC at 525 nm. As discussed previously, extinctions from **Pin14** (and to some extent **Pin10**) show much better agreement with observational data for all three latitude bands. Most importantly, model extinction remain close or slightly lower in the mid-latitude compared to

500 SAGE II extinction even after 4 years, suggesting that the sharp decay in ~~S-burden~~ sulphur burden observed by Baran and Foot (1994) may be unrealistic. Interestingly, in the SH mid latitudes, extinction from **Pin14** shows much better agreement with SAGE II extinctions at 20 and 24 km. This again confirms biases discussed in Figure 2 that could be attributed to the weaker lower stratospheric transport in the SH mid-latitudes, and Cerro Hudson eruption must have only slight contribution to the sAOD. At 1020 nm, agreement is even better (See Supplementary Figure **S1S3**). Also as observed in

505 Figure 1 and 2, extinction differences between runs **Pin10**, **Pin14** and **Pin20** are largest for the first few months after the eruption but extinction lines almost overlap within ensemble variance from each eruption. This again confirms that the more as greater amount of volcanic SO<sub>2</sub> injection, the faster growth and removal within first few months after the eruption is injected into the stratosphere, the cloud evolves to a larger average particle sizes, leading faster sedimentation.

510 One of the A key feature seen in Figure 3 that is not captured well in any model **Pinatubo** simulation is the plateau in the SAGE-II SAGE-II (and GloSSAC) tropical peak extinction. For example, at 24 km (where the effect of instrument saturation instrument saturation effect should be minimal), after reaching peak values within first 3 three months, extinction values remain almost flat approximately constant for at least 6 months. At 20 km, this plateau in extinction in the tropics is visible for almost 12 months in the GloSSAC CMIP6-GloSSAC data (not shown). Similar features are visible at 1020 nm extinction (Figure **S1S3**). If indeed these plateau features are realistic in observational data in 515 the SAGE-II data are realistic, then they would be maintained by balance between tropical up-welling (need to have been caused by the sustained tropical upwelling (via upward branch of the Brewer-Dobson circulationas well as one from, combined with aerosol-induced heating)and sedimentation of particles that, being offset by sedimentation of the particles that would have grown via coagulation. On the other hand, model-simulated extinction shows more prominent seasonal cycle fluctuations during NH winter when the Brewer-Dobson circulation (tropical upwelling) is strongest 520 (e.g. Dhomse et al., 2008; Weber et al., 2011; Butchart, 2014). condensation and coagulation. These plateau structures in extinctions are not so distinct at mid-latitudes in either hemisphere but seasonal cycle fluctuations that are determined by the wintertime circulation are apparent in the mid-latitudes of either hemisphere, with a clear seasonal cycle occurring due to preferential wintertime circulation (e.g. Dhomse et al., 2006, 2008), that is visible in both SAGE-II and model data. Another important difference model and SAGE-II data.

525 A notable discrepancy is that modelled extinctions are extinction is low-biased (by up to 50%) during pre-eruption months. This could be associated with low background ~~S-burden~~ sulphur burden in our model or slightly elevated stratospheric aerosol due to small volcanic eruptions (such as Mt. Redoubt 1989/90, Kelud,1990) that are not present included in our simulations. Another explanation could be due to the fact that model not resolving the model does not resolve the uptake of organics, with observations Murphy et al. (2007) and modelling (Yu et al., 2016) suggesting into the particle phase. Observations (Murphy et al., 2007) and modelling studies (Yu et al., 2016) have shown that organic-sulphate particles (Murphy et al., 2014) are the dominant aerosol type in the tropical and mid-latitude upper troposphere and lower stratosphere, and the omission of this interaction might have introduced systematic low bias during background periods.

530 Next, we compare we evaluate the meridional, vertical and temporal variations in effective radius (Reff) at similar altitudes in the Pinatubo UM-UKCA datasets. The particle size variations in these interactive simulations of the Pinatubo

535 cloud reflect the chemical and microphysical processes resolved by the chemistry-aerosol module, in association with the stratospheric circulation and dynamics occurring in the general circulation model. We analyse these model-predicted size variations alongside those in the benchmark observation-based  $Reff$  dataset from CMIP6-GloSSAC, which applies the 3- $\lambda$  size retrieval from the 453 nm, 525 nm and 1020 nm aerosol extinction measurements from SAGE-II (Thomason et al., 1997a, 2018).

540 Figure 4 shows zonal mean  $Reff$  at 20 and 25 km ~~from runs~~, within the altitude range of the volcanic  $SO_2$  injection, and at 20 km, underneath the main volcanic cloud. Results are shown from 3-member means from the 10, 14 and 20 Tg  $SO_2$  emission runs (Pin10, Pin14 ~~along with observation-based  $Reff$  described in Luo (2016)~~. As shown in previous sections, ~~and Pin20~~ clearly shows a high bias compared to S-burden,  $sAOD_{550}$  as well as extinction observations, hence it is excluded in Figure 4. Overall, the temporal and spatial evolution of  $Reff$  estimated using observational data seems to be well captured in ~~compared to (although  $Reff$  magnitude is high-biased by about )~~. For comparability with the equivalent figure from Dhomse et al. (2014), the Supplementary Material (Figure S6) shows the updated comparison to the Bauman et al. (2003)  $Reff$  dataset. Overall, the model captures the general spatio-temporal progression in the  $Reff$  variations seen in the GloSSAC dataset. However, whereas the 10%). Another important feature is that  $Reff$  at 25 km in the model simulations persists much longer than CMIP6  $Reff$ . It is important to note that Russell et al. (1996) analysed a range of ~~in-situ~~ Tg and 14 Tg simulations agree best with the HIRS-2 sulphur burden (Figure 1) and the GloSSAC  $sAOD$  and extinction (Figures 2 and ~~ground-based remote sensing measurements from the post-Pinatubo period, showing that optical depth spectra observed from Mauna Loa are consistent with  $Reff$  values of 0.6 to 0.8 microns continuing until mid to late 1992 at this near-tropical latitude, with dust sonde (OPC) measurements from Laramie balloon soundings measurements also showing  $Reff$  of 0.4 to 0.6 microns in 3), the magnitude of the  $Reff$  enhancement is best captured in the mid-latitude lower stratosphere. Hence,  $Reff$  enhancement after Pinatubo, in CMIP and model simulation are broadly in good agreement with the measurements analysed in Russell et al. (1996)~~. And this clearly shows significant improvement since Dhomse et al. (2014) where  $Reff$  was underestimated by about 50%. The updated comparison to the Bauman et al. (2003)  $Reff$  dataset, derived from SAGE II and CLAES measurements, is shown in Supplementary Figure S4. These improvements were noticed during model development after Dhomse et al. (2014) to include meteoric smoke particles and their interactions at version 8.2 of 20 Tg run (Pin20). The comparisons suggest the low bias in simulated  $Reff$  seen in the previous UM-UKCA Pinatubo study (Dhomse et al., 2014) is still present here. However, this low bias in particle size/growth may simply be reflecting the required downward-adjustment of the Pinatubo  $SO_2$  emission, as a larger  $Reff$  enhancement in the GLOMAP codebase (~~?Mann et al., 2019a; Marshall et al., 2019~~) 20 Tg simulation is clearly apparent. It is possible that the two-moment modal aerosol dynamics in GLOMAP-mode may affect its predicted  $Reff$  enhancement. However, the model requirement for reduced  $SO_2$  emission is attributed to be likely due to a missing, or poorly resolved, model loss pathway, such as accommodation onto co-emitted volcanic ash. The sustained presence of ash within the Pinatubo cloud (e.g. Winker and Osborn, 1992) will likely have altered particle size and growth rates in the initial months after the eruption.

In the tropics, where  $R_{eff}$  increases are largest, the timeseries of  $R_{eff}$  is noticeably different at 20km and 25km. At 570 25km, the model simulations are somewhat counter-intuitive. Initially, they show decrease in  $R_{eff}$ , likely due to this in the core of the tropical reservoir (10°S to 10°N) to that in the edge regions (10°N-20°N and 10°S-20°S), at both 20 km and 25 km. The  $R_{eff}$  increases in these edge regions occur when tropics to mid-latitude transport is strongest, 575 in phase with the seasonal cycle of the Brewer-Dobson circulation, which tends to transport air towards the winter pole (Butchart, 2014). The  $R_{eff}$  increases are due primarily to particle growth from coagulation and condensation, and the simulations also illustrate how the simulated Pinatubo cloud comprises much smaller particles at 25 km than at 20 km. 580 The 25 km level is in the central part of the volcanic cloud Pinatubo cloud, particles there being younger (and smaller) particles formed as because the oxidation of the volcanic  $SO_2$  emitted volcanic  $SO_2$  that occurs at that level triggers extensive new particle formation in the initial months after the eruption (e.g. Dhomse et al., 2014). By contrast, at 20km, below the altitude at which the volcanic plume detrains the  $SO_2$  (injection height range is 21-23km) the effective radius shows a steady increase, as relatively larger particles sediment to these altitudes as the tropical volcanic aerosol reservoir progresses. 585 The 20 km level particles will almost exclusively have sedimented from the main cloud, and therefore be larger. There is a slow but substantial growth in the sustained increase in average particle size in this the equatorial core of the tropical Pinatubo cloud, with the 20km 20 km level reaching peak  $R_{eff}$  values only during mid-1992, in contrast to the peak S-burden sulphur burden and  $sAOD_{550}$  which have already peaked at this time, being in decay phase since the start 590 of 1992 (see Figures 1 and 2).

Whereas the simulated peak  $R_{eff}$  enhancement occurs by mid-1992 in the tropics, in the NH the peak  $R_{eff}$  in NH mid-latitudes, the peak  $R_{eff}$  occurs at the time of the peak meridional transport, the  $R_{eff}$  variation there mainly reflecting the seasonal cycle of the BD circulation (Butchart, 2014) Brewer-Dobson circulation, as also seen in the tropical reservoir edge region. The different timing of the volcanic  $R_{eff}$  enhancement in the tropics and mid-latitudes is important 595 when interpreting or interpolating the in-situ measurement record from the post-Pinatubo OPC soundings from Laramie (Deshler, 2003). Russell et al. (1996) show that the  $R_{eff}$  values derived from the Mauna Loa ground-based remote sensing are substantially larger than those from the dust sondes dust-sonde measurements at Laramie. Model simulation confirms this inherent coupling between dynamics, circulation and microphysical growth processes causes a different relationship between The interactive Pinatubo simulations here confirm this expected meridional gradient in effective radius, with the chemical, dynamical and microphysical processes also causing a vertical gradient in the tropical to mid-latitude ratio in  $R_{eff}$  in the upper and lower portions of the volcanic aerosol cloud  $R_{eff}$  ratio. The current ISA-MIP activity (Timmreck et al., 2018) brings a potential opportunity to identify a consensus among interactive stratospheric aerosol models for the expected broad-scale spatio-temporal variations in uncertain volcanic aerosol metrics such as effective radius.

600 An important aspect of volcanically enhanced stratospheric aerosol is that they provide surface area for catalytic ozone loss (e.g. Cadle et al., 1975; Hofmann and Solomon, 1989). Stratospheric A comparison of stratospheric sulphate area density comparison for three different months (December 911991, June 1992 and December 1992) is shown in Figure 5. SAD derived using observational data (Arfeuille et al., 2014), also known as  $3\lambda$  SAD, is also shown. Again, Pin20 SAD

shows a high ~~bias~~<sup>bias</sup>, whereas **Pin10** SAD seems to show good agreement with  $3\lambda$  data. Our simulations do not include the  $\text{SO}_2$  injection from the August 1991 ~~Mt. Cerro~~ Hudson eruption (Chile), ~~and~~ yet the model captures ~~well~~ the volcanic SAD enhancement in the SH mid-latitude stratosphere ~~very well~~. The model does not capture the enhanced SAD signal at ~~10-12km in the Southern Hemisphere~~ ~~10-12 km in the SH~~ in December 1991, the altitude of that feature in the  $3\lambda$  dataset ~~is~~ consistent with lidar measurements of the Hudson [aerosol](#) cloud from Aspendale, Australia (Barton et al., 1992). The most critical differences are that  $3\lambda$  SAD are confined in the lowermost stratosphere. ~~A~~ A deeper cloud of enhanced SAD, with steeper low-high latitude SAD gradients ~~are~~ ~~is~~ visible in all the model simulations. As seen in Figure 3, by June 1992 tropical SAD from runs **Pin10** and **Pin14** are low-biased, indicating lower aerosol in the tropical pipe which could be either due to faster transport to the high latitudes (weaker subtropical barrier in the middle stratosphere) and/or quicker coagulation ~~thereby causing~~ faster sedimentation.

Figure 6 shows the time series of observed SW and LW radiative near-global mean flux anomalies ( $60^\circ\text{S}$  -  $60^\circ\text{N}$ ), with respect to a 1985 to 1989 (pre-Pinatubo) baseline. ~~ERBE~~ [The ERBE data](#) (black symbols) ~~data~~ is from Edition 3 Revision 1, non-scanner, wide ~~field-of-view~~ [field-of-view](#) observations (Wielicki et al., 2002). Coloured lines indicate ensemble mean ~~forcings~~ [forcing](#) anomalies from three Pinatubo  $\text{SO}_2$  emission scenarios. The **Pin10** simulation generates a peak solar dimming of  $4 \text{ W/m}^2$ , matching well both the timing and magnitude of the peak in the ERBE SW anomaly timeseries. It is notable that if the ERBE SW anomaly is calculated relative the 1995-1997 baseline, we ~~see~~ [estimate](#) a peak solar dimming of  $5.5 \text{ W/m}^2$  (not shown), which then compares best with the Pinatubo SW forcing from **Pin14**. ~~Consistently~~ [Consistent](#) with the the ~~S-burden~~ [sulphur burden](#),  $\text{sAOD550}$  and mid-visible extinction comparisons (Figures 1, 2 and 3), the **Pin20** simulation also ~~overpredicts~~ [over-predicts](#) the magnitude of the Pinatubo forcing compared to ERBE. It is important to note here that the model Pinatubo forcings are not only from the volcanic aerosol cloud, but include also any effects from the simulated post-Pinatubo changes in other climate forcers (e.g. stratospheric ozone and water vapour). As expected run **Pin20** shows largest anomalies in both SW and LW radiation and distinct differences between **Pin10**, **Pin14** and **Pin20** are visible until the end of 1992. For this 10 to 20Tg emission range, we find the global-mean SW forcing scales approximately linearly with increasing  ~~$\text{SO}_2$~~  [SO<sub>2</sub>](#) emission amount, the 40% increase from 10 to ~~14Tg~~ [14 Tg](#) and 43% increase from 14 to ~~20Tg~~ [20 Tg](#) causing the Pinatubo SW forcing to be stronger by 34% ( $4.1$  to  $5.5 \text{ W/m}^2$ ) and 36% ( $5.5$  to  $7.5 \text{ W/m}^2$ ), respectively.

In contrast to the SW forcings, the magnitude of the anomaly in the peak LW forcing is best matched in the **Pin20** simulation, although the **Pin14** simulation also agrees quite well with the ERBE anomaly timeseries. Whereas the Pinatubo SW forcing ~~will follow closely~~ [closely follows](#) the mid-visible aerosol changes, the LW forcing is more complex to interpret, ~~simulated~~. [Simulated](#) LW aerosol absorption ~~not analysed~~ [is not studied](#) in this paper, and almost certainly ~~having~~ [has](#) a different temporal variation than the 550 nm and 1020 nm extinction variations analysed here. Also, the model LW forcing also includes effects from the dynamical changes in stratospheric water vapour which partially ~~offsets~~ [offset](#) the SW dimming (e.g. Joshi et al., 2003) adding to the LW aerosol effect. Our simulations do not include co-emission of water vapour, which might have ~~influenced~~ [influenced](#) stratospheric chemistry (e.g. LeGrande et al., 2016) and altered observed Pinatubo forcing. Another possible explanation for this discrepancy might be much weaker signal in LW radiation

alongside ERBE temporal coverage (36 days vs 72 days). Again, as in the sulphur burden and extinction comparisons, 640 after January 1992 observed SW anomalies seem to decay at a faster rate compared to all the model simulations.

Another important volcanic impact is the aerosol-induced heating in the lower stratosphere as large particles absorb outgoing LW radiation. Since the ERA-interim analysis assimilates radiosonde observations from large number of sites in the tropics, we can compare the temperature anomaly to the model predictions, as a further independent test. However, 645 exact quantification of this mechanism is somewhat ~~complicated as the ERA-interim~~ complicated as the ERA-Interim stratospheric temperature anomalies also ~~includes~~ include influence from other chemical and dynamical changes such as ~~variation~~ variations in ozone and water vapour as well as QBO and ~~ENSO-related~~ ENSO-related changes in tropical upwelling (e.g. Angell, 1997b; Randel et al., 2009). ~~Assuming~~ We can assume the 5-year anomalies will remove effects of some of the short-term processes. Modelled temperature anomalies are simply differences between the sensitivity (**Pin10**, **Pin14** and **Pin20**) and control (**Pin00**) simulations. Although we compare the simulated Pinatubo warming (temperature 650 difference) to ERA-interim temperature anomalies, this is only intended to provide an approximate observational constraint for the magnitude of the effect and the altitude at which it reaches a maximum. The **Pin10** simulation best captures the magnitude of the ~~ERA-interim~~ ERA-Interim post-Pinatubo tropical temperature anomalies, and the model simulations and re-analysis both show maximum warming occurred in the 30 to 50 hPa range around 3-4 months after the eruption. The model predicts Pinatubo aerosol cloud continued to cause a substantial warming (> 2 K) throughout 1992, ~~that~~ which 655 propagates downwards as in ~~ERA-interim~~ ERA-Interim temperature anomalies.

## 4.2 El Chichón aerosol cloud

Whereas Pinatubo is often the main case study to evaluate interactive stratospheric aerosol models, El Chichón provides a different test ~~for the models~~, as its volcanic aerosol cloud ~~dispersing~~ dispersed almost exclusively to the NH. We 660 ~~also~~ therefore seek to understand whether the biases seen for Pinatubo (over-predicted tropical sAOD and discrepancy between literature estimates of ~~SO2~~ SO<sub>2</sub> emission and the peak global aerosol loading) are also seen for this alternative major eruption case.

Both El Chichón and Pinatubo eruptions occurred in the modern satellite era, however there are far fewer datasets available for the evaluation of El Chichón aerosol properties as it occurred in the important gap period between SAGE-I and SAGE II (see Thomason et al., 2018). ~~Although~~ As there are quite extensive observational data records for the El 665 Chichón volcanic aerosol clouds (e.g McCormick and Swissler, 1983; Hofmann and Rosen, 1983a), combining these ~~data~~ with satellite datasets would greatly reduce large uncertainties ~~about~~ concerning the evolution of the El-Chichón aerosol cloud (e.g. Sato et al., 1993; SPARC, 2006).

Here, our analysis focuses primarily on comparing simulated mid-visible stratospheric AOD at 550 nm (sAOD<sub>550</sub>) to the CMIP6 and Sato datasets. We also test the simulated vertical extent of the El Chichón cloud, comparing extinction at 670 20 km and 25 km to the SAGE II (and GloSSAC) data record, and compare the ~~models~~ model's simulated warming in the tropical lower stratospheric to temperature anomalies in the ERA-Interim reanalyses.

Figure 8 compares ensemble mean sAOD<sub>550</sub> from **EIC05**, **EIC07**, **EIC10** and three observation-based datasets. Overall, there are significant differences between simulated sAOD<sub>550</sub> and the observations. The **CMIP6-CMIP6-GloSSAC** dataset enacts strongest solar dimming in NH mid-latitudes (peak sAOD<sub>550</sub> of **0.28**0.14), the tropical reservoir never exceeding a sAOD of **0.16**0.08, whereas the Sato and Ammann datasets, enact highest sAOD<sub>550</sub> in the tropics. The model simulations 675 also find highest solar dimming occurred in the tropical reservoir, with the mean of the 5 Tg simulations predicting a maximum sAOD<sub>550</sub> of about 0.28. With the QBO in the westerly phase, and timing of the eruption (4th April), **BD circulation exported the Brewer-Dobson circulation readily exported a** large fraction of the plume **readily** to the NH, but the meridional gradient in the solar dimming is an important uncertainty to address in future research

680 In the model, how deep the the depth of the tropical volcanic aerosol reservoir that forms is closely linked to the altitude of the volcanic **SO<sub>2</sub>-SO<sub>2</sub>** emission. We aligned our experiments with the ISA-MIP HERSEA experiment design (Timmreck et al., 2018), specifying a 24-27 km injection height based on the information from the airborne lidar measurements in airborne lidar measurement surveys of the tropical stratosphere that provide the main constraint for the gap-filled dataset (see Figure 4.34 in the ASAP report (SPARC, 2006) **SPARC (2006)**). Balloon measurements from **Southern** southern 685 Texas and Laramie (Hofmann and Rosen, 1983b), and the constraints from the airborne lidar survey flights in July, September and October (McCormick and Swissler, 1983) will likely provide a good constraint for the interactive models, showing, together show that a large part of the plume was transported early to NH mid-high latitudes via middle branch of the **Brewer-Dobson** Brewer-Dobson circulation at around **25km**, the 25 km, with lower altitudes of the cloud remaining confined to the tropical reservoir. The evolution of the cloud is complex and strongly influenced by several effects: factors, 690 including the rate of SO<sub>2</sub> conversion to aerosol and the depletion of oxidants, the tropical upwelling of the **Brewer-Dobson** Brewer-Dobson circulation, sedimentation of the ash and sulphuric acid droplets (and their interactions) and the downward propagating QBO. The multiple interacting processes within the tropical reservoir make analysing makes analysis of this early phase dispersion a complex problem, yet their combined net effects determines the subsequent transport of the aerosol to mid-latitudes, and the **radiative forcing that results** resulting radiative forcing.

695 Due to significant differences observed in Figure 8, even with limited **SAGE-II** SAGE-II observations, simulated extinctions are compared in Figure 9. Simulated extinctions for all three SO<sub>2</sub> emission scenarios show an excellent agreement with **SAGE-II** SAGE-II from October 1984 onwards. Similarly at extinction at 1020 nm also shows very good agreement with SAGE-II data that is shown in Supplementary Figure S4. A sudden jump in the **GloSSAC-CMIP6-GloSSAC** data at the start of the **SAGE-II** SAGE-II period is evident, and other unexplained sudden increases in extinction earlier in the 700 CMIP6 dataset, e.g. in the SH at **24km**24 km. On the other hand, somewhat elevated SAGE-II the somewhat elevated SAGE-II extinction in the NH mid-latitudes compared to model extinctions highlight possible highlights possible a model discrepancy due to the injection altitude leading to faster removal. GloSSAC extinction in the SH mid-latitude shows very little seasonal variation, and the sudden changes seen at both 20 and **24km**24 km are surprising and difficult to reconcile with expected variation, and. They could potentially be artefacts from the interpolation procedure. Overall, Figure 705 9 clearly suggests potential areas where combining with models may help improve the **GloSSAC-CMIP6-GloSSAC**

(and other) datasets, highlighting the need for combining observational data with El Chichón-related model simulations to better represent the consistency and variations within the El Chichón surface cooling included in climate models.

Figure 10 shows the tropical warming of the stratosphere predicted by the model, comparing again to the **ERA-interim** **ERA-Interim** temperature anomaly (compared to the mean for 1982-1986). As in **the** Pinatubo case (Figure 7), the speed of downward propagation of these anomalies seems to be well captured by all the simulations. Peak warming of about 3 K observed in **ERA-interim** **ERA-Interim** between 30-50 hPa seems to be well reproduced in **Elc07**. Warm anomalies (up to 1 K) visible in **ERA-interim** **ERA-Interim** data between 10-20 hPa suggest the downward propagating westerly QBO contributed to up to 1 K warming, hence **the** simulated warming will be about **+K-1 K** less than the **ERA-interim** **ERA-Interim** anomalies. Overall, **Elc05** seems to reproduce **the** El Chichón-related warming more realistically but the slight warming persisting near 70 hPa until March 1983 is absent in this simulation. Again this **suggest** **suggests** that for UM-UKCA, 5 Tg and 7 Tg are reasonable lower and upper limits of SO<sub>2</sub> injection required to simulate observed lower stratospheric warming.

#### 4.3 Mt. Agung aerosol cloud

The El **Chichón** **Chichón** and Pinatubo eruptions occurred when satellite instruments were monitoring the stratospheric aerosol layer, and the global dispersion of their volcanic aerosol clouds are relatively well characterised. For the Agung period our knowledge of the global dispersion is less certain and primarily based on the synthesis of surface radiation measurements from Dyer and Hicks (1968). These measurements show the Agung cloud dispersed mainly to the SH, although aerosol measurements from 10 balloon-borne particle counter soundings from Minneapolis in 1963-65 (Rosen, 1964, 1968) and ground-based lidar from Lexington, **Massachusetts** **Massachusetts** in 1963 and 1964 (Grams and Fiocco, 1967) show substantial enhancement in the NH as well. For this period, the Sato forcing dataset enacts solar dimming following the ground-based solar radiation measurements discussed in Dyer and Hicks (1968), whereas the **CMIP6** **CMIP6-AER2D** dataset is based on **simulations with a 2D a 2-D** interactive stratospheric aerosol model **simulations**.

To address these limitations, **the** SPARC (Stratosphere-Troposphere Process and their Role in Climate Project) project entitled SSiRC (Stratospheric Sulphur and its Role in Climate) initiated a stratospheric aerosol data rescue project (see <http://www.sparc-ssirc.org/data/datarescueactivity.html>). Its primary aim is to gather and in some cases re-calibrate post-Agung aerosol measurements from major volcanic periods to provide new constraints for stratospheric aerosol models. For example, ship-borne lidar measurements of the tropical volcanic aerosol reservoir after Pinatubo have recently been recovered (Antuna-Marrero et al., 2020; Mann et al., 2020). As part of this **paper** **study**, we are contributing to this SSiRC activity and have recovered the Lexington post-Agung ground-based lidar measurement from Grams and Fiocco (1967) and use these to constrain the vertical extent of the Agung aerosol cloud.

Figure 11 compares sAOD<sub>550</sub> from model simulations with **CMIP6** **CMIP6-AER2D**, Sato and Ammann data. Both CMIP6 and Sato datasets suggest **the** **that** tropical volcanic aerosol cloud dispersed rapidly, and almost exclusively, to the SH, **consistent also which is also consistent** with our understanding of QBO-dependent meridional transport (Thomas et al., 2009). This means that during the westerly QBO phase the volcanic plume is quickly transported towards the winter

740 hemisphere whereas during the easterly phase the tropics-to-high-latitude transport is slower, hence some part of the plume is available for the wintertime transport into the opposite hemisphere. In contrast, the Ammann dataset suggests a significant part of the cloud was transported to the NH, the dispersion parameterisation considering only seasonal changes in stratospheric circulation. Hence, the modulation of meridional transport caused by the QBO, in the Agung case, increasing the export from low to mid-latitudes, is not represented in the Ammann dataset.

745 Figure 11 also shows that for the post-Agung period, there are very large differences in the  $sAOD_{550}$  between **CMIP6** **CMIP6-AER2D** and Sato data. Hence, climate simulations performed using these two forcing data sets would have significantly different response between two CMIP assessment. Overall, the CMIP6 dataset generates much stronger peak  $sAOD_{550}$  than Sato, with a peak of around **0.4** **0.2** in the tropics, a few months after the eruption. Sato data shows a peak value of about 0.12, which suddenly drops to below 0.05 within couple of months. **Then** **after** **Then** **after** there 750 is a steady build-up with a local peak in  $sAOD_{550}$  occurring in November 1963, 8 months after the eruption. The Sato dataset then enacts a much stronger second peak in tropical  $sAOD_{550}$  in August-September 1964 that must be based on measurements from Kenya and the Congo (Dyer and Hicks, 1968). By contrast, **CMIP6, based on the AER-2D model**, **CMIP6-AER2D**, predicts the Agung cloud dispersed rapidly to the SH with the tropical reservoir reducing to  $sAOD_{550}$  of less than 0.05 at that time. Our simulations predict the Agung aerosol dispersed to the SH with similar timing to the 755 CMIP6 dataset, but with a larger proportion remaining in the tropical reservoir. Similar to CMIP6 datasets our simulations also predict secondary  $sAOD_{550}$  peak in SH mid-latitudes near  $40^{\circ}$ S. Although a similar pattern is produced in almost all simulations,  $sAOD_{550}$  from **Agu06** seems to be in much better agreement with CMIP6 data.

760 These comparisons highlight that there is still substantial uncertainty about the global dispersion of the Agung cloud. However, there are extensive set of stratospheric aerosol measurements carried out during this period (see <http://www.sparc-ssirc.org/data/datarescueactivity.html>). Hence, there is potential to reduce this uncertainty combining these observations also with interactive stratospheric model simulations (Timmreck et al., 2018). Dyer and Hicks (1968) discuss the 765 transport pathways for the volcanic aerosol, in relation to seasonal export from the tropical reservoir. Stothers (2001) analysed a range of measurements to derive the turbidity of the Agung cloud, but they neglected measurement from Kenya and Congo sites in their analysis, attributing a lower accuracy in those data. It is notable those observations were 770 during the dry season, when other sources of aerosol could potentially have caused additional solar dimming. In terms of modeling, Niemeier et al. (2019) discussed possible implications of two separate Agung eruptions in 1963. They performed two model simulations, one with a single eruption and one with two separate eruptions on 17th March and 16th May with 4.7 Tg and 2.3 Tg  $SO_2$  injection, respectively. They found significant differences between simulated aerosol properties and available evaluation datasets. They suggested that two separate eruptions are necessary to simulate the climatic impact. However, due to limited observational data they could not validate their model results extensively. They also discussed that simulated  $sAOD_{550}$  differences with respect to evaluation data are larger than the differences 775 between their two simulations. **Pitari et al. (2016a)** **Pitari et al. (2016b)** also present global mean  $sAOD_{550}$  changes after the Agung eruption with single eruption (12 Tg on 16 May 1963), but they did not show the latitudinal extent of the Agung volcanic cloud dispersion.

775 Figure 12 compares simulated and ~~CMIP6~~<sup>CMIP6-AER2D</sup> extinctions at 550 nm at 16, 20 and 24 km. As in previous figures ~~the~~ tropical comparison is shifted upwards by 4 km. Overall, modelled and CMIP6 extinctions show ~~an~~ almost identical decay rate. At 16 km, nearly all the model simulations show ~~a~~ high bias compared to CMIP6 data and model extinction. On the other hand, at 20 km, tropical CMIP6 extinction seems to peak a bit later and there is better agreement in the mid-latitude extinction in both ~~the~~ hemispheres. The UM-UKCA extinctions reflect the primary influence from the  
780 QBO because of changing the sub-tropical edge of the tropical reservoir as well as peak wintertime meridional transport in either hemisphere. On the other hand, CMIP6 extinctions ~~show~~ show a strong seasonal cycle in the tropics. The differences between our model and CMIP6 extinction must be primarily due to injection altitude and the simplified aerosol microphysical model used to construct CMIP6 data. ~~Similar evolution is observed in the extinctions at 1020 nm as shown in supplementary Figure S3.~~

785 Figure 12 also shows the extinction from the early ground-based lidar at Lexington, Massachusetts ( $42^{\circ}44'N$ ,  $71^{\circ}15'W$ ) as presented in Grams and Fiocco (1967). The method used to convert lidar backscatter to extinction is described in the Supplementary Material. Although lidar data shows large variability, these single location measurements still provide better insight ~~about~~ into the transport of Agung aerosol cloud in the NH. At 16km, **Agu09** seem to show better agreement with lidar data, although by spring 1965, simulated extinctions are lower than the lidar data, suggesting faster decay in the  
790 model at this level. A similar pattern is observed at 20 km. ~~The somewhat~~ **Somewhat** larger lidar extinction in spring 1965 compared to model simulations might be due to either weak model tropics-to-NH-mid-latitude transport (more transport to the SH), or aerosol removal is too fast in the simulations. Extinctions at 24 km are shown in supplementary Figure **S4S5**, and again confirm good agreement between lidar and **Agu09**. Overall, the extinction comparison with Lexington lidar data suggests that transport of the Agung volcanic cloud and its vertical extent in to the NH mid-latitude is well represented in  
795 **Agu09**.

800 Finally, we compare tropical warming in Figure 12. As ERA-Interim reanalyses ~~start~~ starts in 1979, ~~hence~~ we calculate observational-based anomalies from ERA-40 data. Bearing in mind that almost all the reanalysis datasets have significant inhomogeneities in the pre-satellite era, observation-based warming estimates should be treated carefully. However, as expected ERA-40 data show almost 1 K warming in the middle stratosphere before the eruption indicating downward propagation of warmer anomalies associated with the westerly QBO. Using radiosonde data, Free et al. (2009) estimated about 1.5 K warming near 50 hPa, which is somewhat consistent with ERA-40 (after removing 1 K warming due to westerly QBO). However, almost all of the simulations show 1-2 K more warming compared to ERA-40 data as modelled temperature differences do not include QBO-related anomalies.

## 5 Conclusions

805 We have applied the interactive stratospheric aerosol configuration of the UM-UKCA model to simulate the formation and global dispersion of the volcanic aerosol clouds from the three largest tropical eruptions of the 20th century, ~~the~~ Agung, El Chichón and Pinatubo. The simulations are analysed to assess the evolution of each eruption cloud, from an initial tropical

reservoir of volcanic aerosol to a hemispherically dispersed stratospheric aerosol cloud. For each eruption, 3-member ensembles are carried out for each of upper, lower and mid-point of the literature range of SO<sub>2</sub> emission, aligning with 810 the design of the co-ordinated HErSEA experiment, part of the multi-model ISA-MIP interactive stratospheric aerosol modelling initiative (see Timmreck et al., 2018). The analysis is also designed to provide new "microphysically-consistent and **observationally-constrained** **observationally-constrained**" volcanic forcing datasets for climate models, to represent each **eruption** **eruption**'s surface cooling more realistically.

Simulated aerosol optical properties are compared against a range of satellite datasets. The model captures the observed 815 variation in global stratospheric sulphur from 1991-3 HIRS measurements very well, and experiments **Pin10** and **Pin14** defining a model-specific 10 to 14 Tg emissions uncertainty range and identifying a potential weighting to define a best-fit forcing dataset for Pinatubo. Our simulations also show that the aerosol decay rate is inversely proportional to the SO<sub>2</sub> injection amount, illustrating how increased aerosol particle size causes faster sedimentation. The model ensembles **compares** **compare** very well to mid-visible and near-infra-red aerosol extinction from **SAGE-II** **SAGE-II** measurements. 820 Although, the model shows higher sAOD biases in the tropics, it is common feature seen in interactive stratospheric aerosol models (e.g. Mills et al., 2016; Sukhodolov et al., 2018; Niemeier et al., 2019). We have also compared the Pinatubo ensembles to the three widely used forcing datasets (CMIP6–GloSSAC, Sato and Ammann) and we find that **the** **Pin14** model ensemble shows overall best agreement. A plateau in lower stratospheric tropical extinction seen in **GloSSAC** **CMIP6-GloSSAC** data for almost one year after the Pinatubo eruption, is not reproduced in our simulations and 825 thus remains as an open scientific question. The **10-14Tg** **10-14 Tg** SO<sub>2</sub> emissions rage for the model is lower than the 14-23 Tg observed to be present after the eruption (Guo et al., 2004b), and the tropical sAOD<sub>550</sub> high bias is consistent with the models missing an important removal process. Plausible suggestions for these are: a) the vertical redistribution of the volcanic cloud due to ash, b) changes in SO<sub>2</sub> oxidation due to OH decrease inside the plume, and c) too strong a subtropical barrier in the models.

830 The simulated Reff shows good agreement with **CMIP6 data**, **CMIP6-GloSSAC data**, although the model simulates a deeper global layer of enhanced SAD than in the  $3\lambda$  dataset (Luo, 2016). Simulated global-mean SW forcing (solar dimming) in run **Pin10** shows excellent agreement with the magnitude of the anomaly in the ERBE data, and the LW forcing in the model also **matching** **matches** well with the magnitude and shape of the ERBE anomaly. Assuming a 1 K colder temperature anomaly in ERA-Interim tropical temperatures due to the downward propagating QBO, a warming 835 of 3 K near 50 hPa is well simulated in both **Pin10** and **Pin14** simulations. Overall, most of the comparisons suggest that about 10-14 Tg SO<sub>2</sub> injection between 21-23 km is sufficient to simulate the climate and chemical impact of the Mt. Pinatubo eruption.

840 For the El Chichón eruption, there are significant differences between observation-based sAOD<sub>550</sub> estimates, hence evaluation of the simulations is somewhat restricted. However, NH mid-latitudes generally have a good quality observational data record, and sAOD<sub>550</sub> from run **Elc05** shows good agreement with CMIP6 **data but run shows best agreement with Sato dataset and** in the tropics **model compares better with Sato dataset**. Our extinction comparisons also show that there are **clear** inhomogeneities in the **GloSSAC** **CMIP6-GloSSAC** data during this period, hence El Chichón-related

aerosol properties must be treated with caution. Based on comparisons of the lower stratospheric warming of about 2 K, 5 Tg and 7 Tg SO<sub>2</sub> injections seem to be reasonable lower and upper limits for what is required to simulate observed 845 temperature changes.

Finally, evaluation of Mt. Agung aerosol is more complicated due to much larger differences in the observation-based datasets. Due to the westerly phase of QBO and timing of the eruption, CMIP6 data show a tropical peak in sAOD<sub>550</sub> within a month of the March eruption which is transported to SH mid-latitudes by October. Sato dataset suggest two 850 peaks in the tropics 8 and 14 months after the eruption. Run **Agu06** shows reasonable agreement with limited amount of observational extinction data, although that is not conclusive. Comparison with the lidar measurements from Lexington suggests that the vertical extent of the Agung volcanic cloud in the NH mid-latitudes ~~is~~ is in good agreement with run **Agu09**. Comparisons with ERA-40 temperature anomalies also suggests that 3 K warming in the tropical stratosphere (2 K in the model simulation due to westerly phase of QBO). Assuming CMIP6-simulated sAOD<sub>550</sub> is realistic, 6 Tg and 9 Tg SO<sub>2</sub> injection seem to be the best lower and upper estimates required to simulate Mt. Agung-related aerosol in the 855 UM-UKCA.

Overall, we have validated the interactive stratospheric aerosol configuration of the GA4 UM-UKCA model ~~is~~ and have shown the simulated aerosol properties for the Pinatubo ensemble are consistently in good agreement to a range of satellite-based observational datasets. For Pinatubo, we have also compared to three different independent tests of the 860 radiative effects from the volcanic aerosol cloud: the ERBE flux anomaly timeseries in the SW and LW, and the stratospheric warming in the ERA-interim re-analysis. These comparisons confirm that a 10 to 14 Tg emission flux of SO<sub>2</sub> would accurately represent the effects ~~that~~ the new forcing datasets would enact for Pinatubo in ~~chemistry-climate-model~~ CCM integrations. For El Chichón and Agung, the magnitude of the volcanic forcing is highly uncertain, the volcanic aerosol datasets used in CMIP5 and CMIP6 historical integrations showing substantial differences. We contend there is 865 substantial potential to improve on this situation, by identifying consensus forcings from multi-model simulations (Timmerreck et al., 2018), with comparison to additional in-situ and active remote sensing measurements such as those being initiated within the SSIRC data rescue activity (Antuna-Marrero et al., 2020; Mann et al., 2020).

*Data availability.* Simulated aerosol data are publicly available from [http://homepages.see.leeds.ac.uk/~fbsssdh/Dhomse2019\\_Volcanic\\_Aerosol\\_Data/](http://homepages.see.leeds.ac.uk/~fbsssdh/Dhomse2019_Volcanic_Aerosol_Data/) We will get doi for Data once manuscript is online

870 *Author contributions.* SD and GM led the initial experiments design, model simulations, data analysis and the writing of the paper. The figures were prepared by SD. GM, SS and JCA retrieved and processed Lexington LIDAR data. GM, LM, LA and CJ contributed towards this GA4-UM-UKCA interactive stratospheric chemistry-aerosol model capability. All co-authors contributed to either advising/co-ordinating the UKCA developments, writing sections of the paper, performing evaluation and/or reviewing drafts of the paper.

*Competing interests.* The authors declare that they have no conflict of interest.

875 *Acknowledgements.* We thank Dr. We thank Larry Thomason (NASA Langley) and Dr. Beiping Luo (ETH-Zurich) for useful discussions about use of ~~GloSSAC CMIP6-GloSSAC~~ and CMIP6 datasets. We also acknowledge the contributions of James Brooke (Univ. Leeds), Nicolas Bellouin (Univ. Reading), Anja Schmidt (Univ. Cambridge) and Mohit Dalvi (Joint Weather and Climate Research Programme, UK Met Office) in ~~contributing to help helping to~~ develop this interactive stratospheric chemistry-aerosol configuration of GA4-UM-UKCA. SD was supported by the NERC SISLAC project (NE/R001782/1) ~~and NCEO (NE/N018079/1). MPC thanks NCEO~~  
880 ~~for funding (NE/R016518/1)~~. SD, GM and KC received funding via the NERC highlight topic consortium project SMURPHS ("Securing Multidisciplinary UndeRstanding and Prediction of Hiatus and Surge periods", NERC grant NE/N006038/1). GM also received funding from the NCAS, via the ACSIS long-term science programme on the Atlantic climate system. GM was also part-funded from the Copernicus Atmospheric Monitoring Service (CAMS), one of six services that form Copernicus, the European Union's Earth Observation programme. Juan Carlos Antuna-Marrero acknowledges travel and subsistence funding from CAMS that enabled his 1-month  
885 visit in March 2019 to the ~~School of Earth and Environment (SEE)~~, University of Leeds, with CAMS and SEE also co-funding Sarah Shallcross's PhD studentship. We thank the European Centre for Medium-Range Weather Forecasts for providing ~~their the~~ ERA-interim meteorological re-analyses, which were obtained via the UK Centre for Environmental Data Access (CEDA). Simulations were performed on the UK ARCHER national supercomputing service and data analysis used the UK collaborative JASMIN data facility.

## References

890 Abraham, N. L., Archibald, A. T., Bellouin, N., Boucher, O., Braesicke, P., Bushell, A., Carslaw, K., Collins, B., Dalvi, M., Emmerson, K., and Others: Unified Model Documentation Paper No. 84: United Kingdom Chemistry and Aerosol (UKCA) Technical Description MetUM Version 8.4, UK Met Office, Exeter, UK, <https://www.ukca.ac.uk/images/b/b1/Umdp{ }084-umdp84.pdf>, 2012.

895 Ammann, C. M., Meehl, G. A., Washington, W. M., and Zender, C. S.: A monthly and latitudinally varying volcanic forcing dataset in simulations of 20th century climate, *Geophysical Research Letters*, 30, <https://doi.org/10.1029/2003GL016875>, <http://doi.wiley.com/10.1029/2003GL016875>, 2003.

Angell, J. K.: Stratospheric warming due to Agung, El Chichón, and Pinatubo taking into account the quasi-biennial oscillation, *Journal of Geophysical Research: Atmospheres* (1984–2012), 102, 9479–9485, <https://doi.org/10.1029/96JD03588>, <http://onlinelibrary.wiley.com/doi/10.1029/96JD03588/full>, 1997a.

900 Angell, J. K.: Estimated impact of Agung, El Chichon and Pinatubo volcanic eruptions on global and regional total ozone after adjustment for the QBO, *Geophysical Research Letters*, 24, 647–650, <https://doi.org/10.1029/97GL00544>, <http://doi.wiley.com/10.1029/97GL00544>, 1997b.

Antuña, J. C.: Lidar measurements of stratospheric aerosols from Mount Pinatubo at Camaguey, Cuba, in: *Atmospheric Environment*, vol. 30, pp. 1857–1860, Elsevier Ltd, [https://doi.org/10.1016/1352-2310\(95\)00386-X](https://doi.org/10.1016/1352-2310(95)00386-X), 1996.

905 Antuña, J. C.: Spatial and temporal variability of the stratospheric aerosol cloud produced by the 1991 Mount Pinatubo eruption, *Journal of Geophysical Research*, 108, 4624, <https://doi.org/10.1029/2003JD003722>, <http://doi.wiley.com/10.1029/2003JD003722>, 2003.

Antuña, J. C., Robock, A., Stenchikov, G. L., Thomason, L. W., and Barnes, J. E.: Lidar validation of SAGE II aerosol measurements after the 1991 Mount Pinatubo eruption, *Journal of Geophysical Research Atmospheres*, 107, 4194, <https://doi.org/10.1029/2001JD001441>, <http://doi.wiley.com/10.1029/2001JD001441>, 2002.

910 Antuna-Marrero, J. C., Mann, G. W., Keckhut, P., Avdyushin, S., Nardi, B., and Thomason, L. W.: Early ship borne lidar measurements of the Pinatbo in the Antarctic, *Earth System Science Data*, NA, NA—NA, <https://doi.org/10.xxxx/essd-submitted>, <https://www.earth-syst-sci-data.net>, 2020.

Aquila, V., Oman, L. D., Stolarski, R., Douglass, A. R., and Newman, P. A.: The Response of Ozone and Nitrogen Dioxide to the Eruption of Mt. Pinatubo at Southern and Northern Midlatitudes, *Journal of the Atmospheric Sciences*, 70, 894–900, <https://doi.org/10.1175/JAS-D-12-0143.1>, <http://journals.ametsoc.org/doi/abs/10.1175/JAS-D-12-0143.1>, 2013.

915 Archibald, A. T., O'Connor, F. M., Abraham, N. L., Archer-Nicholls, S., Chipperfield, M. P., Dalvi, M., Folberth, G. A., Dennison, F., Dhomse, S. S., Griffiths, P. T., Hardacre, C., Hewitt, A. J., Hill, R. S., Johnson, C. E., Keeble, J., Köhler, M. O., Morgenstern, O., Mulcahy, J. P., Ordóñez, C., Pope, R. J., Rumbold, S. T., Russo, M. R., Savage, N. H., Sellar, A., Stringer, M., Turnock, S. T., Wild, O., and Zeng, G.: Description and evaluation of the UKCA stratosphere–troposphere chemistry scheme (StratTrop vn 1.0) implemented in UKESM1, *Geoscientific Model Development*, 13, 1223–1266, <https://doi.org/10.5194/gmd-13-1223-2020>, <https://gmd.copernicus.org/articles/13/1223/2020/>, 2020.

920 Arfeuille, F., Luo, B. P., Heckendorn, P., Weisenstein, D., Sheng, J. X., Rozanov, E., Schraner, M., Brönnimann, S., Thomason, L. W., and Peter, T.: Modeling the stratospheric warming following the Mt. Pinatubo eruption: Uncertainties in aerosol extinctions, *Atmospheric Chemistry and Physics*, 13, 11 221–11 234, <https://doi.org/10.5194/acp-13-11221-2013>, <https://www.atmos-chem-phys.net/13/11221/2013/http://www.atmos-chem-phys.net/13/11221/2013/acp-13-11221-2013.html>, 2013.

925 Arfeuille, F. X., Weisenstein, D., MacK, H., Rozanov, E., Peter, T., and Brönnimann, S.: Volcanic forcing for climate modeling: a new microphysics-based data set covering years 1600–present, *Climate of the Past*, 10, 359–375, <https://doi.org/10.5194/cp-10-359-2014>, 2014.

930 Baran, A. J. and Foot, J. S.: New application of the operational sounder HIRS in determining a climatology of sulphuric acid aerosol from the Pinatubo eruption, *Journal of Geophysical Research*, 99, 25 673–25 679, <https://doi.org/10.1029/94JD02044>, <http://doi.wiley.com/10.1029/94JD02044>, 1994.

Baran, A. J., Foot, J. S., and Dibben, P. C.: Satellite detection of volcanic sulphuric acid aerosol, *Geophysical Research Letters*, 20, 1799–1801, <https://doi.org/10.1029/93GL01965>, <https://agupubs.onlinelibrary.wiley.com/doi/abs/10.1029/93GL01965>, 1993.

Barnes, J. E. and Hofmann, D. J.: Lidar measurements of stratospheric aerosol over Mauna Loa Observatory, *Geophysical Research Letters*, 24, 1923–1926, <https://doi.org/10.1029/97GL01943>, 1997.

935 Barton, I. J., Prata, A. J., Watterson, I. G., and Young, S. A.: Identification of the Mount Hudson volcanic cloud over SE Australia, *Geophysical Research Letters*, 19, 1211–1214, <https://doi.org/10.1029/92GL01122>, <http://doi.wiley.com/10.1029/92GL01122>, 1992.

Bauman, J. J., Russell, P. B., Geller, M. A., and Hamill, P.: A stratospheric aerosol climatology from SAGE II and CLAES measurements: 1. Methodology, *Journal of Geophysical Research: Atmospheres*, 108, n/a–n/a, <https://doi.org/10.1029/2002JD002992>, <http://doi.wiley.com/10.1029/2002JD002992>, 2003.

940 Bekki, S., Toumi, R., and Pyle, J. A.: Role of Sulphur Photochemistry in Tropical Ozone Changes After the Eruption of Mount Pinatubo, *Nature*, 362, 331–333, <https://doi.org/10.1038/362331a0>, <http://www.nature.com/doifinder/10.1038/362331a0>, 1993.

Bittner, M., Schmidt, H., Timmreck, C., and Sienz, F.: Using a large ensemble of simulations to assess the Northern Hemisphere stratospheric dynamical response to tropical volcanic eruptions and its uncertainty, *Geophysical Research Letters*, 43, 9324–9332, <https://doi.org/10.1002/2016GL070587>, <http://doi.wiley.com/10.1002/2016GL070587>, 2016.

945 Brooke, J. S. A., Feng, W., Carrillo-Sánchez, J. D., Mann, G. W., James, A. D., Bardeen, C. G., Marshall, L., Dhomse, S. S., and Plane, J. M. C.: Meteoric Smoke Deposition in the Polar Regions: A Comparison of Measurements With Global Atmospheric Models, *Journal of Geophysical Research: Atmospheres*, 122, 11,111–112,130, <https://doi.org/10.1002/2017JD027143>, <http://doi.wiley.com/10.1002/2017JD027143>, 2017.

Butchart, N.: The Brewer-Dobson circulation, *Reviews of Geophysics*, 52, 157–184, <https://doi.org/10.1002/2013RG000448>, <http://doi.wiley.com/10.1002/2013RG000448>, 2014.

950 Cadle, R. D. and Grams, G. W.: Stratospheric aerosol particles and their optical properties, <https://doi.org/10.1029/RG013i004p00475>, 1975.

Cadle, R. D., Crutzen, P., and Ehhalt, D.: Heterogeneous chemical reactions in the stratosphere, *Journal of Geophysical Research*, 80, 3381–3385, <https://doi.org/10.1029/jc080i024p03381>, 1975.

955 Carty, T., Mascioli, N. R., Smarte, M. D., and Salawitch, R. J.: An empirical model of global climate – Part 1: A critical evaluation of volcanic cooling, *Atmospheric Chemistry and Physics*, 13, 3997–4031, <https://doi.org/10.5194/acp-13-3997-2013>, <https://www.atmos-chem-phys.net/13/3997/2013/>, 2013.

DallaSanta, K., Gerber, E. P., and Toohey, M.: The Circulation Response to Volcanic Eruptions: The Key Roles of Stratospheric Warming and Eddy Interactions, *Journal of Climate*, 32, 1101–1120, <https://doi.org/10.1175/JCLI-D-18-0099.1>, <http://journals.ametsoc.org/doi/10.1175/JCLI-D-18-0099.1>, 2019.

Damadeo, R. P., Zawodny, J. M., Thomason, L. W. L., and Iyer, N.: SAGE version 7.0 algorithm: application to SAGE II, *Atmospheric Measurement Techniques*, 6, 3539–3561, <https://doi.org/10.5194/amt-6-3539-2013>, <http://www.atmos-meas-tech.net/6/3539/2013/amt-6-3539-2013.html>, 2013.

965 Dee, D. P., Uppala, S. M., Simmons, A. J., Berrisford, P., Poli, P., Kobayashi, S., Andrae, U., Balmaseda, M. A., Balsamo, G., Bauer, P., Bechtold, P., Beljaars, A. C. M., van de Berg, L., Bidlot, J., Bormann, N., Delsol, C., Dragani, R., Fuentes, M., Geer, A. J., Haimberger, L., Healy, S. B., Hersbach, H., Hólm, E. V., Isaksen, L., Källberg, P., Köhler, M., Matricardi, M., McNally, A. P., Monge-Sanz, B. M., Morcrette, J.-J. J., Park, B.-K. K., Peubey, C., de Rosnay, P., Tavolato, C., Thépaut, J.-N. N., and Vitart, F.: The ERA-Interim reanalysis: configuration and performance of the data assimilation system, *Quarterly Journal of the Royal Meteorological Society*, 137, 553–597, <https://doi.org/10.1002/qj.828>, <http://doi.wiley.com/10.1002/qj.828>, 2011.

970 Deshler, T.: Large nitric acid particles at the top of an Arctic stratospheric cloud, *Journal of Geophysical Research*, 108, 4517, <https://doi.org/10.1029/2003JD003479>, <http://doi.wiley.com/10.1029/2003JD003479>, 2003.

Dhomse, S., Weber, M., Wohltmann, I., Rex, M., and Burrows, J. P.: On the possible causes of recent increases in northern hemispheric total ozone from a statistical analysis of satellite data from 1979 to 2003, *Atmospheric chemistry and physics*, 6, 1165–1180, <https://doi.org/10.5194/acp-6-1165-2006>, <http://www.atmos-chem-phys.org/6/1165/2006/acp-6-1165-2006.html>, 2006.

975 Dhomse, S., Weber, M., and Burrows, J.: The relationship between tropospheric wave forcing and tropical lower stratospheric water vapor, *Atmospheric Chemistry and Physics*, 8, 471–480, <https://doi.org/10.5194/acp-8-471-2008>, <http://www.atmos-chem-phys.net/8/471/2008/acp-8-471-2008.html>, 2008.

Dhomse, S., Chipperfield, M. P. M. P., Feng, W., and Haigh, J. D.: Solar response in tropical stratospheric ozone: a 3-D chemical transport model study using ERA reanalyses, *Atmospheric Chemistry and Physics*, 11, 12 773–12 786, <https://doi.org/10.5194/acp-11-12773-2011>, <http://www.atmos-chem-phys.net/11/12773/2011/acp-11-12773-2011.html>, 2011.

980 Dhomse, S., Chipperfield, M., Feng, W., Hossaini, R., Mann, G., and Santee, M.: Revisiting the hemispheric asymmetry in midlatitude ozone changes following the Mount Pinatubo eruption: A 3-D model study, *Geophysical Research Letters*, 42, 3038–3047, <https://doi.org/10.1002/2015GL063052>, <http://doi.wiley.com/10.1002/2015GL063052>, 2015.

985 Dhomse, S. S., Chipperfield, M. P., Feng, W., Ball, W. T., Unruh, Y. C., Haigh, J. D., Krivova, N. A., Solanki, S. K., and Smith, A. K.: Stratospheric O<sub>3</sub> changes during 2001–2010: the small role of solar flux variations in a chemical transport model, *Atmospheric Chemistry and Physics*, 13, 10 113–10 123, <https://doi.org/10.5194/acp-13-10113-2013>, <http://www.atmos-chem-phys.net/13/10113/2013/acp-13-10113-2013.html>, 2013.

Dhomse, S. S., Emmerson, K. M., Mann, G. W., Bellouin, N., Carslaw, K. S., Chipperfield, M. P., Hommel, R., Abraham, N. L., Telford, P., Braesicke, P., Dalvi, M., Johnson, C. E., O'Connor, F., Morgenstern, O., Pyle, J. A., Deshler, T., Zawodny, J. M., and Thomason, L. W.: 990 Aerosol microphysics simulations of the Mt. Pinatubo eruption with the UM-UKCA composition-climate model, *Atmospheric Chemistry and Physics*, 14, 11 221–11 246, <https://doi.org/10.5194/acp-14-11221-2014>, <http://www.atmos-chem-phys.net/14/11221/2014/acp-14-11221-2014.html>, 2014.

Driscoll, S., Bozzo, A., Gray, L. J., Robock, A., and Stenchikov, G.: Coupled Model Intercomparison Project 5 (CMIP5) simulations of climate following volcanic eruptions, *Journal of Geophysical Research: Atmospheres*, 117, D17105, <https://doi.org/10.1029/2012JD017607>, <http://doi.wiley.com/10.1029/2012JD017607>, 2012.

Dyer, A.: ANISOTROPIC DIFFUSION COEFFICIENTS AND THE GLOBAL SPREAD OF VOLCANIC DUST, *J Geophys Res*, 75, 3007–3012, <https://doi.org/10.1029/jc075i015p03007>, 1970.

1000 Dyer, A. J.: The effect of volcanic eruptions on global turbidity, and an attempt to detect long-term trends due to man, *Quarterly Journal of the Royal Meteorological Society*, 100, 563–571, <https://doi.org/10.1002/qj.49710042606>, <http://doi.wiley.com/10.1002/qj.49710042606>, 1974.

Dyer, A. J. and Hicks, B. B.: Global spread of volcanic dust from the Bali eruption of 1963, *Quarterly Journal of the Royal Meteorological Society*, 94, 545–554, <https://doi.org/10.1002/qj.49709440209>, <http://doi.wiley.com/10.1002/qj.49709440209>, 1968.

Eyring, V., Harris, N. R., Rex, M., Shepherd, T. G., Fahey, D. W., Amanatidis, G. T., Austin, J., Chipperfield, M. P., Dameris, M., Forster, P. M. F., Gettelman, A., Graf, H. F., Nagashima, T., Newman, P. A., Pawson, S., Prather, M. J., Pyle, J. A., Salawitch, R. J., Santer, B. D., and Waugh, D. W.: A strategy for process-oriented validation of coupled chemistry-climate models, *Bulletin of the American Meteorological Society*, 86, 1117–1133, <https://doi.org/10.1175/BAMS-86-8-1117>, 2005.

Eyring, V., Chipperfield, M. P., Giorgi, M. A., Kinnison, D. E., Manzini, E., Newman, P. A., Shepherd, T. G., Waugh, D. W., Matthes, K., Newman, P. A., Pawson, S., Shepherd, T. G., and Waugh, D. W.: New CCMVal Reference and Sensitivity Simulations Overview of the New CCMVal Reference and Sensitivity Simulations in Support of Upcoming Ozone and Climate Assessments and the Planned SPARC CCMVal Report, *SPARC News*, 30, 20–26, 2008.

Eyring, V., Lamarque, J.-F., Hess, P., Arfeuille, F., Bowman, K., Chipperfield, M. P., Duncan, B., Fiore, A., Gettelman, A., Giorgi, M. A., Granier, C., Hegglin, M., Kinnison, D., Kunze, M., Langematz, U., Luo, B., Martin, R., Matthes, K., Newman, P. A., Peter, T., Peter, T., Robock, A., Ryerson, T., Saiz-Lopez, A., Salawitch, R., Schultz, M., Shepherd, T. G., Shindell, D., Staehelin, J., Tegtmeier, S., Thomason, L., Tilmes, S., Vernier, J.-P., Waugh, D., and Young, P.: Overview of IGAC/SPARC Chemistry-Climate Model Initiative (CCMI) Community Simulations in Support of Upcoming Ozone and Climate Assessments, <http://oceanrep.geomar.de/20227/1/40>{ }SPARCNewsletter{ }Jan2013{ }web.pdf, 2013.

Eyring, V., Bony, S., Meehl, G. A., Senior, C. A., Stevens, B., Stouffer, R. J., and Taylor, K. E.: Overview of the Coupled Model Intercomparison Project Phase 6 (CMIP6) experimental design and organization, *Geoscientific Model Development*, 9, 1937–1958, <https://doi.org/10.5194/gmd-9-1937-2016>, 2016.

1020 Fiocco, G. and Grams, G.: Observations of the Aerosol Layer at 20 km by Optical Radar, *Journal of the Atmospheric Sciences*, 21, 323–324, <https://doi.org/10.1175/1520-0469>, <https://doi.org/10.1175/1520-0469>, 1964.

Folland, C. K., Boucher, O., Colman, A., and Parker, D. E.: Causes of irregularities in trends of global mean surface temperature since the late 19th century, *Science advances*, 4, eaao5297, 2018.

Free, M., Lanzante, J., Free, M., and Lanzante, J.: Effect of Volcanic Eruptions on the Vertical Temperature Profile in Radiosonde Data and Climate Models, *Journal of Climate*, 22, 2925–2939, <https://doi.org/10.1175/2008JCLI2562.1>, <http://journals.ametsoc.org/doi/abs/10.1175/2008JCLI2562.1>, 2009.

Grainger, R. G., Lambert, A., Taylor, F. W., Remedios, J. J., Rodgers, C. D., Corney, M., and Kerridge, B. J.: Infrared absorption by volcanic stratospheric aerosols observed by ISAMS, *Geophysical Research Letters*, 20, 1283–1286, <https://doi.org/10.1029/93GL00823>, <http://doi.wiley.com/10.1029/93GL00823>, 1993.

1030 Grams, G. and Fiocco, G.: Stratospheric aerosol layer during 1964 and 1965, *Journal of Geophysical Research*, 72, 3523–3542, <https://doi.org/10.1029/jz072i014p03523>, <http://onlinelibrary.wiley.com/doi/10.1029/JZ072i014p03523/full>, 1967.

Grams, G. W.: Optical radar studies of stratospheric aerosols., Ph.D. thesis, Massachusetts Institute of Technology, 1966.

Grant, W. B., Browell, E. V., Long, C. S., Stowe, L. L., Grainger, R. G., and Lambert, A.: Use of volcanic aerosols to study the tropical stratospheric reservoir, *Journal Of Geophysical ResearchAtmospheres*, 101, 3973–3988, <http://onlinelibrary.wiley.com/doi/10.1029/95JD03164/full>, 1996.

Guo, S., Bluth, G. J. S., Rose, W. I., Watson, I. M., and Prata, A. J.: Re-evaluation of SO<sub>2</sub> release of the 15 June 1991 Pinatubo eruption using ultraviolet and infrared satellite sensors, *Geochemistry, Geophysics, Geosystems*, 5, n/a–n/a, <https://doi.org/10.1029/2003GC000654>, <http://doi.wiley.com/10.1029/2003GC000654><http://www.agu.org/pubs/crossref/2004/2003GC000654.shtml>, 2004a.

1040 Guo, S., Rose, W. I., Bluth, G. J. S., and Watson, I. M.: Particles in the great Pinatubo volcanic cloud of June 1991: The role of ice, *Geochemistry Geophysics Geosystems*, 5, 101 029/, <https://doi.org/10.1029/2003GC000655>, <http://www.agu.org/pubs/crossref/2004/2003GC000655.shtml>, 2004b.

Hegerl, G. and Zwiers, F.: Use of models in detection and attribution of climate change, *Wiley interdisciplinary reviews: climate change*, 2, 570–591, 2011.

1045 Hofmann, D. J. and Rosen, J. M.: Sulfuric acid droplet formation and growth in the stratosphere after the 1982 eruption of El Chichon, *Science*, 222, 325–327, 1983a.

Hofmann, D. J. and Rosen, J. M. J.: Stratospheric sulfuric acid fraction and mass estimate for the 1982 volcanic eruption of El Chichon, *Geophysical research letters*, 10, 313–316, <https://doi.org/10.1029/GL010i004p00313>, <http://doi.wiley.com/10.1029/GL010i004p00313>, 1983b.

1050 Hofmann, D. J. and Solomon, S.: Ozone destruction through heterogeneous chemistry following the eruption of El Chichón, *Journal of Geophysical Research*, 94, 5029, <https://doi.org/10.1029/JD094iD04p05029>, <http://doi.wiley.com/10.1029/JD094iD04p05029>, 1989.

Holton, J. R., Haynes, P. H., McIntyre, M. E., Douglass, A. R., Rood, R. B., and Pfister, L.: Stratosphere-troposphere exchange, *Reviews of Geophysics*, 33, 403–439, <https://doi.org/10.1029/95RG02097>, <http://www.agu.org/pubs/crossref/1995/95RG02097.shtml>, 1995.

Hommel, R., Timmreck, C., and Graf, H. F.: The global middle-atmosphere aerosol model MAECHAM5-SAM2: comparison with 1055 satellite and in-situ observations, *Geoscientific Model Development*, 4, 809–834, <https://doi.org/10.5194/gmd-4-809-2011>, <https://www.geosci-model-dev.net/4/809/2011/>, 2011.

Jäger, H. and Deshler, T.: Correction to “Lidar backscatter to extinction, mass and area conversions for stratospheric aerosols based on midlatitude balloonborne size distribution measurements”, *Geophysical Research Letters*, 30, 351–354, <https://doi.org/10.1029/2003GL017189>, <http://doi.wiley.com/10.1029/2003GL017189><https://agupubs.onlinelibrary.wiley.com/doi/abs/10.1029/2003GL017189>, 2003.

1060 Jones, A. C., Haywood, J. M., Jones, A., and Aquila, V.: Sensitivity of volcanic aerosol dispersion to meteorological conditions: A Pinatubo case study, *Journal of Geophysical Research: Atmospheres*, 121, 6892–6908, <https://doi.org/10.1002/2016JD025001>, <http://doi.wiley.com/10.1002/2016JD025001>, 2016.

Joshi, M. M., Shine, K. P., Joshi, M. M., and Shine, K. P.: A GCM Study of Volcanic Eruptions as a Cause of Increased 1065 Stratospheric Water Vapor, [http://dx.doi.org/10.1175/1520-0442\(2003\)016<3525:AGSOVE>2.0.CO;2](http://dx.doi.org/10.1175/1520-0442(2003)016<3525:AGSOVE>2.0.CO;2), [https://doi.org/10.1175/1520-0442\(2003\)016<3525:AGSOVE>2.0.CO;2](https://doi.org/10.1175/1520-0442(2003)016<3525:AGSOVE>2.0.CO;2), 2003.

Kinne, S., Toon, O. B., and Prather, M. J.: Buffering of stratospheric circulation by changing amounts of tropical ozone - A Pinatubo case 1070 study, *Geophysical Research Letters*, 19, 1927–1930, <https://doi.org/10.1029/92GL01937>, <http://doi.wiley.com/10.1029/92GL01937>, 1992.

Kovilakam, M., Thomason, L., Ernest, N., Rieger, L., Bourassa, A., and Millán, L.: A Global Space-based Stratospheric Aerosol Climatology (Version 2.0): 1979–2018, *Earth System Science Data Discussions*, 2020, 1–41, <https://doi.org/10.5194/essd-2020-56>, <https://essd.copernicus.org/preprints/essd-2020-56/>, 2020.

Kremser, S., Thomason, L. W., von Hobe, M., Hermann, M., Deshler, T., Timmreck, C., Toohey, M., Stenke, A., Schwarz, J. P., Weigel, R., Fueglistaler, S., Prata, F. J., Vernier, J. P., Schlager, H., Barnes, J. E., Antuña-Marrero, J. C., Fairlie, D., Palm, M., Mahieu, E.,  
1075 Notholt, J., Rex, M., Bingen, C., Vanhellemont, F., Bourassa, A., Plane, J. M., Klocke, D., Carn, S. A., Clarisse, L., Trickl, T., Neely, R., James, A. D., Rieger, L., Wilson, J. C., and Meland, B.: Stratospheric aerosol—Observations, processes, and impact on climate, <https://doi.org/10.1002/2015RG000511>, 2016.

Lacis, A., Hansen, J., and Sato, M.: Climate forcing by stratospheric aerosols, *Geophysical Research Letters*, 19, 1607–1610, <https://doi.org/10.1029/92GL01620>, <http://doi.wiley.com/10.1029/92GL01620>, 1992.

1080 Lambert, A., Grainger, R. G., Remedios, J. J., Rodgers, C. D., Corney, M., and Taylor, F. W.: Measurements of the evolution of the Mt. Pinatubo aerosol cloud by ISAMS, *Geophysical Research Letters*, 20, 1287–1290, 1993.

Lambert, A., Grainger, R. G., Rodgers, C. D., Taylor, F. W., Mergenthaler, J. L., Kumer, J. B., and Massie, S. T.: Global evolution of the Mt Pinatubo volcanic aerosols observed by the infrared limb-sounding instruments CLAES and ISAMS on the Upper Atmosphere Research Satellite, *Journal of Geophysical Research - Atmospheres*, 102, 1495–1512, 1997.

1085 Lee, H. and Smith, A.: Simulation of the combined effects of solar cycle, quasibiennial oscillation, and volcanic forcing on stratospheric ozone changes in recent decades, *Journal of Geophysical Research*, 108, 1–16, <https://doi.org/10.1029/2001JD001503>, <http://onlinelibrary.wiley.com/doi/10.1029/2001JD001503/full>, 2003.

LeGrande, A. N., Tsigaridis, K., and Bauer, S. E.: Role of atmospheric chemistry in the climate impacts of stratospheric volcanic injections, *Nature Geoscience*, <https://doi.org/10.1038/ngeo2771>, <http://www.nature.com/doifinder/10.1038/ngeo2771>, 2016.

1090 Long, C. S. and Stowe, L. L.: Using the NOAA/AVHRR to study stratospheric aerosol optical thicknesses following the Mt Pinatubo eruption, *Geophysical Research Letters*, 21, 2215–2218, <http://onlinelibrary.wiley.com/doi/10.1029/94GL01322/full>, 1994.

Luo, B.: Stratospheric aerosol data for use in CMIP6 models, [ftp://iacftp.ethz.ch/pub/\\_/read/luo/CMIP6/Readme{\\_}Data{\\_}Description.pdf](ftp://iacftp.ethz.ch/pub/_/read/luo/CMIP6/Readme{_}Data{_}Description.pdf), 2016.

Mann, G., Dhomse, S., Deshler, T., Timmreck, C., Schmidt, A., Neely, R., and Thomason, L.: Evolving particle size is the key to improved  
1095 volcanic forcings, *Past Global Change Magazine*, 23, 52–53, <https://doi.org/10.22498/pages.23.2.52>, <http://www.pastglobalchanges.org/products/pages-magazine/7166>, 2015.

Mann, G., Brooke, J., Sengupta, K., Marshall, L., Dhomse, S., Feng, W., Neely, R., Bardeen, C., Bellouin, N., Dalvi, M., and Others: The prevalence of meteoric-sulphuric particles within the stratospheric aerosol layer and their influence on how pure sulphuric particles are transported and transformed., in: *Geophysical Research Abstracts*, vol. 21, 2019a.

1100 Mann, G. W., Carslaw, K. S., Spracklen, D. V., Ridley, D. A., Manktelow, P. T., Chipperfield, M. P., Pickering, S. J., and Johnson, C. E.: Description and evaluation of GLOMAP-mode: a modal global aerosol microphysics model for the UKCA composition-climate model, *Geoscientific Model Development*, 3, 519–551, <https://doi.org/10.5194/gmd-3-519-2010>, <http://www.geosci-model-dev.net/3/519/2010/>, 2010.

Mann, G. W., Shallcross, S., Antuña-Marrero, J. C., Dhomse, S., Schmidt, A., Neely, R., Carslaw, K. S., Bellouin, N., Winker, D. M.,  
1105 Vaughan, G., and Others: Ash-sulphuric interactions: Simulating major volcanic aerosol clouds as global dust veils, in: *AGU Fall Meeting 2019*, 2019b.

Mann, G. W., Antuña-Marrero, J. C., Shallcross, S., Dhomse, S., Thomason, L., Beiping, L., Deshler, T., and Rosen, J.: Recovered measurements of the 1960s stratospheric aerosol layer for new constraints for volcanic forcing in the years after 1963 Agung, in: *EGU Assembly 2020*, 2020.

1110 Marotzke, J. and Forster, P. M.: Forcing, feedback and internal variability in global temperature trends, *Nature*, 517, 565–570, <https://doi.org/10.1038/nature14117>, <http://www.nature.com/articles/nature14117>, 2015.

Marshall, L., Schmidt, A., Toohey, M., Carslaw, K., Mann, G., Sigl, M., Khodri, M., Timmreck, C., Zanchettin, D., Ball, W., Bekki, S., Brooke, J., Dhomse, S., Johnson, C., Lamarque, J.-F., Legrande, A., Mills, M., Niemeier, U., Pope, J., Poulain, V., Robock, A., Rozanov, E., Stenke, A., Sukhodolov, T., Tilmes, S., Tsigaridis, K., and Tummon, F.: Multi-model comparison of the volcanic sulfate deposition from the 1815 eruption of Mt. Tambora, *Atmospheric Chemistry and Physics*, 18, <https://doi.org/10.5194/acp-18-2307-2018>, 2018.

1115 Marshall, L., Johnson, J. S., Mann, G. W., Lee, L., Dhomse, S. S., Regayre, L., Yoshioka, M., Carslaw, K. S., and Schmidt, A.: Exploring How Eruption Source Parameters Affect Volcanic Radiative Forcing Using Statistical Emulation, *Journal of Geophysical Research: Atmospheres*, <https://doi.org/10.1029/2018JD028675>, <http://doi.wiley.com/10.1029/2018JD028675>, 2019.

1120 McCormick, M.: Sage II: An overview, *Advances in Space Research*, 7, 219–226, [https://doi.org/10.1016/0273-1177\(87\)90151-7](https://doi.org/10.1016/0273-1177(87)90151-7), <https://www.sciencedirect.com/science/article/pii/0273117787901517>, 1987.

McCormick, M. P. and Swissler, T. J.: Stratospheric aerosol mass and latitudinal distribution of the El Chichon eruption cloud for October 1982, *Geophysical research letters*, 10, 877–880, 1983.

McCormick, M. P., Thomason, L. W., and Trepte, C. R.: Atmospheric effects of the Mt Pinatubo eruption, *Nature*, 373, 1125 399–404, <https://doi.org/10.1038/373399a0>, [http://jack.pixe.lth.se/kfgu/KOO090\\_{\\_}FKF075/Artiklar/P05.pdf](http://jack.pixe.lth.se/kfgu/KOO090_{_}FKF075/Artiklar/P05.pdf) <http://www.nature.com/articles/373399a0>, 1995.

Mills, M. J., Schmidt, A., Easter, R., Solomon, S., Kinnison, D. E., Ghan, S. J., Neely, R. R., Marsh, D. R., Conley, A., Bardeen, C. G., and Gettelman, A.: Global volcanic aerosol properties derived from emissions, 1990–2014, using CESM1(WACCM), *Journal of Geophysical Research: Atmospheres*, 121, 2332–2348, <https://doi.org/10.1002/2015JD024290>, <http://doi.wiley.com/10.1002/2015JD024290>, 1130 2016.

Morgenstern, O., Braesicke, P., O'Connor, F. M., Bushell, A. C., Johnson, C. E., Osprey, S. M., and Pyle, J. A.: Evaluation of the new UKCA climate-composition model – Part 1: The stratosphere, *Geoscientific Model Development*, 2, 43–57, <https://doi.org/10.5194/gmd-2-43-2009>, <http://www.geosci-model-dev.net/2/43/2009/>, 2009.

1135 Morgenstern, O., Akiyoshi, H., Bekki, S., Braesicke, P., Butchart, N., Chipperfield, M. P., Cugnet, D., Deushi, M., Dhomse, S. S., Garcia, R. R., Gettelman, A., Gillett, N. P., Hardiman, S. C., Jumelet, J., Kinnison, D. E., Lamarque, J. F., Lott, F., Marchand, M., Michou, M., Nakamura, T., Olivie, D., Peter, T., Plummer, D., Pyle, J. A., Rozanov, E., Saint-Martin, D., Scinocca, J. F., Shibata, K., Sigmond, M., Smale, D., Teyssèdre, H., Tian, W., Volodire, A., and Yamashita, Y.: Anthropogenic forcing of the Northern Annular Mode in CCMVal-2 models, *Journal of Geophysical Research*, 115, 1–15, <https://doi.org/10.1029/2009JD013347>, <http://www.agu.org/pubs/crossref/2010/2009JD013347.shtml>, 2010.

1140 Morgenstern, O., Hegglin, M., Rozanov, E., O'Connor, F., Luke Abraham, N., Akiyoshi, H., Archibald, A., Bekki, S., Butchart, N., Chipperfield, M., Deushi, M., Dhomse, S., Garcia, R., Hardiman, S., Horowitz, L., Jöckel, P., Josse, B., Kinnison, D., Lin, M., Mancini, E., Manyin, M., Marchand, M., Marécal, V., Michou, M., Oman, L., Pitari, G., Plummer, D., Revell, L., Saint-Martin, D., Schofield, R., Stenke, A., Stone, K., Sudo, K., Tanaka, T., Tilmes, S., Yamashita, Y., Yoshida, K., and Zeng, G.: Review of the global models used within phase 1 of the Chemistry-Climate Model Initiative (CCMI), *Geoscientific Model Development*, 10, 639–671, 1145 <https://doi.org/10.5194/gmd-10-639-2017>, 2017.

Murphy, D. M., Cziczo, D. J., Hudson, P. K., and Thomson, D. S.: Carbonaceous material in aerosol particles in the lower stratosphere and tropopause region, *Journal of Geophysical Research*, 112, D04203, <https://doi.org/10.1029/2006JD007297>, <http://doi.wiley.com/10.1029/2006JD007297>, 2007.

Murphy, D. M., Froyd, K. D., Schwarz, J. P., and Wilson, J. C.: Observations of the chemical composition of stratospheric aerosol particles, *Quarterly Journal of the Royal Meteorological Society*, 140, 1269–1278, <https://doi.org/10.1002/qj.2213>, <http://doi.wiley.com/10.1002/qj.2213>, 2014.

Niemeier, U., Timmreck, C., and Krüger, K.: Revisiting the Agung 1963 volcanic forcing – impact of one or two eruptions, *Atmospheric Chemistry and Physics*, 19, 10 379–10 390, <https://doi.org/10.5194/acp-19-10379-2019>, <https://www.atmos-chem-phys.net/19/10379/2019/>, 2019.

O'Connor, F. M., Johnson, C. E., Morgenstern, O., Abraham, N. L., Braesicke, P., Dalvi, M., Folberth, G. A., Sanderson, M. G., Telford, P. J., Voulgarakis, A., Young, P. J., Zeng, G., Collins, W. J., and Pyle, J. A.: Evaluation of the new UKCA climate-composition model – Part 2: The Troposphere, *Geoscientific Model Development*, 7, 41–91, <https://doi.org/10.5194/gmd-7-41-2014>, <https://www.geosci-model-dev.net/7/41/2014/>, 2014.

Pitari, G., Cionni, I., Di Genova, G., Visioni, D., Gandolfi, I., and Mancini, E.: Impact of Stratospheric Volcanic Aerosols on Age-of-Air and Transport of Long-Lived Species, *Atmosphere*, 7, 149, <https://doi.org/10.3390/atmos7110149>, <http://www.mdpi.com/2073-4433/7/11/149>, 2016a.

Pitari, G., Genova, G. D., Mancini, E., Visioni, D., Gandolfi, I., Cionni, I., Di Genova, G., Mancini, E., Visioni, D., Gandolfi, I., and Cionni, I.: Stratospheric aerosols from major volcanic eruptions: A composition-climate model study of the aerosol cloud dispersal and e-folding time, *Atmosphere*, 7, 75, <https://doi.org/10.3390/atmos7060075>, <http://www.mdpi.com/2073-4433/7/6/75>, 2016b.

Pitts, M. C. and Thomason, L. W.: The impact of the eruptions of Mount Pinatubo and Cerro Hudson on antarctic aerosol levels during the 1991 austral spring, *Geophysical Research Letters*, 20, 2451–2454, 1993.

Plumb, R. A.: A “tropical pipe” model of stratospheric transport, *Journal of Geophysical Research: Atmospheres*, 101, 3957–3972, <https://doi.org/10.1029/95JD03002>, <http://doi.wiley.com/10.1029/95JD03002>, 1996.

Poberaj, C. S., Staehelin, J., and Brunner, D.: Missing Stratospheric Ozone Decrease at Southern Hemisphere Middle Latitudes after Mt. Pinatubo: A Dynamical Perspective, *Journal of the Atmospheric Sciences*, 68, 1922–1945, <https://doi.org/10.1175/JAS-D-10-05004.1>, <http://journals.ametsoc.org/doi/abs/10.1175/JAS-D-10-05004.1>, 2011.

Prather, M.: Catastrophic loss of stratospheric ozone in dense volcanic clouds, *Journal of Geophysical Research*, 97, 10 187–10 191, <https://doi.org/10.1029/92jd00845>, 1992.

Randel, W. J., Garcia, R. R., Calvo, N., and Marsh, D.: ENSO influence on zonal mean temperature and ozone in the tropical lower stratosphere, *Geophysical Research Letters*, 36, 1–5, <https://doi.org/10.1029/2009GL039343>, <http://www.agu.org/pubs/crossref/2009/2009GL039343.shtml>, 2009.

Robock, A.: Volcanic eruptions and climate, *Reviews of Geophysics*, 38, 191–219, <https://doi.org/10.1029/1998RG000054>, <http://doi.wiley.com/10.1029/1998RG000054>, 2000.

Robock, A. and Matson, M.: Circumglobal transport of the El Chichón volcanic dust cloud, *Science*, 221, 195–197, <https://doi.org/10.1126/science.221.4606.195>, 1983.

Roche, A. E., Kumer, J. B., Mergenthaler, J. L., Ely, G. A., Uplinger, W. G., Potter, J. F., James, T. C., and Sterritt, L. W.: The cryogenic limb array etalon spectrometer (CLAES) on UARS: Experiment description and performance, *Journal of Geophysical Research*, 98, 10 763, <https://doi.org/10.1029/93JD00800>, <http://doi.wiley.com/10.1029/93JD00800>, 1993.

Rosen, J.: The vertical distribution of dust to 30 kilometers, *Journal of Geophysical Research*, <http://onlinelibrary.wiley.com/doi/10.1029/JZ069i021p04673/full>, 1964.

Rosen, J.: Simultaneous dust and ozone soundings over North and Central America, *Journal of Geophysical Research*, 73, 479–486, 1968.

Rosen, J. M., Kjome, N. T., McKenzie, R. L., and Liley, J. B.: Decay of Mount Pinatubo Aerosol At Midlatitudes in the Northern and Southern Hemispheres, *Journal Of Geophysical ResearchAtmospheres*, 99, 25 733–25 739, <http://onlinelibrary.wiley.com/doi/10.1029/94JD02312/full>, 1994.

Russell, P. B., Livingston, J. M., Pueschel, R. F., Bauman, J. J., Pollack, J. B., Brooks, S. L., Hamill, P., Thomason, L. W., Stowe, L. L., Deshler, T., Dutton, E. G., and Bergstrom, R. W.: Global to microscale evolution of the Pinatubo volcanic aerosol derived from diverse measurements and analyses, *Journal of Geophysical Research*, 101, 18 745–18 763, <https://doi.org/10.1029/96JD01162>, <http://doi.wiley.com/10.1029/96JD01162><http://www.agu.org/pubs/crossref/1996/96JD01162.shtml>, 1996.

1185 Santer, B. D., Wigley, T. M. L., Doutriaux, C., Boyle, J. S., Hansen, J. E., Jones, P. D., Meehl, G. A., Roeckner, E., Sengupta, S., and Taylor, K. E.: Accounting for the effects of volcanoes and ENSO in comparisons of modeled and observed temperature trends, *Journal of Geophysical Research: Atmospheres*, 106, 28 033–28 059, <https://doi.org/10.1029/2000JD000189>, <http://doi.wiley.com/10.1029/2000JD000189>, 2001.

1190 Santer, B. D., Bonfils, C., Painter, J. F., Zelinka, M. D., Mears, C., Solomon, S., Schmidt, G. A., Fyfe, J. C., Cole, J. N., Nazarenko, L., Taylor, K. E., and Wentz, F. J.: Volcanic contribution to decadal changes in tropospheric temperature, *Nature Geoscience*, 7, 185–189, <https://doi.org/10.1038/ngeo2098>, 2014.

Sato, M., Hansen, J. E. J. E., McCormick, M. P., and Pollack, J. B.: Stratospheric aerosol optical depths, 1850–1990, *Journal of Geophysical Research*, 98, 22 987, <https://doi.org/10.1029/93JD02553>, <http://doi.wiley.com/10.1029/93JD02553>, 1993.

1200 Schmidt, G. A., Ruedy, R., Hansen, J. E., Aleinov, I., Bell, N., Bauer, M., Bauer, S., Cairns, B., Canuto, V., Cheng, Y., Del Genio, A., Faluvegi, G., Friend, A. D., Hall, T. M., Hu, Y., Kelley, M., Kiang, N. Y., Koch, D., Lacis, A. A., Lerner, J., Lo, K. K., Miller, R. L., Nazarenko, L., Oinas, V., Perlitz, J., Perlitz, J., Rind, D., Romanou, A., Russell, G. L., Sato, M., Shindell, D. T., Stone, P. H., Sun, S., Tausnev, N., Thresher, D., and Yao, M.-S.: Present-Day Atmospheric Simulations Using GISS ModelE: Comparison to In Situ, Satellite, and Reanalysis Data, *Journal of Climate*, 19, 153–192, <https://doi.org/10.1175/JCLI3612.1>, <https://doi.org/10.1175/JCLI3612.1>, 2006.

1210 Sheng, J.-X., Weisenstein, D. K., Luo, B.-P., Rozanov, E., Arfeuille, F., and Peter, T.: A perturbed parameter model ensemble to investigate Mt. Pinatubo's 1991 initial sulfur mass emission, *Atmospheric Chemistry and Physics*, 15, 11 501–11 512, <https://doi.org/10.5194/acp-15-11501-2015>, <https://www.atmos-chem-phys.net/15/11501/2015/>, 2015a.

Sheng, J.-X. X., Weisenstein, D. K., Luo, B.-P. P., Rozanov, E., Stenke, A., Anet, J., Bingemer, H., and Peter, T.: Global atmospheric sulfur budget under volcanically quiescent conditions: Aerosol-chemistry-climate model predictions and validation, *Journal of Geophysical Research: Atmospheres*, 120, 256–276, <https://doi.org/10.1002/2014JD021985>, <http://doi.wiley.com/10.1002/2014JD021985>, 2015b.

Soden, B. J., Wetherald, R. T., Stenchikov, G. L., and Robock, A.: Global cooling after the eruption of Mount Pinatubo: a test of climate feedback by water vapor., *Science*, 296, 727–730, <https://doi.org/10.1126/science.296.5568.727>, <http://www.ncbi.nlm.nih.gov/pubmed/11976452><http://www.sciencemag.org/cgi/doi/10.1126/science.296.5568.727>, 2002.

1220 Solomon, S.: Stratospheric ozone depletion: A review of concepts and history, *Reviews of Geophysics*, 37, 275–316, <https://doi.org/10.1029/1999RG900008>, <http://onlinelibrary.wiley.com/doi/10.1029/1999RG900008/full>, 1999.

SPARC: SPARC Assessment of stratospheric aerosol properties (ASAP), Tech. rep., World Climate Research Programme, <http://www.sparc-climate.org/publications/sparc-reports/sparc-report-no4/>, 2006.

SPARC: SPARC Report on the Evaluation of Chemistry-Climate Models, in: SPARC report, vol. No. 5, p. 426 pp., World Climate Research Programme, wcrp - 30 edn., <http://www.sparc-climate.org/publications/sparc-reports/sparc-report-no5/><http://www.sparc-climate.org/publications/sparc-reports/>, 2010.

1225 Stenchikov, G. L. G. G. L., Kirchner, I., Robock, A., Graf, H.-F., Antuña, J. C., Grainger, R. G., Lambert, A., and Thomason, L.: Radiative forcing from the 1991 Mount Pinatubo volcanic eruption, *Journal of Geophysical Research*, 103, 13 837–13 857, <https://doi.org/10.1029/98JD00693>, <http://www.agu.org/pubs/crossref/1998/98JD00693.shtml><http://onlinelibrary.wiley.com/doi/10.1029/98JD00693/full>, 1998.

1230 Stothers, R.: Major optical depth perturbations to the stratosphere from volcanic eruptions: Pyrheliometric period, 1881–1960, *Journal of Geophysical Research: Atmospheres*, <http://onlinelibrary.wiley.com/doi/10.1029/95JD03237/full>, 1996.

Stothers, R. B.: Major optical depth perturbations to the stratosphere from volcanic eruptions: Stellar extinction period, 1961–1978, *Journal of Geophysical Research: Atmospheres*, 106, 2993–3003, <https://doi.org/10.1029/2000JD900652>, <http://doi.wiley.com/10.1029/2000JD900652>, 2001.

1235 Sukhodolov, T., Sheng, J.-X., Feinberg, A., Luo, B.-P., Thomas, P., Revell, L., Stenke, A., Weisenstein, D. K., and Rozanov, E.: Stratospheric aerosol evolution after Pinatubo simulated with a coupled size-resolved aerosol-chemistry-climate model, SOCOL-AERv1.0, *Geoscientific Model Development*, 11, 2633–2647, 2018.

Thomas, M. A., Giorgetta, M. A., Timmreck, C., Graf, H. F., and Stenchikov, G.: Simulation of the climate impact of Mt. Pinatubo eruption using ECHAM5 – Part 2: Sensitivity to the phase of the QBO and ENSO, *Atmospheric Chemistry and Physics*, 9, 3001–3009, <https://doi.org/10.5194/acp-9-3001-2009>, <http://www.atmos-chem-phys.net/9/3001/2009/>, 2009.

Thomason, L. W.: Observations of a new SAGE II aerosol extinction mode following the eruption of Mt. Pinatubo, *Geophysical Research Letters*, 19, 2179–2182, <https://doi.org/10.1029/92GL02185>, <https://agupubs.onlinelibrary.wiley.com/doi/abs/10.1029/92GL02185>, 1992.

1245 Thomason, L. W., Kent, G. S., Trepte, C. R., and Poole, L. R.: A Comparison of the Stratospheric Aerosol Background Periods of 1979 and 1989–1991, *Journal Of Geophysical ResearchAtmospheres*, 102, 3611–3616, 1997a.

Thomason, L. W., Poole, L. R., and Deshler, T.: A global climatology of stratospheric aerosol surface area density deduced from stratospheric aerosol and gas experiment II measurements: 1984–1994, *Journal of Geophysical ResearchAtmospheres*, 102, 8967–8976, <https://doi.org/10.1029/96JD02962>, <http://doi.wiley.com/10.1029/96JD02962>, 1997b.

1250 Thomason, L. W., Ernest, N., Millán, L., Rieger, L., Bourassa, A., Vernier, J.-P., Manney, G., Luo, B., Arfeuille, F., and Peter, T.: A global space-based stratospheric aerosol climatology: 1979–2016, *Earth System Science Data*, 10, 469–492, 2018.

Timmreck, C., Mann, G. W., Aquila, V., Hommel, R., Lee, L. A., Schmidt, A., Brühl, C., Carn, S., Chin, M., Dhomse, S. S., Diehl, T., English, J. M., Mills, M. J., Neely, R., Sheng, J., Toohey, M., and Weisenstein, D.: The Interactive Stratospheric Aerosol Model Intercomparison Project (ISA-MIP): Motivation and experimental design, *Geoscientific Model Development*, 11, 2581–2608, <https://doi.org/10.5194/gmd-11-2581-2018>, 2018.

1255 Trepte, C. C. R., Veiga, R. E., and McCormick, M. P.: The Poleward Dispersal of Mount Pinatubo Volcanic Aerosol, *Journal of Geophysical Research*, 98, 18 563–18 573, <https://doi.org/10.1029/93JD01362>, <http://www.agu.org/pubs/crossref/1993/93JD01362.shtml><http://onlinelibrary.wiley.com/doi/10.1029/93JD01362/full>, 1993.

Turco, R., Whitten, R., and Toon, O.: Stratospheric aerosols: Observation and theory, *Reviews of Geophysics*, <http://onlinelibrary.wiley.com/doi/10.1029/RG020i002p00233/full>, 1982.

1260 Uppala, S. M., KÅllberg, P. W., Simmons, A. J., Andrae, U., Bechtold, V. D. C., Fiorino, M., Gibson, J. K., Haseler, J., Hernandez, A., Kelly, G. A., Li, X., Onogi, K., Saarinen, S., Sokka, N., Allan, R. P., Andersson, E., Arpe, K., Balmaseda, M. A., Beljaars, A. C. M., Berg, L. V. D., Bidlot, J., Bormann, N., Caires, S., Chevallier, F., Dethof, A., Dragosavac, M., Fisher, M., Fuentes, M., Hagemann, S., Hólm, E., Hoskins, B. J., Isaksen, L., Janssen, P. A. E. M., Jenne, R., McNally, A. P., Mahfouf, J.-F., Morcrette, J.-J., Rayner, N. A., Saunders, R. W., Simon, P., Sterl, A., Trenberth, K. E., Untch, A., Vasiljevic, D., Viterbo, P., and Woollen, J.: The ERA-40 re-analysis, *Quarterly Journal of the Royal Meteorological Society*, 131, 2961–3012, <https://doi.org/10.1256/qj.04.176>, <http://doi.wiley.com/10.1256/qj.04.176>, 2005.

1265 Vaughan, G., Wareing, D. P., Jones, S. B., Thomas, L., and Larsen, N.: Lidar measurements of Mt. Pinatubo aerosols at Aberystwyth from August 1991 through March 1992, *Geophysical Research Letters*, 21, 1315–1318, <https://doi.org/10.1029/93GL02893>, <http://doi.wiley.com/10.1029/93GL02893>, 1994.

1270 Walters, D. N., Williams, K. D., Boutle, I. A., Bushell, A. C., Edwards, J. M., Field, P. R., Lock, A. P., Morcrette, C. J., Stratton, R. A., Wilkinson, J. M., and Others: The Met Office Unified Model global atmosphere 4.0 and JULES global land 4.0 configurations, *Geoscientific Model Development*, 7, 361–386, 2014.

1275 Weber, M., Dikty, S., Burrows, J. P., Garry, H., Dameris, M., Kubin, A., Abalichin, J., and Langematz, U.: The Brewer-Dobson circulation and total ozone from seasonal to decadal time scales, *Atmospheric Chemistry and Physics*, 11, 11221–11235, <https://doi.org/10.5194/acp-11-11221-2011>, <https://www.atmos-chem-phys.net/11/11221/2011/>, 2011.

1280 Wielicki, B. A., Wong, T., Allan, R. P., Slingo, A., Kiehl, J. T., Soden, B. J., Gordon, C. T., Miller, A. J., Yang, S. K., Randall, D. A., Robertson, F., Susskind, J., and Jacobowitz, H.: Evidence for large decadal variability in the tropical mean radiative energy budget. - PubMed - NCBI, *Science*, 295, 841–844, <https://doi.org/10.1126/science.1065837>, <https://www.ncbi.nlm.nih.gov/pubmed/11823638>, 2002.

1285 Winker, D. M. and Osborn, M. T.: Airborne lidar observations of the Pinatubo volcanic plume, *Geophysical Research Letters*, 19, 167–170, 1992.

1290 Yoshioka, M., Regayre, L. A., Pringle, K. J., Johnson, J. S., Mann, G. W., Partridge, D. G., Sexton, D. M., Lister, G. M., Schutgens, N., Stier, P., Kipling, Z., Bellouin, N., Browse, J., Booth, B. B., Johnson, C. E., Johnson, B., Molland, J. D., Lee, L., and Carslaw, K. S.: Ensembles of Global Climate Model Variants Designed for the Quantification and Constraint of Uncertainty in Aerosols and Their Radiative Forcing, *Journal of Advances in Modeling Earth Systems*, 11, 3728–3754, <https://doi.org/10.1029/2019MS001628>, 2019.

1295 Young, R. E., Houben, H., and Toon, O. B.: Radiatively forced dispersion of the Mt. Pinatubo volcanic cloud and induced temperature perturbations in the stratosphere during the first few months following the eruption, *Geophysical Research Letters*, 21, 369–372, <http://adsabs.harvard.edu/abs/1994GeoRL..21..369Y>, 1994.

Young, S. A., Manson, P. J., and Patterson, G. R.: Southern Hemisphere Lidar Measurements of the Aerosol Clouds from Mt. Pinatubo and Mt. Hudson, in: NASA Technical Report, NASA. Langley Research Center, Sixteenth International Laser Radar Conference, Part 1, <https://ntrs.nasa.gov/search.jsp?R=19920019987>, 1992.

Yu, P., Murphy, D. M., Portmann, R. W., Toon, O. B., Froyd, K. D., Rollins, A. W., Gao, R.-S., and Rosenlof, K. H.: Radiative forcing from anthropogenic sulfur and organic emissions reaching the stratosphere, *Geophysical Research Letters*, 43, 9361–9367, <https://doi.org/10.1002/2016GL070153>, <http://doi.wiley.com/10.1002/2016GL070153>, 2016.

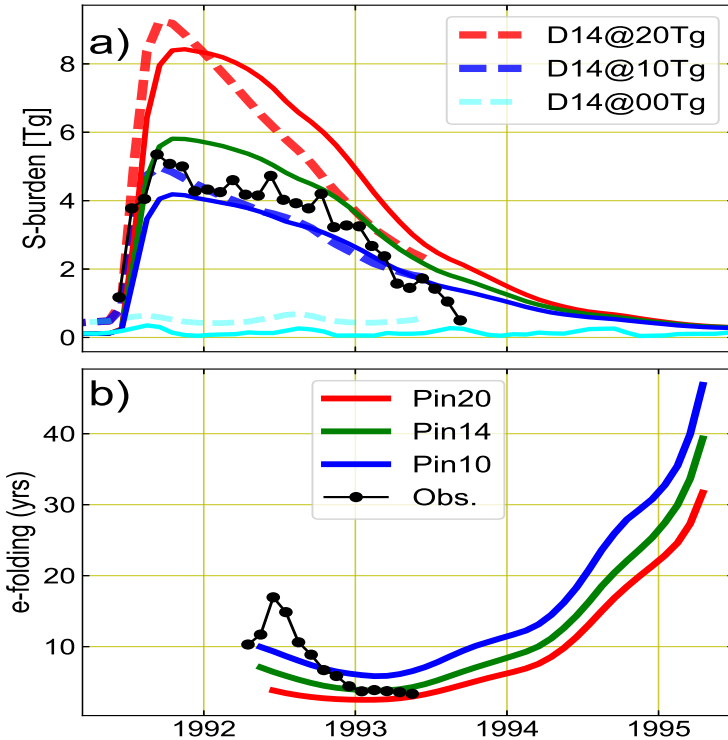


**Figure 1.** (a, top) Monthly mean stratospheric aerosol (globally integrated above 400 hPa) sulphur burden (S-burden, blue line) from simulations Pin00 (aqua line), Pin10 (blue line), Pin14 (green line) and Pin20 (red line). S-burden The S-burden from Dhomse et al. (2014) for 0, 10 and 20 Tg  $\text{SO}_2$  injection are shown with dashed aqua, red and blue dashed and red lines, respectively. (b, bottom) Estimated S-burden derived from High-resolution Infrared Radiation Sounder (HIRS) satellite measurements is shown with black dots (Baran and Foot, 1994). (b, lower) S-burden decay rates (e-folding lifetime) calculated using simple linear fit using 6-month 7-month S-burden ( $\pm 3$  for mid-point) time series.

Zanchettin, D., Khodri, M., Timmreck, C., Toohey, M., Schmidt, A., Gerber, E. P., Hegerl, G., Robock, A., Pausata, F. S. R., Ball, W. T., Bauer, S. E., Bekki, S., Dhomse, S. S., LeGrande, A. N., Mann, G. W., Marshall, L., Mills, M., Marchand, M., Niemeier, U., Poulain, V., Rozanov, E., Rubino, A., Stenke, A., Tsigaridis, K., and Tummon, F.: The Model Intercomparison Project on the climatic response to Volcanic forcing (VolMIP): experimental design and forcing input data for CMIP6, Geoscientific Model Development, 9, 2701–2719,

**Table 1.** Set up of UM-UKCA simulations.

Simulation	Injection amount (Tg SO <sub>2</sub> )	Date	Height (km)	QBO phase
<b>Pin00</b>	0	15 June 1991	NA	Easterly
<b>Pin10</b>	10	As <b>Pin00</b>	21–23	As <b>Pin00</b>
<b>Pin14</b>	14	As <b>Pin00</b>	As <b>Pin10</b>	As <b>Pin00</b>
<b>Pin20</b>	20	As <b>Pin00</b>	As <b>Pin10</b>	As <b>Pin00</b>
<b>Elc00</b>	0	4 April 1982	NA	Westerly
<b>Elc05</b>	5	As <b>Elc00</b>	24–26	As <b>Elc00</b>
<b>Elc07</b>	7	As <b>Elc00</b>	As <b>Elc05</b>	As <b>Elc00</b>
<b>Elc10</b>	10	As <b>Elc00</b>	As <b>Elc05</b>	As <b>Elc00</b>
<b>Agu00</b>	0	17 March 1963	NA	Westerly
<b>Agu06</b>	6	As <b>Agu00</b>	20–22	As <b>Agu00</b>
<b>Agu09</b>	9	As <b>Agu00</b>	As <b>Agu06</b>	As <b>Agu00</b>
<b>Agu12</b>	12	As <b>Agu00</b>	As <b>Agu06</b>	As <b>Agu00</b>

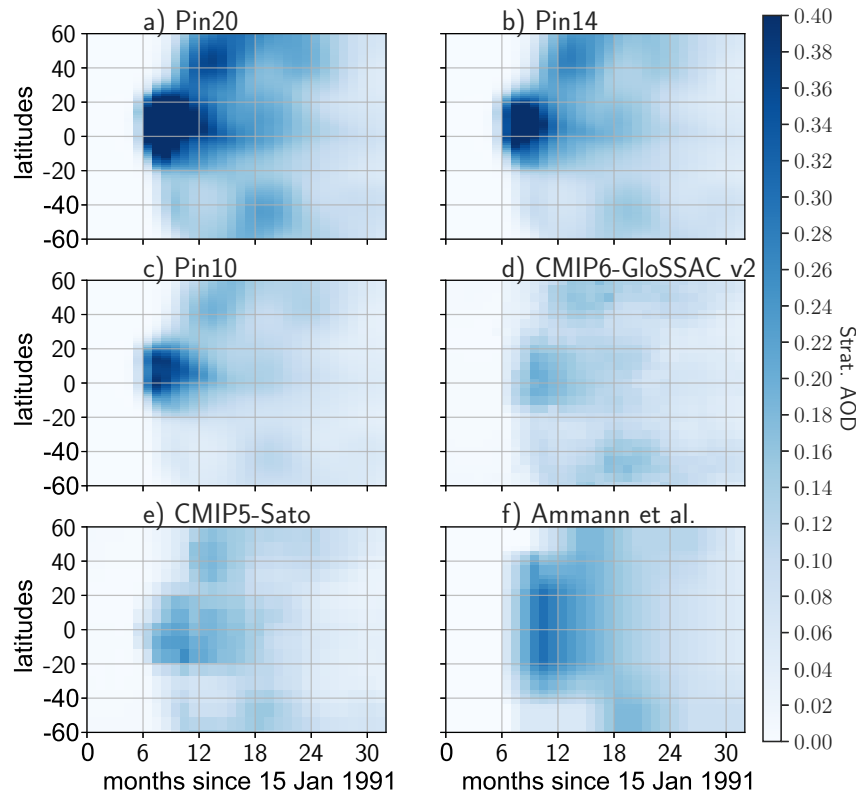


**Figure 2.** Ensemble mean stratospheric Aerosol Optical Depth (sAOD) from simulations (a) **Pin20**, (b) **Pin14**, and (c) **Pin10**. Panels (d)-(f) show sAOD<sub>550</sub> from [CMIP6-GloSSAC](#) (Thomason et al., 2018), [Sato et al. \(1993\)](#) [Sato](#) (Sato et al., 1993) and [Ammann et al. \(2003\)](#) [Ammann](#) (Ammann et al., 2003), respectively.

DIF >

Table 2: [Some important aspects of the evaluation dataset.](#)

<a href="#">Aerosol property</a>	<a href="#">Key Aspects</a>
<b>Global stratospheric sulphur burden</b>	

---

## High-resolution Infrared Radiation Sounder (HIRS)

- 1.1 Derived from HIRS measurements onboard NOAA-10, -11, -12 satellites
- 1.2 Aqueous sulphuric acid aerosol retrieval using  $8.2\mu\text{m}$  and  $12.5\mu\text{m}$  HIRS water vapour  
(Baran et al., 1993).
- 1.3 Derived sulphur burden based on assumed aerosol composition of 75% weight aqueous sulphuric acid solution droplets.
- 1.4 Global sulphur burden dataset is digitized from Figure 3 of Baran and Foot (1994)

---

## Stratospheric AOD ( $\text{sAOD}_{550}$ ) and extinction ( $\text{ext}_{550}$ ) at 550 nm

---

### The CMIP6-GloSSAC forcing dataset <https://eosweb.larc.nasa.gov/project/glossac/glossac>

- 2.1 Pinatubo aerosol cloud primarily from SAGE-II, HALOE and CLAES observations (Thomason et al., 2018).
- 2.2 Improved Pinatubo gap-fill in mid-latitudes from combining SAGE-II with CLAES
- 2.3 Tropical Pinatubo gap-fill from combining SAGE-II with Mauna Loa lidar (SPARC, 2006).
- 2.4 El Chichon aerosol cloud mostly derived from high-latitude SAM-II data (64°N to 64°S-84°S)
- 2.5 Tropical and mid-latitude El Chichon cloud from combining SAM-II with lidar data from ground-based surveys (13°N to 80°N) and from Hampton, Virginia (37°N).

---

### The CMIP6-AER2D forcing dataset (<ftp://iacftp.ethz.ch/pub/read/luo/CMIP6/>)

- 3.1 From 2D interactive stratospheric aerosol simulations (Arfèuille et al., 2014).
- 3.2 Primarily from the 8 major eruption clouds in 1850-1979 (29 in 1600-present dataset).
- 3.3 Additional minor eruption clouds from Stothers (1996) are also included.

---

### The CMIP5-Sato forcing dataset (<https://data.giss.nasa.gov/modelforce/strataer/>)

- 4.1 NASA GISS observation-based forcing data for 1850-2012 ( $\text{sAOD}_{550}$  only).
- 4.2 Satellite era, uses SAGE-I, SAM-II, SAGE-II and OSIRIS measurements.
- 4.3 Pre-satellite era uses syntheses of different measurements
- 4.4 Surface radiation measurement dataset for Agung (Dyer and Hicks, 1968) highly uncertain tropics (Stothers, 2001).

---

---

The CMIP5-Ammann dataset  
([ftp://ftp.ncdc.noaa.gov/pub/data/paleo/climate\\_forcing/volcanic\\_aerosols/ammann2003b\\_volcanics.txt](ftp://ftp.ncdc.noaa.gov/pub/data/paleo/climate_forcing/volcanic_aerosols/ammann2003b_volcanics.txt))

- 5.1 Simple model-based dataset for 13 eruption clouds 1880-2000 (sAOD<sub>550</sub> only).
- 5.2 Based on parameterisation for meridional dispersion from tropical reservoir to mid-latitudes determined by Brewer-Dobson circulation seasonal cycle.
- 5.3 12-month e-folding timescale for decay of tropical volcanic aerosol reservoir
- 5.4 Peak sAOD<sub>550</sub> for each eruption scaled to match aerosol loadings from Stothers (1996); Hofmann and Rosen (1983b); Stenchikov et al. (1998), assuming  $\text{R}_0 = 12$  months and  $\text{R}_{\text{decay}} = 12$  months.

---

The post-Agung Lexington lidar dataset from Grams (1966) (see Supplementary Information)

- 6.1 694nm backscatter ratio profiles from Lexington, Massachusetts (42°N, 71°W Fiocco and Grams, 1964; Grams and Fiocco, 1967) (ext<sub>550</sub> only).
- 6.2 1-km dataset for 66 lidar soundings (Jan 1964 to July 1965) in Table A1 of Grams (1966).
- 6.3 Backscatter ratio timeseries at 15km, 20km and 24km tabulated into ASCII file.
- 6.4 Conversion to ext<sub>550</sub> using extinction-to-backscatter ratio from Jäger and Deshler (2000).

---

## Vertical profile evolution of Effective Radius (Reff) and Surface Area Density (SAD)

---

CMIP6-GloSSAC (Pinatubo and El Chichon) and CMIP6-AER2D (Agung)

- 7.1 SAD for Pinatubo and El Chichon aerosol clouds from GloSSAC, using SAGE-II 3- $\lambda$  method.
- 7.2 SAD for Agung aerosol cloud from 2D interactive stratospheric aerosol model simulation.
- 7.3 Volume concentration for each cloud derived from same method
- 7.4 Effective radius from 3 times ratio of volume concentration to SAD

---

## Vertical profile of tropical stratospheric temperature anomaly

---

---

From ECMWF reanalysis data

- 8.1 Temperature anomaly based on difference from 5-year mean starting in year of eruption
- 8.2 T-anomalies for Pinatubo and El Chichón from the ERA-interim re-analysis (Dee et al., 2011)
- 8.3 For the Agung period, anomaly derived from the ERA-40 year dataset (Uppala et al., 2005)

---

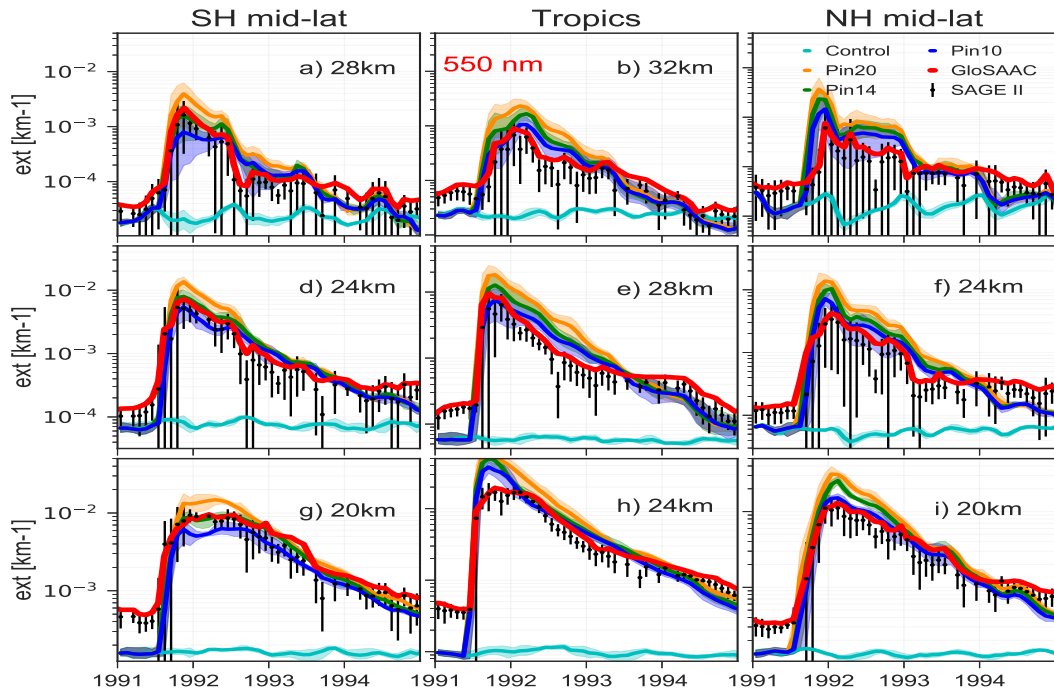


**Figure 3.** Ensemble mean extinctions (550 nm) from simulations **Pin00** (aqua), **Pin10** (blue), **Pin14** (green), and **Pin20** (orange). The shaded regions indicate the variability among ensemble members. Extinctions for SH mid-latitudes ( $35^{\circ}\text{S} - 60^{\circ}\text{S}$  (panels a, d, g)), tropics ( $20^{\circ}\text{S} - 20^{\circ}\text{N}$  (panels b, e, h)), and NH mid-latitudes ( $35^{\circ}\text{N} - 60^{\circ}\text{N}$  (panels c, f, i)) are shown in left, middle and right panels, respectively. Mid-latitude extinctions are shown for 20, 24 and 28 km, whereas tropical profiles are shown for 24, 28 and 32 km. Monthly mean extinction from SAGE II v7.2 measurements for a given latitude band are shown with black filled circles and vertical lines indicate standard deviation from all the measurements for a given month. Gap-filled extinctions from the [GloSSAC-CMIP6-GloSSAC v2](#) dataset ([Thomassen et al., 2018](#)) ([Kovilakam et al., 2020](#)) are shown with a red line.

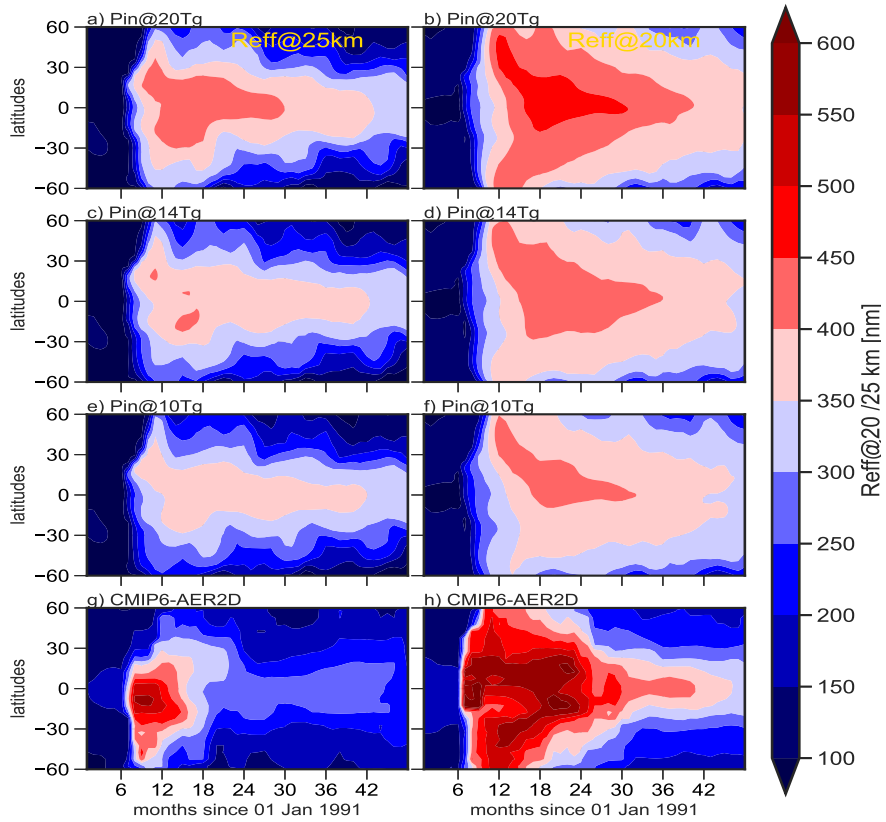


**Figure 4.** Modelled (from simulations and) and CMIP6-effective radii (Reff, in  $\mu\text{m}$ ) at from (a, b) -simulation Pin20, (c, d) 25simulation Pin14, (e, f) simulation Pin10 km and (g, h) -CMIP6-GloSSAC V2 at (left) 25 km and (right) 20 km.

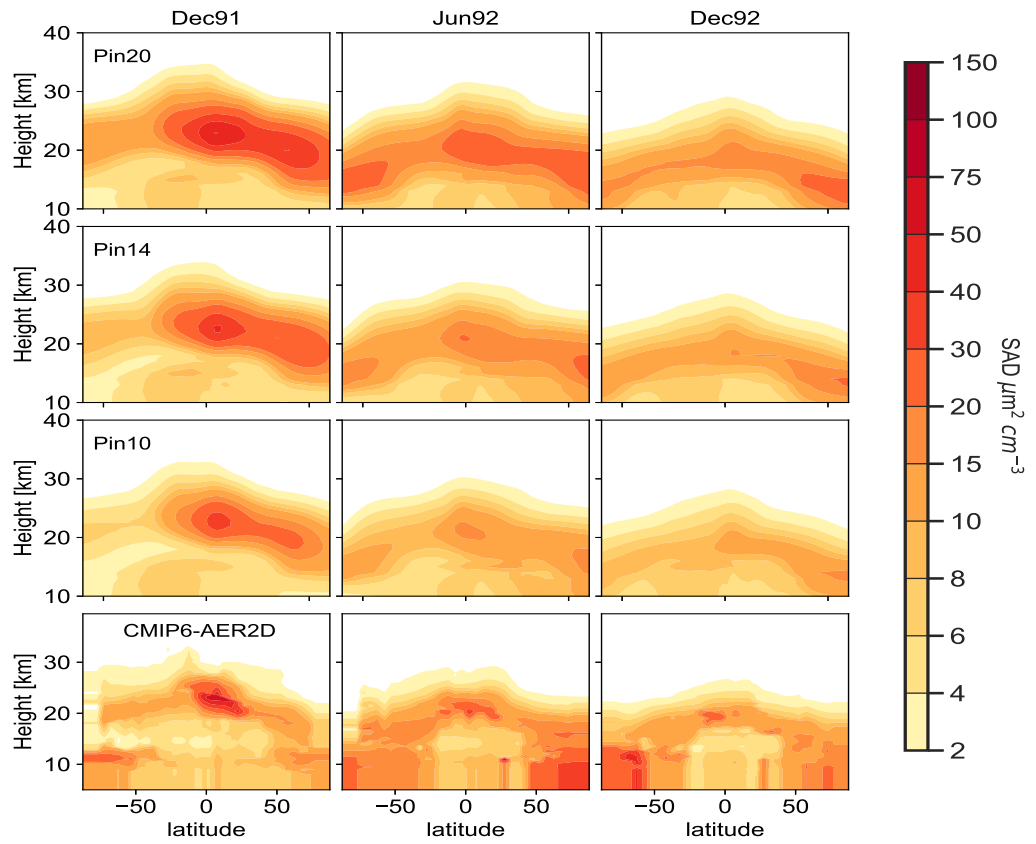


**Figure 5.** Zonal mean monthly mean Surface Area Density (SAD,  $\mu\text{m}^2 \text{cm}^{-3}$ ) for December 1991, June 1992 and December 1992 from ensemble mean simulations (top row) **Pin20**, (second row) **Pin14**, and (third row) **Pin10**. The bottom row shows observation-based SAD estimates from Arfeuille et al. (2014).

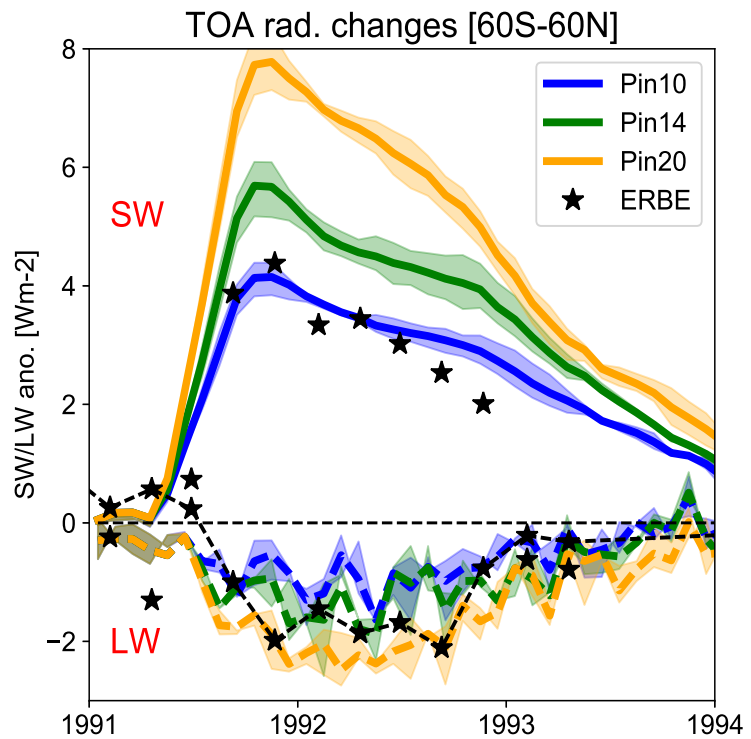


**Figure 6.** Near-global ( $60^{\circ}\text{S}$ - $60^{\circ}\text{N}$ ) longwave (LW) and shortwave (SW) heating anomalies ( $\text{W m}^{-2}$ ) from the ensemble mean of simulations **Pin20** (blue), **Pin14** (green), and **Pin10** (orange). Estimated anomalies from the Earth Radiation Budget Experiment (ERBE) satellite data are shown with black stars.

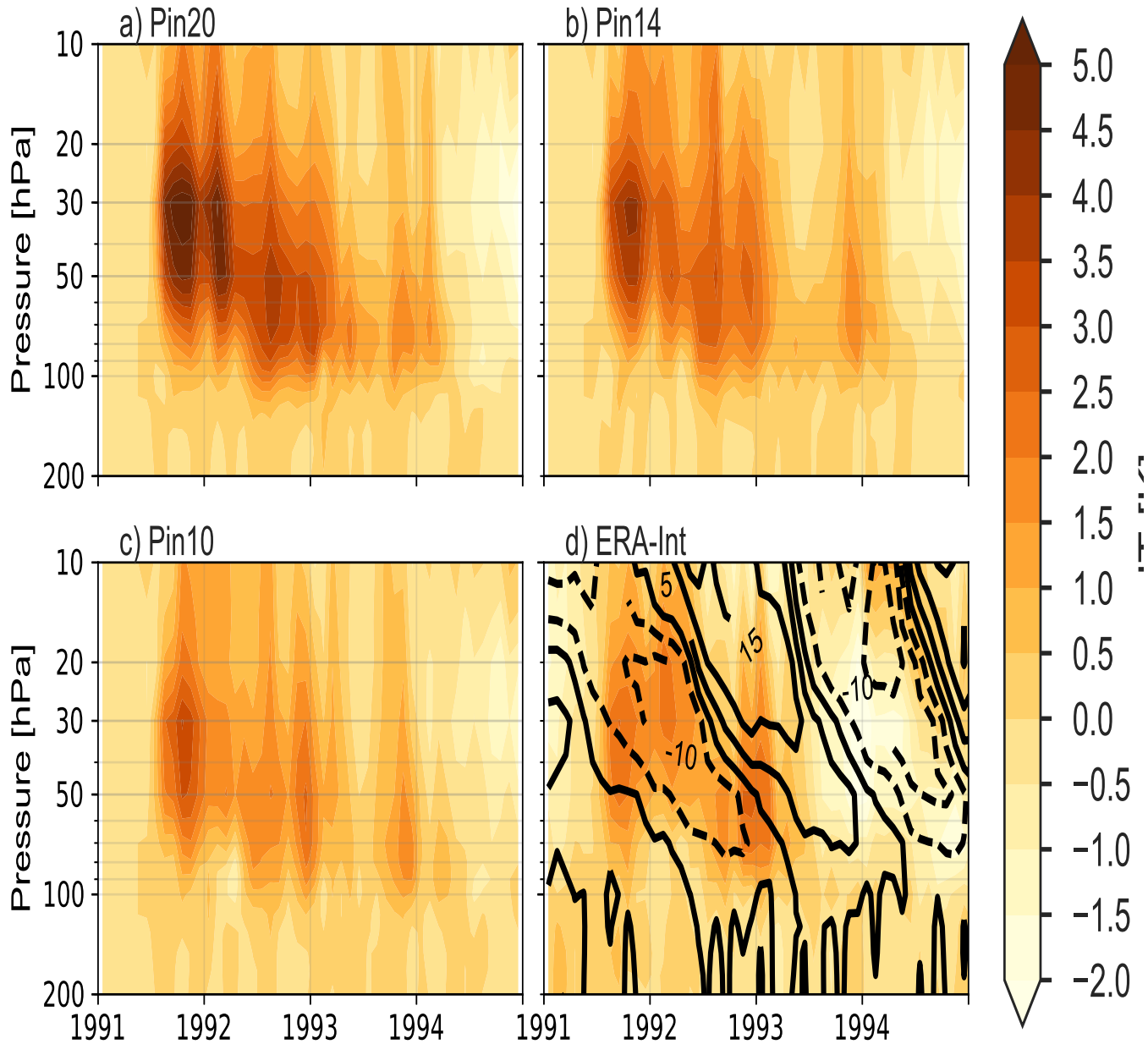


**Figure 7.** (a)-(c) Ensemble mean aerosol-induced heating (K) in the tropical ( $20^{\circ}\text{S} - 20^{\circ}\text{N}$ ) stratosphere, calculated by subtracting temperature fields from a control simulation for simulations **Pin20**, **Pin14** and **Pin10**. (d) Tropical temperature (shaded) and zonal wind (contour) anomalies from ERA-Interim reanalysis data (for 1991–1995 time period). Contour intervals for wind anomalies are 4 m/s and negative anomalies are shown with dashed lines.

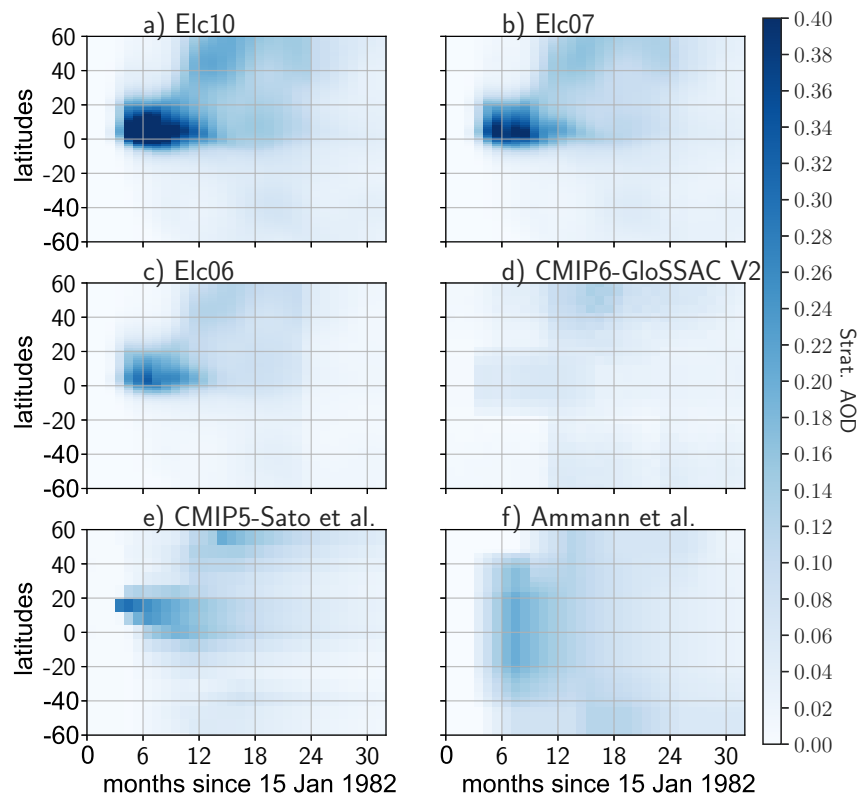


**Figure 8.** Same as **Fig. 2**, but for El Chichón simulations (a) **Elc10**, (b) **Elc07**, and (c) **Elc05**.

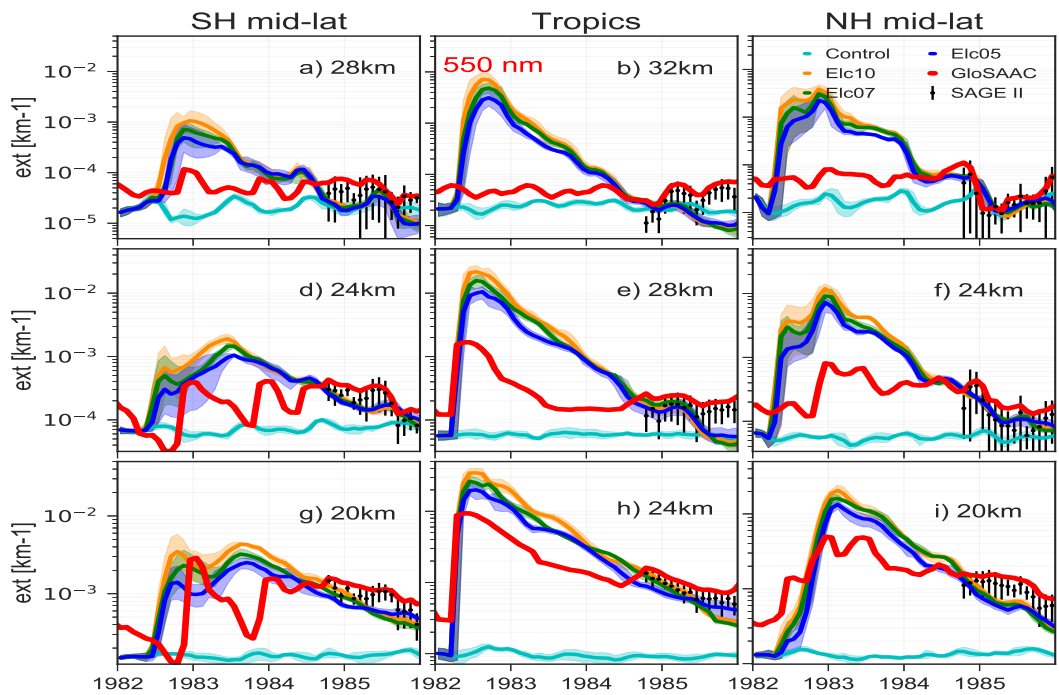


**Figure 9.** Same as **Fig. 3**, but for El Chichón simulations (a) **Elc05**, (b) **Elc07** and (c) **Elc10**.

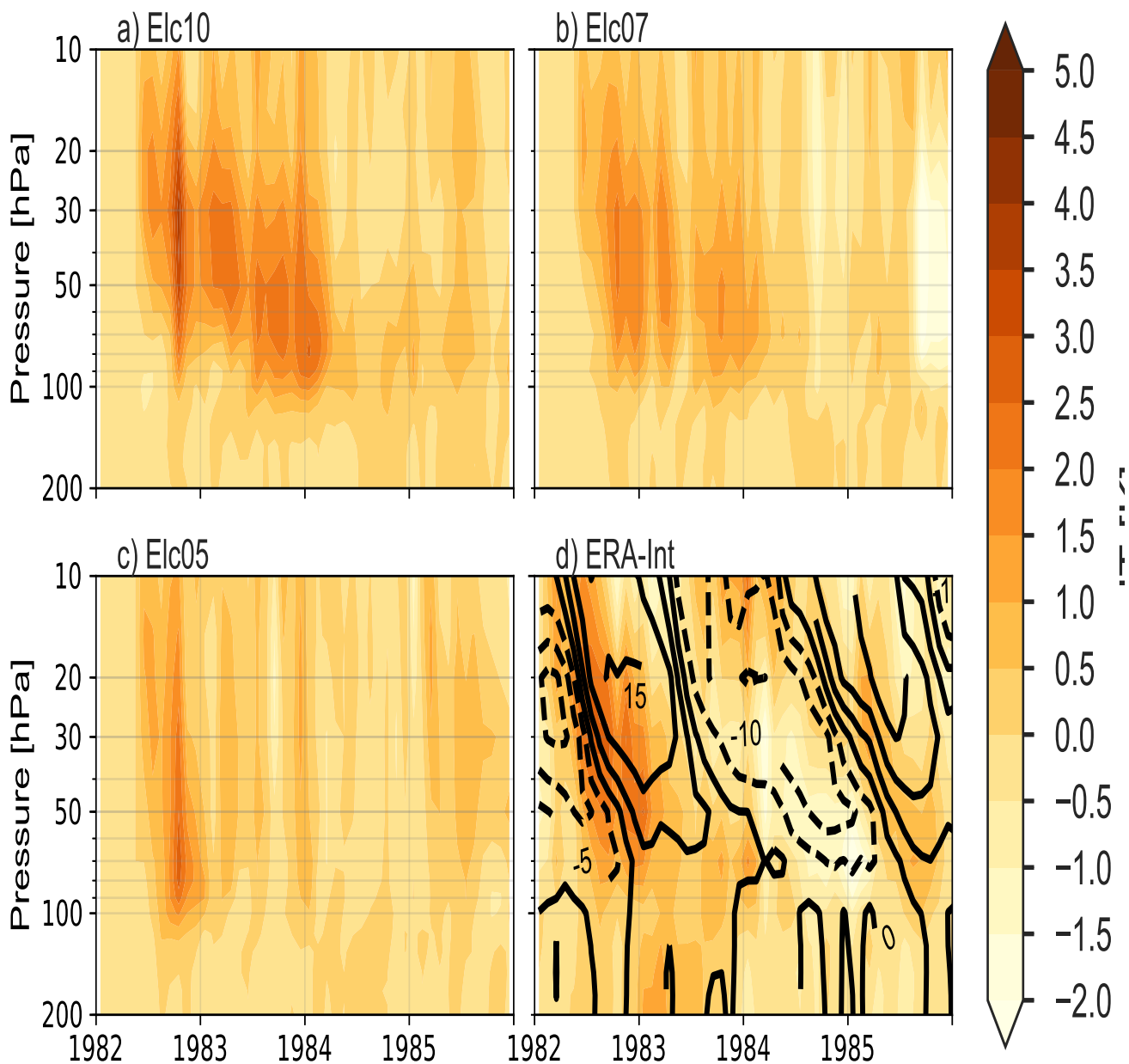


**Figure 10.** Same as **Fig. 7**, but for El Chichón simulations (a) **Elc10**, (b) **Elc07** and (c) **Elc05**.

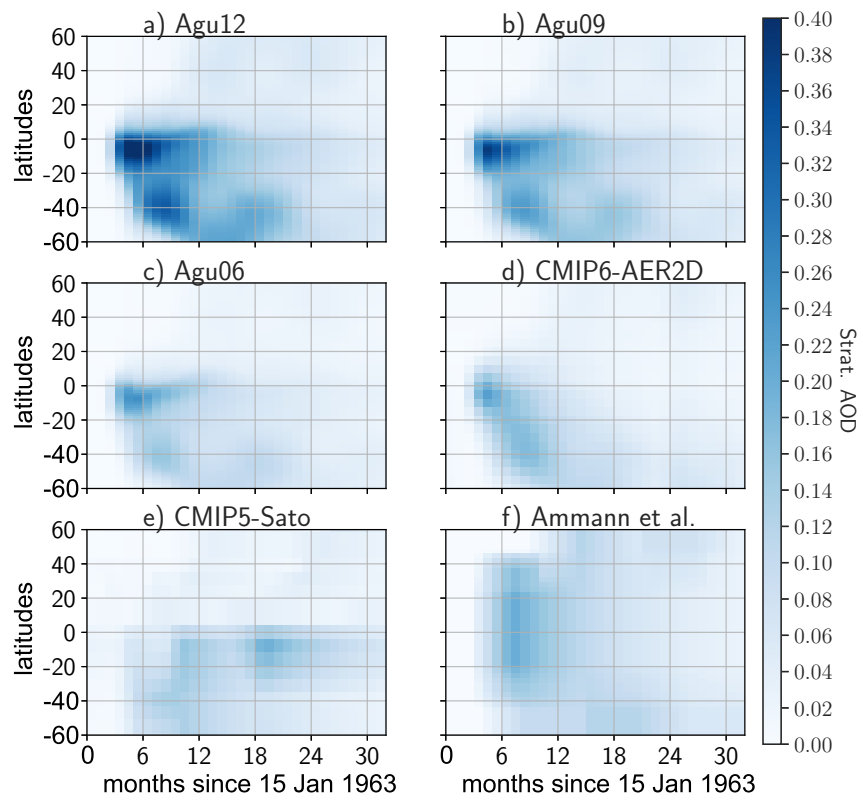


**Figure 11.** Same as **Fig. 2**, but for Mt. Agung simulations (a) **Agu12**, (b) **Agu09**, and (c) **Agu06**.

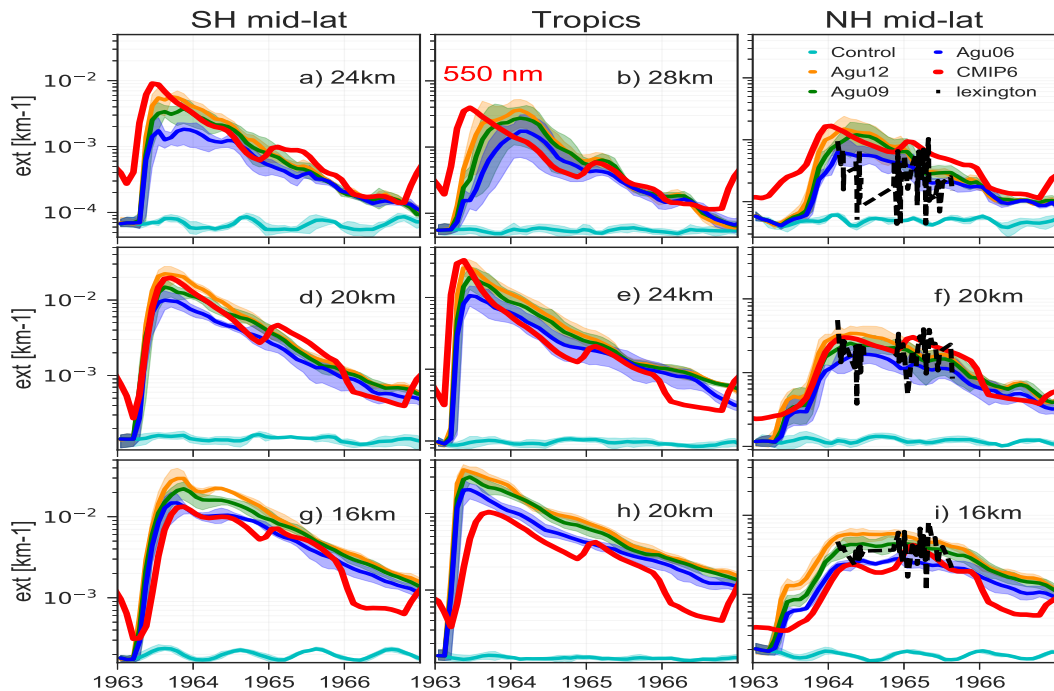


**Figure 12.** Same as **Fig. 3**, but for Mt. Agung simulations **Agu06**, **Agu09** and **Agu12**. Extinctions—Mid-visible aerosol extinction are shown for at 16, 20 and 24 km for mid-latitudes and at 20, 24 and 28 km for the tropics. As GloSSAC data is not available before 1979, model extinctions—Also shown are compared with CMIP6 data aerosol extinction from the CMIP6-AER2D dataset (Arfeuille et al., 2014) and from LIDAR measurements from at a NH mid-latitude station, site (Lexington, Massachusetts, USA) (Grams and Fiocco, 1967).

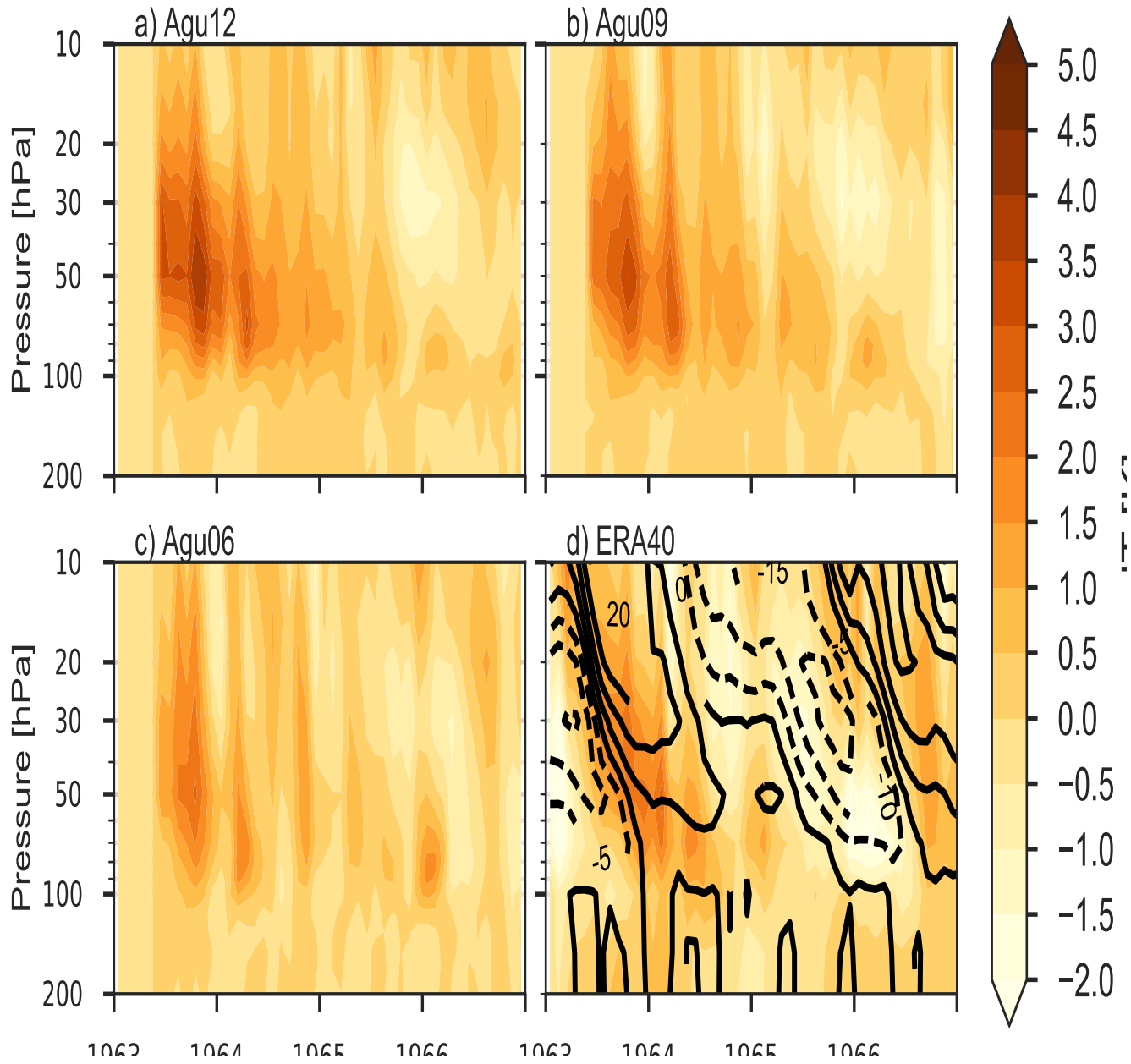


**Figure 13.** Same as **Fig. 7**, but for Agung simulations (a) **Agu12**, (b) **Agu09** and (c) **Agu06** and for (d) temperature anomalies calculated using ERA-40 reanalysis data.